6-12-2018

New Polynuclear Copper-Pyrazolate Complexes: Towards the Synthesis of Photo- and Redox-Active Metal Organic Frameworks

Kaige Shi
kshi002@fiu.edu

FLORIDA INTERNATINAL UNIVERSITY

Miami, Florida

NEW POLYNUCLEAR COPPER-PYRAZOLATE COMPLEXES: TOWARDS THE SYNTHESIS OF PHOTO- AND REDOX-ACTIVE METAL ORGANIC FRAMEWORKS

A dissertation submitted in partial fulfillment of the

requirements for the degree of

DOCTOR OF PHILOSOPHY

in

CHEMISTRY

by

Kaige Shi

2018

To: Dean Michael R. Heithaus
College of Arts, Sciences and Education

This dissertation, written by Kaige Shi, and entitled New Polynuclear Copper-Pyrazolate Complexes: Towards the Synthesis of Photo- and Redox-Active Metal Organic Frameworks, having been approved in respect to style and intellectual content, is referred to you for judgment.

We have read this dissertation and recommend that it be approved.

_____
Konstantinos Kavallieratos

_____
Yuk-Ching Tse-Dinh

_____
Jaroslava Miksovska

_____
Chunlei (Peggy) Wang

_____
Raphael G. Raptis, Major Professor

Date of Defense: June 12, 2018

The dissertation of Kaige Shi is approved

_____
Dean Michael R. Heithaus
College of Arts, Sciences and Education

_____
Andrés G. Gil
Vice President for Research and Economic Development
and Dean of the University Graduate School

Florida International University, 2018

DEDICATION

I dedicate this thesis to my parents. Without their patience, understanding, support, and most of all love, the completion of this work would not have been possible.

ACKNOWLEDGMENTS

Firstly, I would like to express my sincere gratitude to my advisor Professor Dr. Raphael G Raptis for the continuous support of my PhD study and related research, for his patience, expertise, understanding, motivation, and immense knowledge. His guidance helped me in all the time of research and writing of this thesis. I could not have imagined having a better advisor for my PhD study. His advice on both research as well as on my career have been invaluable.

Besides my advisor, I would like to thank my committee members: Prof. Konstantinos Kavallieratos, Prof. Yuk-Ching Tse-Dinh, Prof. Jaroslava Miksovska and Prof. Chunlei (Peggy) Wang, for their insightful comments and encouragement, but also for the questions which helped me to widen my research in various perspectives. I also want to thank them for investing their time and providing interesting and valuable feedback. I feel proud and honored that you have accepted to be on my committee.

I would like to thank our collaborators and their group members for their help and input: Prof. Arturo Hernández-Maldonado (Univ. of Puerto Rico, Mayaguez; surface, porosity and adsorption measurements), Dr. Athanasios K. Boudalis (Univ. Strasbourg, France; EPR measurements), Dr. Radovan Herchel (Palacky University, Czech Republic; Magnetic measurements) and Dr. Vadym Drozd (FIU, XPRD under high pressure).

There is no way to express how much it means to me to have been a member of Dr Raptis' lab. These brilliant friends and colleagues inspired me over the many years: Dr. Logesh Mathivathanan, Dr. Guang Yang, Dr. Indranil Chakraborty, Dr. Ievgen Govor, Dr. Xin-Yi Cao, Alan Rodriguez-Santiago, Shambhu Kandel, Jessica López-Pla, David Kreiger, Konstantinos Lazarou and Tahereh Mousavinejad. Thanks for their friendship and support, and for creating a cordial working environment and share their expertise and experiences. Especially Logesh, who encouraged and

helped me at every stage of my academic life in U.S. I gained a lot from their valuable feedback throughout this project.

Of course, I would also like to thank my parents and sisters for their unconditional trust, timely encouragement, and endless patience.

ABSTRACT OF THE DISSERTATION

NEW POLYNUCLEAR COPPER-PYRAZOLATE COMPLEXES: TOWARDS THE SYNTHESIS OF PHOTO- AND REDOX-ACTIVE METAL ORGANIC FRAMEWORKS

by

Kaige Shi

Florida International University, 2018

Miami, Florida

Professor Raphael G Raptis, Major Professor

The main objectives of this project are the synthesis and redox- or photo-active modification and CO_2 adsorption studies of metal-organic frameworks (MOFs) based on Cu_3-pyrazolate secondary building units (SBUs). Trinuclear copper(II) complexes of the formula $[Cu_3(\mu_3\text{-}O)(\mu\text{-}4\text{-}R\text{-}pz)_3X_3]^z$ have been studied extensively due to their redox, magnetic and catalytic properties. In earlier work, we have shown that trinuclear copper(II) complexes of the formula $[Cu_3(\mu_3\text{-}O)(\mu\text{-}4\text{-}R\text{-}pz)_3X_3]^z$ pz = pyrazolato anion; R = H, CH(O), Cl, Br and NO_2; X = Cl, NCS, CH_3COO, CF_3COO and pyridine – can be oxidized to the corresponding z+1, formally $Cu^{II}_2Cu^{III}$, species. In this project, fourteen (14) new copper-pyrazolate complexes of varying nuclearities (Cu_3, Cu_6, Cu_7 and Cu_{12}), terminal ligands (-NO_2, py, -N_3, -Cl) and bridging ligands (4-Cl-pzH and 4-Ph-pzH) have been synthesized. Efforts have been made to prepare MOFs based on the $Cu_3(\mu_3\text{-}O)$-SBUs. While attempting to design the most suitable SBU for redox-active MOF construction, it was found that the one-electron oxidation of the all-Cu^{II} complex $[Cu_3(\mu_3\text{-}O)(\mu\text{-}pz)_3(NO_2)_3]^{2-}$, $[8]^{2-}$, was achieved at redox potential more cathodic than any other $Cu_3(\mu_3\text{-}O)$-complexes studied in our laboratory. The mixed-valent compound, $[Cu_3(\mu_3\text{-}O)(\mu\text{-}pz)_3(NO_2)_3]^{-}$, $[8]^{-}$, the easiest accessible $Cu^{II}_2Cu^{III}$ species known to date, was characterized spectroscopically. Compound [8] and analogous [11] release NO almost quantitatively upon the addition of PhSH or acetic acid. The system is catalytic in the presence of excess nitrite.

Before embarking on the study of photo-active MOFs, a simpler model compound – a dimer of trimer $[\{Cu_3(\mu_3\text{-}OH)(\mu\text{-}4\text{-}Cl\text{-}pz)_3(py)_2\}_2(\mu\text{-}abp)](ClO_4)_4$ [21], where abp = 4,4'-azopyridine, was synthesized and its photochemistry was studied. The absorption spectra recorded before and after irradiation indicated a structural change. Two dimensional (2D) and three dimensional (3D) materials with $\{[Cu_3(\mu_3\text{-}OH)(\mu\text{-}4\text{-}R\text{-}pz)_3]^{2+}\}_n$ SBUs where R = Ph or Cl , which can potentially undergo *cis/trans*-isomerization, have been prepared during this project. A Phenyl substituent at 4-position on the pyrazole ligand leads to the formation of new class of 2D sheets. Three new 3D porous MOFs based on $\{[Cu_3(\mu_3\text{-}OH)(\mu\text{-}4\text{-}Cl\text{-}pz)_3]^{2+}\}_n$ SBUs have interpenetrated- lattice structures and are capable of adsorbing CO_2 selectively. Compounds FIU-1 and FIU-3 also exhibit hysteretic sorption-desorption profiles indicating the flexibility of the MOFs upon adsorption. Compound FIU-1 demonstrates the usefulness of a hexanuclear Cu^{II} -pyrazolate moiety as an SBU for generating 3-fold interpenetrated 3D polymeric network. Complexes FIU-2 and FIU-3 have novel 3-fold interpenetrating 3D hexagonal framework structures. Compound FIU-2 crystallizes in the monoclinic crystal system with the $P2_1/c$ space group, whereas FIU-3 crystallizes in triclinic space group $P\bar{1}$. Both structures contain Cu_3-SBUs connected by the linkers through the Cu-termini.

TABLE OF CONTENTS

CHAPTER PAGE

LIST OF TABLES

TABLE PAGE

LIST OF FIGURES

FIGURE PAGE

LIST OF SCHEMES

SCHEME PAGE

LIST OF ABBREVIATIONS

General abbreviations

2D	Two-dimensional
3D	Three-dimensional
4-Methyl-pyrazole	4-Me-pzH
4-Phenyl-pyrazole	4-Ph-pzH
abp	4,4’-azobis(pyridine)
bpe	1, 2-bis(4-pyridyl)ethylene
CAN	Ceric ammonium nitrate
$E_{1/2}$	Half-wave potential
E_{pa}	Anodic peak potential
E_{pc}	Cathodic peak potential
Fc^{+}/Fc	Ferricenium/Ferrocene couple
IVCT	Intervalence charge transfer
IR	Infrared spectroscopy
J	Magnetic exchange coupling
pz	Pyrazolate
Pyridine	py
PPN	Bis(triphenylphosphoranylidene)ammonium
PPNCl	Bis(triphenylphosphine)iminium chloride
SBU	Secondary Building Unit
TBA	Tetra-n-butylammonium hexafluorophosphate
TGA	Thermogravimetric analysis
XRPD	X-ray powder diffraction

List of Copper pyrazolate complexes

Trinuclear Copper-pyrazolate complexes

$(PPN)(C_5H_{10}NH_2)[Cu_3(\mu_3\text{-}OH)\,(\mu\text{-}Cl)(\mu\text{-}4\text{-}Ph\text{-}Pz)_3Cl_3]$ [1]

$(PPN)[Cu_3(\mu_3\text{-}OH)\,(\mu\text{-}4\text{-}Ph\text{-}pz)_3Cl_3]\cdot CH_2Cl_2$ [2]

$(PPN)[Cu_3(\mu_3\text{-}OH)(\mu\text{-}4\text{-}Ph\text{-}pz)_3Cl_3]\cdot CH_3CN$ [3]

$(PPN)[Cu_3(\mu_3\text{-}OH)(\mu\text{-}pz)_3(\mu_{1,1}\text{-}N_3)_2(N_3)]$ [4]

$[Cu_3(\mu_3\text{-}OMe)(\mu\text{-}Cl)(\mu\text{-}pz)_3(py)_2]Cl$ [5]

$[Cu_3(\mu_3\text{-}OH)(\mu\text{-}Cl)(\mu\text{-}pz)_3(py)_2Cl](py)$ [6]

$Cu_3(\mu_3\text{-}OH)(\mu\text{-}4\text{-}Cl)_3(py)_3(ClO_4)_2](CH_2Cl_2)[(CH_3)_2CO)]$ [7]

Cu-NO_2 complexes

$(PPN)_2\,[Cu_3(\mu_3\text{-}O)(\mu\text{-}pz)_3(\eta^1\text{-}NO_2)_2(\eta^2\text{-}NO_2)]$ [8]

$(PPN)_3[\,Cu_3(\mu_3\text{-}OH)(\mu\text{-}pz)_3(\eta^1\text{-}NO_2)_3](OH)(NO_3)$ [9]

$(PPN)_2[Cu_3(\mu_3\text{-}O)(\mu\text{-}pz)_3(\eta^1\text{-}NO_2)_2Cl]$ [10]

$(PPN)[Cu_3(\mu_3\text{-}OH)(\mu\text{-}4\text{-}Ph\text{-}pz)_3(\eta^1\text{-}NO_2)_3](CH_2Cl_2)_{0.5}$ [11]

$(PPN)_3[Cu_3(\mu_3\text{-}O)(\mu\text{-}4\text{-}Me\text{-}pz)_3(\eta^1\text{-}NO_2)_3](NO_3)$ [12]

$(PPN)_3[Cu_3(\mu_3\text{-}O)(\mu\text{-}4\text{-}Cl\text{-}pz)_3(\eta^1\text{-}NO_2)_3](NO_3)$ [13]

$[PPN][Cu_3(\mu_3\text{-}O)(\mu\text{-}pz)_3(N_3)_2(\eta^2\text{-}NO_2)]$ [14]

Hexanculear copper pyrazolate complex

$[\{Cu_3(\mu_3\text{-}OCH_3)(\mu\text{-}C_3H_2N_2Cl)_3\}_2(\mu\text{-}C_3H_2N_2Cl)_3(\mu_6\text{-}Cl)]$ [15]

Heptanuclear copper pyrazolate complexes

$[\{Cu_3(\mu_3\text{-}OH)(\mu\text{-}4\text{-}Ph\text{-}pz)_3(4\text{-}Ph\text{-}pzH)(Cl)_2\}_2][Cu(CH_3CNHpz)_2\,(\mu\text{-}Cl_2)]$ [16]

$[PPN]_2[\{Cu_3(\mu_3\text{-}OH)(\mu\text{-}4\text{-}Ph\text{-}pz)_3Cl_3\}_2\{CuCl_2(4\text{-}Ph\text{-}pzH)_2\}]$ [17]

$[PPN]_2[\{Cu_3(\mu_3\text{-}OH)(\mu\text{-}4\text{-}Ph\text{-}pz)_3Cl_3\}_2\{Cu(\mu\text{-}Cl)_2(4\text{-}Ph\text{-}pzH)_4\}]\cdot(CH_3CN)_2$ [18]

Cu_{12}

$[Cu_6(\mu_3\text{-}OMe)_2(\mu_4\text{-}Cl)(\mu\text{-}4\text{-}Ph\text{-}pz)_8Cl]_2[bpe]\{Cu_6\text{-}bpe\text{-}Cu_6\}$ [19]

$[Cu_6(\mu_3\text{-}OMe)_2(\mu_4\text{-}Cl)(\mu\text{-}4\text{-}Ph\text{-}pz)_8Cl]_2[abp]\{Cu_6\text{-}abp\text{-}Cu_6\}$ [20]

Dimer of trimers

$[\{Cu_3(\mu_3\text{-}OH)(\mu\text{-}4\text{-}Cl\text{-}pz)_3(py)_2\}_2(\mu\text{-}abp)](ClO_4)_4$ [21]

1D

$\{[Cu_3(\mu_3\text{-}OH)(\mu\text{-}Cl)(\mu\text{-}pz)_3Cl(tmpy)(CH_3CN)]\}_n$ [22]

2D- sheet

$\{[Cu_3(\mu_3\text{-}OH)(\mu\text{-}Cl)(\mu\text{-}pz)_3Cl]_2(tmpy)_2](CH_3CN)_2\}_n$ [23]

$\{[Cu_3(\mu_3\text{-}OH)(\mu\text{-}Cl)(\mu\text{-}pz)_3Cl(tmpy)](CH_3CN)\}_n$ [24]

$\{[Cu_3(\mu_3\text{-}OH)(\mu\text{-}4\text{-}Ph\text{-}pz)_3(abp)_{1.5}][(CF_3SO_3)_2]\ \}_n$ [25]

$\{[Cu_3(\mu_3\text{-}OH)(\mu\text{-}4\text{-}Ph\text{-}pz)_3(CH_3CN)(abp)_{1.5}][(\mu\text{-}4\text{-}Ph\text{-}pz)(\mu\text{-}Cl)Cu(py)(abp)_{0.5}](CF_3SO_3)_2\}_n$ [26]

$\{Cu_6(\mu_3\text{-}OH)(\mu\text{-}pz)_7(\mu\text{-}Cl)Cl_2(bpe)_2\}_n$ [27]

3D-MOFs

$\{[Cu_3(\mu_3\text{-}OH)(\mu\text{-}4\text{-}Cl\text{-}pz)_3\,(bpe)_3][CF_3SO_3]_2\}_n$ [28]

$\{[Cu_3(\mu_3\text{-}OH)(\mu\text{-}4\text{-}Cl\text{-}pz)_3(abp)_2][CF_3SO_3]_2\}_n$ [29]

$\{[Cu_3(\mu_3\text{-}OH)(\mu\text{-}4\text{-}Cl\text{-}pz)_3(abp)_{2.5}][CF_3SO_3]_2\}_n$ [30]

Chapter 1. Trinuclear copper pyrazolate complexes

1.1. Introduction

Pyrazoles (Scheme 1) have been studied for over 40 years as common ligands in coordination chemistry. Simple 1H-pyrazole (pzH) and its derivatives act as monodentate ligands, usually binding a metal in κ^1 fashion through N^2.[1] Deprotonated pyrazolate anions (pz^-) are expected to function as N, N'-bridges, acting as versatile ligands that can coordinate to metal ions in a monodentate, chelating (η^2-pz), or bridging bidentate (μ-pz) fashion. Scheme 2 summarizes the various terminal or bridging coordination modes that have been identified for pyrazolates up to now.[2] In most cases the ligand bridges between two metal ions to form dinuclear, trinuclear, tetranuclear or higher-nuclear complexes.[3, 4] Their formation occurs by self-assembly or templated synthesis of Cu centers and pyrazoles. The pyrazolate anion is an excellent ligand for the construction of cyclic trinuclear and higher nuclearity metal complexes, leading to a variety of molecular architectures.

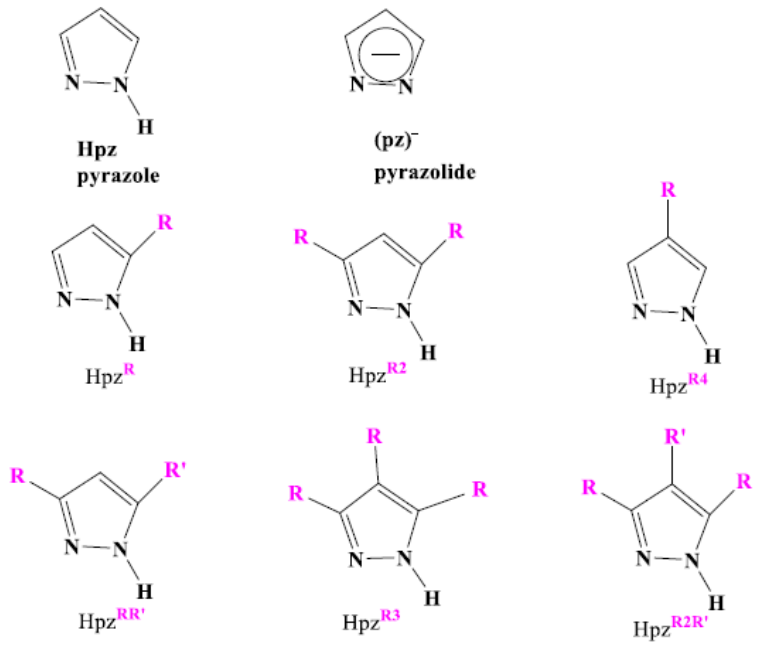

Scheme 1. Pyrazole and its C-substituted relatives. Redrawn from Halcrow et al.[2]

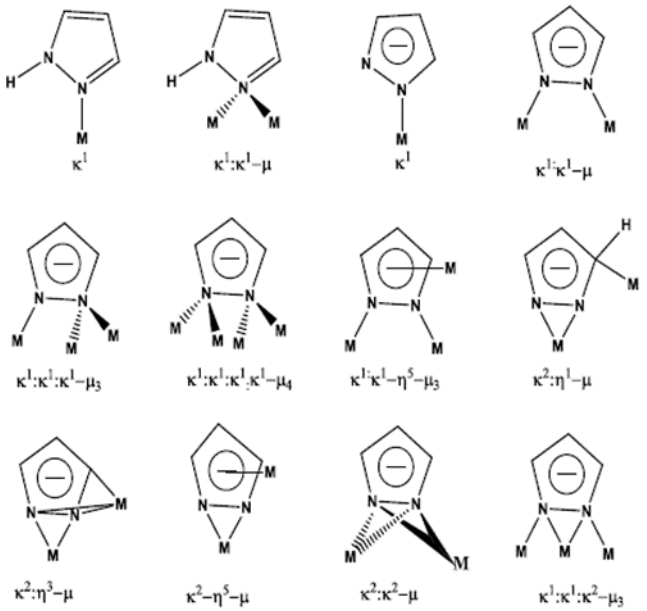

Scheme 2. Known coordination modes of Hpz and pz^-. Redrawn from Halcrow et al.[2]

In particular, copper atoms in any of its three common oxidation states, Cu(I), Cu(II) and Cu(III), can form a rich variety of coordination complexes. Cu(I) prefers ligands having soft donor atoms, such as thioethers, aromatic amines, C and P. In addition, because Cu(I) is d^{10} ion, it has a flexible coordination geometry, forming mostly 4-coordinated species adopting a tetrahedral geometry (T_d), but also 2-coordinate linear ($D_{\infty h}$) and 3-coordinate trigonal planar (D_{3h}) complex- es.[5,6] In Cu(II) complexes, the coordination number varies from four to six, including 4-coordinate square planar (D_{4h}), 5-coordinate square-pyramidal (C_{4v}), or trigonal bipyramidal (D_{3h}) and 6-coordinate octahedral (O_h) and distorted octahedral (D_{4h}, Jahn-Teller distortions of its d^9 electron configuration) geometries.[7,8]

In the past few decades, copper pyrazolate compounds have been extensively investigated as a result of their structural diversity and their potential applications in catalysis,[9] magnetism,[10] and

luminescence. The structures of the reported copper pyrazolate compounds range from di-,[11] to tri-,[12] tetra,[13] penta, hexa,[14] hepta,[14] and polynuclear,[15] and from chains, to layers,[16] and three-dimensional networks.[17] Particularly, numerous trinuclear triangular copper complexes possessing a $Cu_3(\mu_3\text{-}OH)$ core have been reported and structurally characterized.

1.1.1. Triangular copper pyrazolate complexes

Trinuclear complexes have been synthesized by reacting copper(II) salts with Hpz and water, which upon deprotonation give pz^- and OH^- anions, respectively. In some cases, the deprotonation was achieved by adding an exogenous base, such as NaOH,[18] Et_3N,[19] Bu_4NOH.[20] In recent years, Pettinari's group has developed a procedure for the synthesis of a series of trinuclear compounds based on the triangular $[Cu_3(\mu_3\text{-}OH)(\mu\text{-}pz)_3]^{2+}$ moiety with the positive charge neutralized by two carboxylates. According to Scheme 3, compounds 1a-j, having the general formula a $[Cu_3(\mu_3\text{-}OH)(\mu\text{-}pz)_3(RCOO)_2L_xL'_y]$, were obtained by reacting pyrazole (Hpz) with $Cu(RCOO)_2$ in protic solvents (H_2O, MeOH, alcohols).[21]

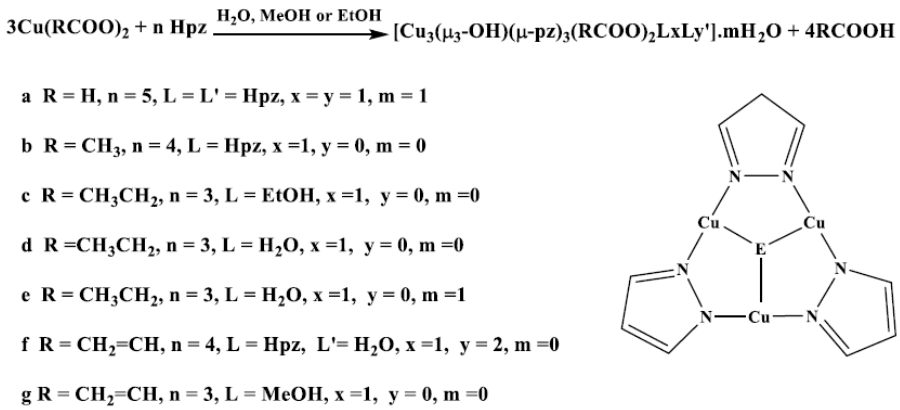

Scheme 3. Synthetic method of Cu-pyrazolate complexes. Redrawn from Di Nicola et al. [21]

The copper pyrazolate triangular complexes contain the distinguishable feature a nine-membered Cu_3N_6 metallacycle. The void at the center of the metallacycle is filled by μ_3-ligands. Although μ_3-OH^- and μ_3-O^{2-} ions are the most common central triply bridging ligands in these compounds,[10] some μ_3-Cl,[22] μ_3-Br,[22] and μ_3-MeO[23] clusters have been described as well. In all trinuclear triangular Cu^{II}-pyrazolate derivatives the oxygen is placed approximately 0.2-0.6 Å out of the plane established by the three Cu ions, while in the [$Cu_3(\mu_3$-O)] moieties the oxygen lies in that plane. Finally, there are one or two more terminal ligands X at each of the Cu(II) atoms (Scheme 4).

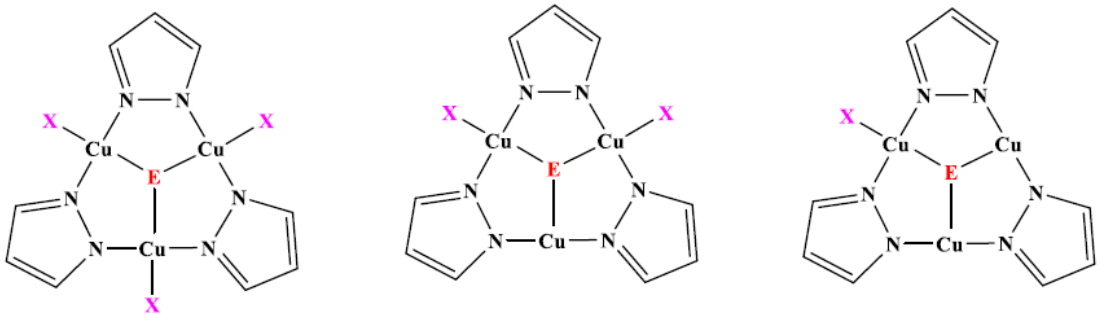

Scheme 4. Cu^{II}_3-pz triangular complex showing the supporting pzs, μ_3-bridging (E), and terminal positions (X).

1.1.2. Mixed-valent triangular copper pyrazolate complexes

1.1.2.1 Classification of mixed-valence complexes

Mixed valence compounds, containing an element present in more than one oxidation state, have been reviewed and classified earlier by Robin and Day and reviewed by Allen and Hush.[24] In mixed valence complexes, the focus of the analysis is the extent of delocalization between redox centers, which can be varied by changing the solvent or ancillary/bridging ligands. The Robin-Day classification of the degree of electronic coupling (H_{ab}) in MV compounds is as follows (Scheme 5).

In Class I compounds, the electron is localized on one center, the valences are trapped. There are distinct sites with different specific valences in the complex that do not interconvert. Class I

compounds have H_{ab} = 0, meaning that there is no electronic coupling at all between the metal centers. An IVCT band will not be observed in this case.

Class II compounds are intermediate in character. There is some localization of distinct valences, but there is a low activation energy for their interconversion. Class II compounds have moderate values of H_{ab} and exhibit intense IVCT bands with $H_{ab} \leq \lambda/2$. For example, Prussian blue, a cyanide-bridged Fe(II)-Fe(III) material of formula $Fe_4[Fe(CN)_6]_3 \cdot 14H_2O$, is one of the first recognized Robin-Day class II mixed-valence compounds.

Class III MV compounds are characterized by completely delocalized valence, so that the oxidation states of all the metal centers are averaged. One of the earliest known MV complexes to exhibit class III behavior is the Creutz-Taube ion. The oxidation states in the $[(NH_3)_5Ru(pz)Ru(NH_3)_5]^{5+}$ are best represented as +2.5 and +2.5 instead of as +2 and +3.[25, 26]

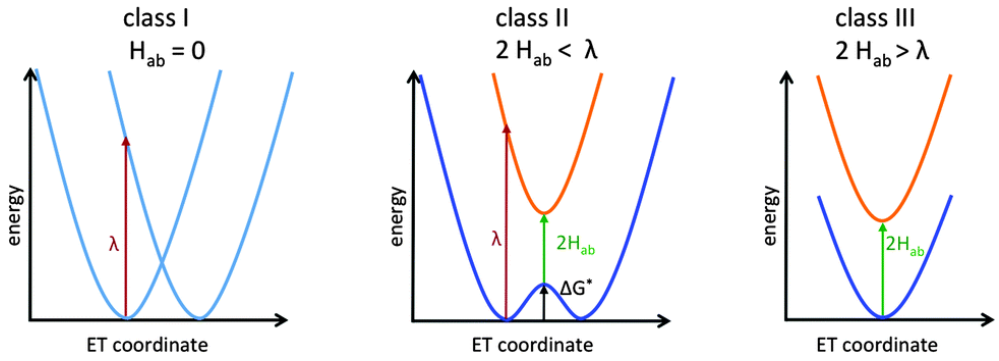

Scheme 5. Potential energy surfaces for a two-center mixed-valence system. Robin-Day classification of the degree of electronic coupling (H_{ab}) in MV compounds. (a) Class I: fully localized; (b) Class II: weakly coupled; (c) Class III: strongly coupled, fully delocalized system.

The magnitude of H_{ab} can be calculated from Equation:

$$H_{ab} = \frac{0.0206}{rab}\sqrt{\varepsilon_{max}\,\nu_{max}\Delta\nu_{1/2}}$$

Where H_{ab} is electronic coupling. ε_{max} is the molar absorptivity of the IT band at its maximum wavenumber (cm^{-1}). $\Delta\nu_{1/2}$ is the width at half height (cm^{-1}). The r_{ab} is the distance between the redox centers involved in the electron transfer.

Hush derived the following equation applicable to all classes of MV systems:

$$H_{ab} = \frac{\mu_{12}\nu_{max}}{eR} \qquad \Delta\nu_{1/2}{}^{0}/cm^{-1} = \sqrt{16RT\ln(2)\nu_{max}} \qquad \Gamma = 1 - \Delta\nu_{1/2}/\Delta\nu_{1/2}{}^{0}$$

Where μ_{12} is the transition dipole moment of the IVCT band. ν_{max} is the IVCT band maximum. $\Delta\nu_{1/2}$ is experimental bandwidth at half height. $\Delta\nu_{1/2}{}^{0}$ is theoretical bandwidth at half height.

The parameter Γ calculated by comparing the experimental and theoretical $\nu_{1/2}$ values of the IVCT band (*vide supra*) classifies a MV species as class II or II: When $0 < \Gamma < 0.5$, the MV complex is classified as a weakly coupled, Class II system, in completely delocalized Class III species, $\Gamma > 0.5$, and these species also exhibit an IVCT band. For Class I MV complexes there is no Γ parameter, because they have no IVCT band.

Table 1. Classification of Mixed-valence Compounds.

Class	Condition	
I	$H_{ab} = 0$	Localized
II	$0 < \Gamma < 0.5$	Weakly coupled
III	$\Gamma > 0.5$	Delocalized

1.1.2.2. Example of mixed-valence copper pyrazolate complex

The Raptis group has reported a mixed-valent copper pyrazolate trinuclear complex, $[Cu_3(\mu_3\text{-}O)(\mu\text{-}pz)_3(O_2CPh)_3]^{1-}$, isolated from the chemical oxidation of a $(TBA)_2[Cu^{II}{}_3(\mu_3\text{-}Cl)_2(\mu\text{-}pz)_3Cl_3]$ with AgO_2CPh, as shown in Scheme 7. Its crystal structure determination revealed a $Cu_3(\mu_3\text{-}O)$ core,

formally $Cu_2^{II}Cu^{III}$, Cu_3^{7+} species, with terminal benzoates. The most striking feature of $[Cu_3(\mu_3\text{-}O)(\mu\text{-}pz)_3(O_2CPh)_3]^{1-}$ was its nearly perfect 3-fold symmetry, which suggested a delocalized electronic distribution, consistent with DFT calculations. The Cu-N bond lengths (1.891(5) Å) were shorted than in the homovalent all-Cu(II) complex, $(PPN)_2[Cu_3(\mu_3\text{-}O)(\mu\text{-}pz)_3Cl_3]$, (1.953(3) Å), in agreement with its higher oxidation state.[27]

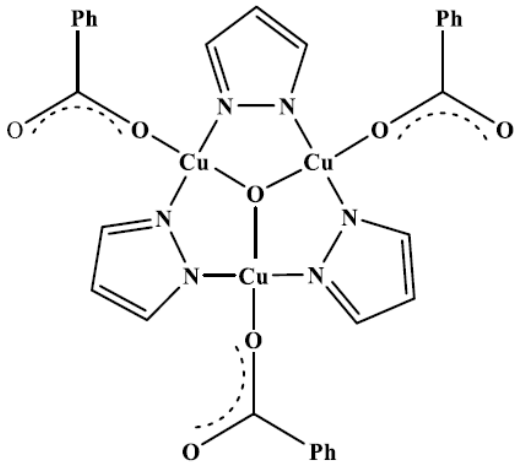

Scheme 6. Schematic representation of $[Cu_3(\mu_3\text{-}O)(\mu\text{-}pz)_3(O_2CPh)_3]^{1-}$. Redrawn from Raptis et al.[27]

1.1.3. Applications of trinuclear Copper pyrazolate complexes

The impetus for exploration of the chemistry of trinuclear Cu(II)-complexes is provided mainly by four fields. First, trinuclear copper(II) complexes are primarily studied for their relevance to enzymes, such as multicopper oxidases (e.g., laccase, ascorbate oxidase, ceruloplasmin), oxygenases (e.g., tyrosinase, particulate methane monooxygenase, ammoniamonooxygenase) and reductases (e.g., nitrite reductase, nitrous oxide reductase).[28, 29] Trinuclear Cu(II) complexes have been of particular significance for their simulation of the bioactive sites of a number of multicopper blue oxidases.

Second, it is interesting to note that Cu(II) ions and N1, N2-bridging ligands (pyrazole and its derivatives) tend to form a trinuclear triangular Cu(II) cluster with coordinatively-unsaturated metal sites, which exhibit interesting magnetic properties.[30] Triangular Cu(II)-complexes are important models for the study of magnetic exchange-coupling and spin frustration.[31, 32] The Raptis group has previously shown that pH-dependent exchange of μ_3-E [E= O, OH, Cl, Br] ligands on a trinuclear copper pyrazolato framework is accompanied by an orderly transition from strong to weak antiferromagnetic coupling and finally to ferromagnetic exchange among the three Cu centers.[18, 33] Ferromagnetically coupled Cu_3-complexes are especially important as they are closely related to the also ferromagnetically coupled active centers of particulate methane monooxygenase.[34]

Third, some trinuclear Cu(II) triethanolamine derivatives (Scheme 7) are highly active and selective catalysts, or catalyst precursors for the peroxidation of cyclohexane, to cyclohexanol and cyclohexanone mixture by hydrogen peroxide (H_2O_2) in acidic medium at room temperature and atmospheric pressure.[13]

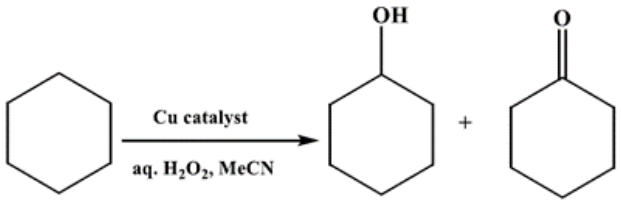

Scheme 7. Copper complexes act as catalyst for oxidation of cyclohexane to a cyclohexanol and cyclohexane mixture. Redrawn from Kirillov et al.[13]

Fourth, these trinuclear copper pyrazolate clusters further self-assemble through carboxylate bridges, often supported by H-bonds, to form hexanuclear systems, 1-, 2- and 3D CPs, showing interesting molecular and supramolecular features in most cases.[35–37] The trinuclear $[Cu_3(\mu_3\text{-}OH)(\mu\text{-}pz)_3]^{2+}$ cluster is quite stable, and can be employed as secondary building block to generate coordination frameworks. These trinuclear $[Cu_3(\mu_3\text{-}OH)(\mu\text{-}pz)_3]^{2+}$ can be connected with rigid

nitrogen ligands (4'4-bipyridine), or flexibible succinate (Suc) dianions, to form CPs under various reaction conditions (solvent, pressure, temperature) and reagents ratios.[17,21]

1.2. Background of Trinuclear Copper pyrazolate complexes

Several triangular Cu_3- pyrazolates with the general formula $[Cu_3(\mu_3\text{-}E)(\mu\text{-}4\text{-}R\text{-}pz)_3X_3]^{n-}$,[18, 22, 27, 35–38] where E = O, OH, OMe, OEt, $(Cl)_2$ and $(Br)_2$; X = Br, Cl, py, SCN, MeCOO; NCO, NO_3; R = H, Cl, Br, I, NO_2, Me, CHO, COOEt, Ph; n = 1, 2 (Scheme 8), have been synthesized and characterized in our group. Our laboratory has worked on the systematic structural and accompanying magnetic and electrochemical manipulation of these triangular copper pyrazolate complexes.

The copper pyrazolate complexes with $Cu_3(\mu_3\text{-}O)$-core are redox active and capable of cycling between a homovalent Cu^{II}_3- state and a mixed-valent $Cu^{II}_2Cu^{III}$- state during an one electron redox process. Studying the electrochemical behavior of $Cu_3(\mu_3\text{-}O)$-containing complexes has been a primary focus in our laboratory. One-electron oxidation of Cu_3-pyrazolates by either $(NH_4)_2Ce(NO_3)_6$ (CAN), $(PhCOO)_2$ or H_2O_2 leads to a mixed-valence species, formally $Cu^{II}_2Cu^{III}$, as shown in Scheme 9. The Raptis group has reported the one-electron chemical oxidation of $[Cu_3(\mu_3\text{-}O(\mu\text{-}pz)_3(O_2CPh)_3]$.[27]

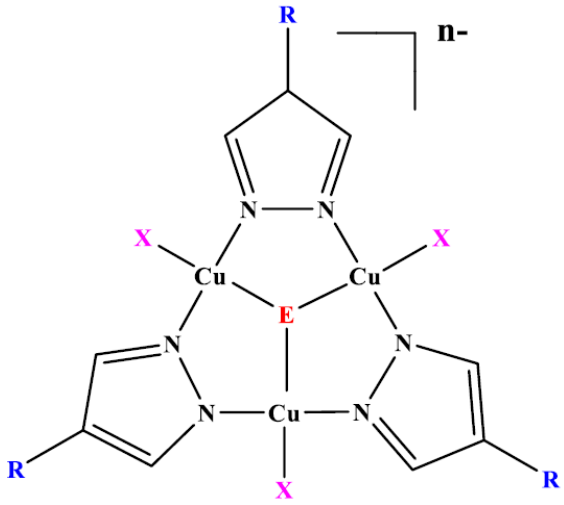

Scheme 8. Formula of $[Cu_3(\mu_3\text{-}E)(\mu\text{-}4\text{-}R\text{-}pz)_3X_3]^{n-}$.

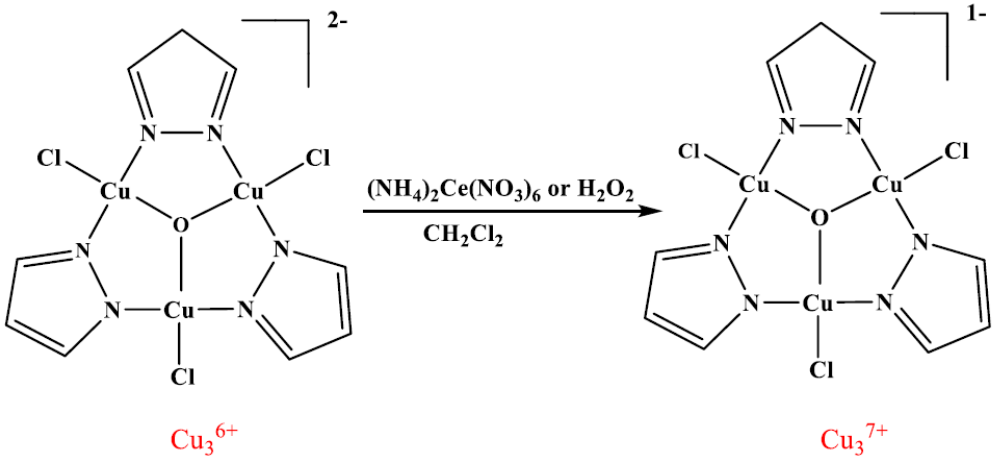

Scheme 9. Chemical oxidation of Cu(II)-pyrazolate complex.

1.3. Hypothesis

Our present work builds on two hypotheses: (i) At constant temperature and pressure, the sorption of MOFs can be changed by varying the redox states: because of the different charge on the metal, the sorbent and sorbate interaction will be different. We postulate that the gas adsorption capacity will change with changing oxidation states. The hypothetical example of Figure 1 shows the

difference between the sorption isotherms for a MOF in its two oxidation states (MOF_{Red} and MOF_{Ox} are reduced and oxidized forms of the given MOF, respectively). The vertical distance between the two curves, Δ%, shows the amount of substance that can be adsorbed and released at constant temperature and pressure. (ii) Similarly, the gas sorption capacity and/or selectivity will be modified by a photochemically- induced structural reorganization of the MOF.

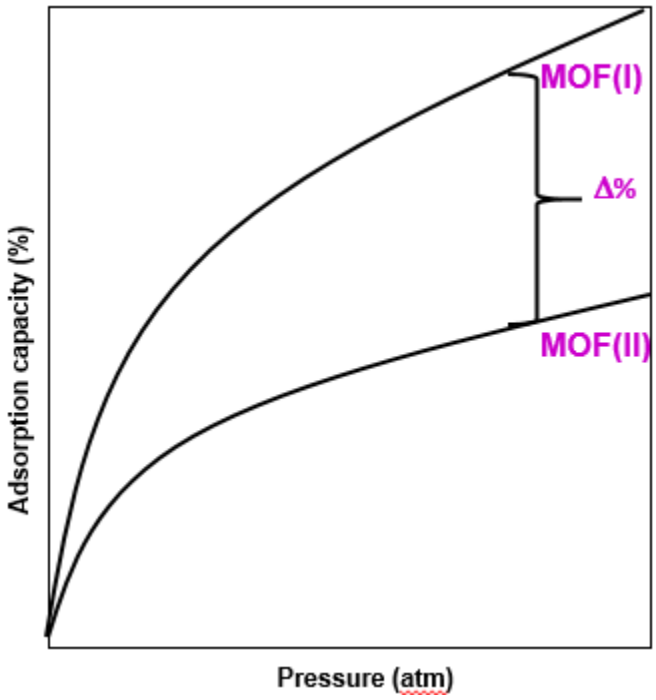

Figure 1. Hypothetical gas sorption isotherms for the reduced and oxidized forms of a redox or photo-active MOF.

To construct and study the photo- or redox-active MOFs Containing on Cu_3-pyrazolato SBU, it is necessary to first study the structural and electronic properties of isolated SBUs. On that front, an objective of this dissertation is to synthesize and characterize new triangular copper pyrazolate complexes with suitable ligands in μ_3- and terminal positions and study their chemical and/or electrochemical properties to find out if it is possible to (i) oxidize to the mixed-valent, formally $[Cu^{III}Cu^{II}_2]$ state and (ii) connect the units with photoactive linkers. The second objective is to

employ these trinuclear units as SBUs to build stable coordination polymers and analyze their potential applications. In our laboratory, one dimensional (1D) chains, two dimensional (2D)-sheets, and three dimensional (3D)-MOFs containing $[Cu_3(\mu_3\text{-}OH)(\mu\text{-}pz)_3]^{2+}$ SBUs have been prepared by controlling the stoichiometry and by replacing terminal monodentate ligands (py), with bridging bidentate 4,4-bipy.[42] We have previously shown that the porous-MOF materials with $\{[Cu_3(\mu_3\text{-}OH)(\mu\text{-}4\text{-}R\text{-}pz)_3]^{2+}\}_n$ SBUs where R = H, Cl, or CHO have interpenetrated-lattice structures and are capable of adsorbing CO_2 selectively.[43] The main project of this dissertation is the synthesis and modification of photo-/ redox-active metal-organic-frameworks (MOFs) based on Cu_3-pyrazolate SBUs and study their gas adsorption properties. (i) For photo-active MOFs, abp and bpe were used as photo-active linkers and photoswitchable tailor-made spacers. Photochemical modification of MOFs will change their pore size and shape, allowing the tuning of their gas adsorption properties. (ii) The Cu-pyrazolato SBUs with $[Cu_3(\mu_3\text{-}O)]^-$ unit will be used to prepare redox-active MOFs. Redox modification of a MOF will result in modulation of its affinity for sorbate molecules and change its overall sorption capacity.

1.4. Experimental Section

1.4.1. Materials and methods

4-chloropyrazole (4-Cl-pzH),[44] 4-Phenyl-pyrazole (4-Ph-pzH),[45] $[PPN]_2[Cu_3(\mu_3\text{-}Cl)_2(\mu\text{-}pz)_3Cl_3]$[18] and $[PPN]_2[Cu_3(\mu_3\text{-}O)(\mu\text{-}pz)_3Cl_3]$[18] were synthesized according to the literature procedures. All other reagents were commercially available and used without further purification. Solvents were purified using standard techniques.[46]

Elemental analysis. Elemental analyses (C, H, N) were performed at Galbraith Laboratories, Inc., Knoxville, Tennessee.

Infrared Spectroscopy (IR). The IR spectra from 4000-500 cm^{-1} were recorded on a Spectrum One Perkin-Elmer FT-IR SPECTROPHOTOMETER with ATR mode.

Ultraviolet-Visible spectroscopy (UV-Vis). The UV-Vis Spectral data were recorded on a Varian Cary 500 scan instrument equipped with a deuterium background correction lamp.

Electrochemistry. Electrochemical measurements were performed in 0.1 M $TBAPF_6/CH_2Cl_2$ at ambient temperature under an Ar atmosphere, using a three-electrode set up (glassy carbon working, Pt-wire auxiliary and $Ag/AgNO_3$ reference electrodes) with a BAS Epsilon-EC electrochemical analyzer. A platinum electrode was used as a working electrode, a platinum-wire was used as the counter electrode, and an Ag/Ag^+ (0.01 M $AgNO_3$ in acetonitrile) electrode was used as the reference electrode. The CV curves were calibrated using the ferricenium/ferrocene (Fc^+/Fc) redox couple, accomplished by adding ferrocene to the solution as an internal standard after recording voltammogram of the analyte.

Single-Crystal X-ray Diffraction. Single crystals X-ray diffraction data were measured on a Bruker D8 QUEST CMOS system equipped with a TRIUMPH curved-crystal monochromator and a Mo Kα fine-focus tube or a Bruker APEX II area detector with graphite monochromated Mo Kα radiation (λ = 0.71073 Å) at ambient or low temperature. Frames were integrated with the Bruker SAINT software package using a narrow-frame algorithm. Absorption effects were corrected using the multi-scan method (SADABS). Structures were solved by intrinsic or direct methods with ShelXT and refined with ShelXL using full-matrix least-squares minimization Using Olex2. All non-hydrogen atoms were refined anisotropically. Hydrogen atoms positions were calculated using the riding model. All the hydrogen atoms were fixed by HFIX and placed in ideal positions. The potential solvent accessible area or void space was calculated using the PlATON.[47]

Thermogravimetric Analysis (TGA). The TGA analyses were performed using a TA-Q500 microbalance with helium (high purity, Praxair) as a carrier gas. The samples (~10 mg) were loaded onto a platinum holder, placed inside the TGA unit chamber and heated from 25 to 800 at 5 K per minute under a constant helium flow rate of 60 mL min^{-1}. The carrier gas was treated with zeolite presorbers to remove any traces of water and impurities prior to entering the TGA chamber.

X-ray powder diffraction (XRD). The patterns of the as-synthesized, activated, and post-CO_2-adsorption samples were obtained using a Rigaku ULTIMA III X-ray diffraction unit. The diffractometer is equipped with cross beam optics and a Cu-K_α target operating at 40 kV and 44 mA.

1.4.2. Synthesis of trinuclear Cu(II)-pz complexes with new ligands in the capping (μ_3) and terminal positions

1.4.2.1. Synthesis of (PPN)($C_5H_{10}NH_2$)[Cu_3(μ_3-OH) (μ-Cl)(μ-4-Ph-Pz)$_3Cl_3$] [1]

The 1,2-Di(4-pyridyl)ethylene (bpe) (0.02 mmol, 3.8 mg) in 5 mL of CH_2Cl_2 was placed in the test tube. A 4 mL 1:1 mixture of CH_2Cl_2:MeOH was layered over the CH_2Cl_2 layer, $CuCl_2 \cdot 2H_2O$ (0.06 mmol, 10.2 mg), 4-Ph-pzH (0.06 mmol, 8.7 mg), piperidine (0.08 mmol, 8 µL), PPNCl (0.04 mmol, 22.9 mg) were stirred in 5 mL CH_2Cl_2 for 2 h, the filtrate (green solution) was layered on the top. Well-shaped green crystals appeared gradually on the walls of the tube in two weeks. Yield, 51%. Anal. calcd/found for $C_{68}H_{64}Cl_4Cu_3N_8OP_2$: C, 58.32 /58.50; H, 4.61/4.58; N, 8.01/8.03.

1.4.2.2. Synthesis of (PPN)[$Cu_3(\mu_3\text{-}OH)\ (\mu\text{-}4\text{-}Ph\text{-}pz)_3Cl_3]\cdot CH_2Cl_2$ [2]

A mixture of $CuCl_2\cdot 2H_2O$ (0.12 mmol, 20.5 mg), 4-Ph-pzH (0.12 mmol, 17.3 mg), NaOH (0.16 mmol, 6.4 mg), PPNCl (0.02 mmol, 11.8 mg) was stirred in CH_2Cl_2 (15 mL) for 24 h. Diffusion of diethyl ether into green solution afforded well-shaped green crystals after filtration. Yield, 72%. Anal. calcd/found for $C_{128}H_{108}Cl_{10}Cu_6N_{14}O_2P_4$: C, 56.39/56.34; H, 4.00/3.99; N, 7.19/7.21.

Method B: (PPN)[$Cu_3(\mu_3\text{-}OH)\ (\mu\text{-}4\text{-}Ph\text{-}pz)_3Cl_3]\cdot THF$

A mixture of $CuCl_2\cdot 2H_2O$ (0.5 mmol, 85.2 mg), 4-Ph-pzH (0.5 mmol, 72.1 mg), Et_3N (1 mmol, 139 µL) and PPNCl (0.34 mmol, 195.3 mg) was stirred in 10 mL THF for 12 h at ambient temperature. Treatment of the green filtrate with Et_2O crushes out the complex. Recrystallization from THF/hexane affords crystals suitable for X-ray diffraction. Yield: 80%.

1.4.2.3. Synthesis of (PPN)[$Cu_3(\mu_3\text{-}OH)(\mu\text{-}4\text{-}Ph\text{-}pz)_3Cl_3]\cdot CH_3CN$ [3]

A similar procedure to synthesize compound **[2]**, using $CuCl_2\cdot 2H_2O$ (0.3 mmol, 51.1 mg), 4-Ph-pzH (0.3 mmol, 43.3 mg), NaOH (0.6 mmol, 24 mg) and PPNCl (0.2 mmol, 114.8 mg) in CH_3CN instead of CH_2Cl_2. Well shaped green-plate crystals suitable for X-ray diffraction were obtained by slow evaporation. Yield, 62%. Anal. calcd/found for $C_{65}H_{55}Cl_3Cu_3N_8OP_2$: C, 59.14/58.85; H, 4.20/4.33; N, 8.49/8.11.

1.4.2.4. Synthesis of (PPN)[$Cu_3(\mu_3\text{-}OH)(\mu\text{-}pz)_3(\mu_{1,1}\text{-}N_3)_2(N_3)$] [4]

Method A:

A solution of NaN_3 (0.38 mmol, 24.42 mg) in 5 mL of MeOH was added dropwise to a solution of $[PPN]_2[Cu_3(\mu_3\text{-}O)(\mu\text{-}pz)_3Cl_3]$ (0.06 mmol, 100 mg) dissolved in 10 mL MeOH, the mixture was stirred overnight at ambient temperature. Upon slow evaporation of filtrate at room temperature for

one week, well-shaped crystals suitable for X-ray diffraction were obtained. The crystals were isolated, washed three times with MeOH ether and dried in the vacuum. The yield was 40%. Anal. calcd/found for $C_{45}H_{41}Cu_3N_{16}OP_2$: C, 50.41/50.01; H, 3.76/3.62; N, 20.91/20.48. UV-vis (CH_2Cl_2, cm^{-1}): 24965, 36499, 37367, 38276.

Method B:

To a 4 mL of CH_2Cl_2 solution of $[PPN]_2[Cu_3(\mu_3\text{-}Cl)_2(\mu\text{-}pz)_3Cl_3]$ (0.06 mmol, 100 mg) was added a solution of NaN_3 (0.51 mmol, 33.1 mg) in 0.5 mL H_2O and 2 mL MeOH. The reaction mixture was stirred for 2 h at ambient temperature. After filtration, single crystals were formed by initially layering the filtrate with hexanes followed by slow evaporation at the ambient temperature; Yield, 62%.

1.4.2.5. Synthesis of $[Cu_3(\mu_3\text{-}OMe)(\mu\text{-}Cl)(\mu\text{-}Pz)_3(py)_2]Cl$ [5]

Method A:

A solution of $[PPN]_2[Cu_3(\mu_3\text{-}Cl)_2(\mu\text{-}pz)_3Cl_3]$ (0.03 mmol, 50 mg) in 5 mL CH_2Cl_2 was placed in the test tube, a 4 mL 1:1 mixture of CH_2Cl_2: MeOH was layered over the CH_2Cl_2 layer, and a third layer of pyridine (0.16 mmol, 13 µL) and thiophenol (0.15 mmol, 16 µL) in 5 ml MeOH was layered on top. Well-shaped purple-polygonal crystals suitable for X-ray diffraction were grown after slow evaporation. Yield: 53%. Anal. Calcd/Found for $C_{20}H_{22}Cl_2Cu_3N_8O$: C, 36.84/36.23; H, 3.4/3.42; N, 17.18/17.27.

Method B:

To the methanolic solution (4 mL) of pyridine (0.16 mmol, 13 µL) was added a CH_2Cl_2 (4 mL) solution of $[PPN]_2[Cu_3(\mu_3\text{-}Cl)_2(\mu\text{-}pz)_3Cl_3]$ (0.03 mmol, 50 mg) with stirring. The mixture was stirred for 24 h at ambient temperature. After keeping the solution in the air for a few days, suitable

for X-ray crystal structural determination were formed on slow evaporation of the solvent. The crystals were isolated, washed three time with MeOH, Et_2O and dried in air. Yield: 70%.

1.4.2.6. Synthesis of $[Cu_3(\mu_3\text{-}OH)(\mu\text{-}Cl)(\mu\text{-}pz)_3(py)_2Cl](py)$ [6]

Compound **[6]** was prepared by the same procedure as described for complex **[5]** by replacing CH_2Cl_2 with CH_3CN and changing the molar ratio to 1:25, instead of 1:5. Upon slow evaporation of the filtrate at room temperature over two weeks, dark blue-polygonal crystals suitable for X-ray diffraction were obtained; Yield: 48%. Anal. Calc/Found for $C_{24}H_{25}Cl_2Cu_3N_9O$: C, 39.22/38.84; H, 3.7/3.44; N, 17.15/17.04. UV-vis (CH_2Cl_2, cm^{-1}): 16583, 28695.

1.4.2.7. $[Cu_3(\mu_3\text{-}OH)(\mu\text{-}4\text{-}Cl\text{-}pz)_3(py)_3(ClO_4)_2](CH_2Cl_2)[(CH_3)_2CO)]$ [7]

$Cu(ClO_4)_2.6H_2O$ (0.1 mmol,37.1 mg), 4-Cl-pzH (0.1mmol, 10.3 mg), NaOH (0.17 mmol, 6.7 mg) were added in 6 ml CH_2Cl_2 and 4ml acetone under stirring for 24h at ambient temperature, the grey solid was filtered out under pressure. Suitable crystals for X-ray diffraction was grown from the slow evaporation for 4 days. Yield: 40%.

1.4.2.8. Synthesis of $(PPN)_2[Cu_3(\mu_3\text{-}O)(\mu\text{-}pz)_3(\eta^1\text{-}NO_2)_2(\eta^2\text{-}NO_2)]$ [8], $(PPN)_3[Cu_3(\mu_3\text{-}OH)(\mu\text{-}pz)_3(\eta^1\text{-}NO_2)_3](OH)(NO_3)$ [9] and $(PPN)_2[Cu_3(\mu_3\text{-}O)(\mu\text{-}pz)_3(\eta^1\text{-}NO_2)_2Cl]$ [10]

To a 4 mL CH_2Cl_2 solution of $[PPN]_2[Cu_3(\mu_3\text{-}Cl)_2(\mu\text{-}pz)_3Cl_3]$ (0.06 mmol, 100 mg) was added a solution of $NaNO_2$ (0.29 mmol, 20.3 mg) in 0.5 mL H_2O and 2 mL MeOH. The reaction mixture was stirred for 24 h at ambient temperature. After filtration and treatment of the filtrate with 10 mL Et_2O, purple crystals of $[PPN]_2[Cu_3(\mu_3\text{-}O)(\mu\text{-}pz)_3(\eta^1\text{-}NO_2)_2(\eta^2\text{-}NO_2)]$ [**8**] were formed by slow evaporation at ambient temperature. Yield, 62%. Anal. Calcd/Foud for $C_{81}H_{69}N_{11}Cu_3O_7P_4$ (%): C,

59.44/59.77; H, 4.28/4.23; N, 9.49/9.41. Infrared (cm^{-1}): 1439m, 1377m, $\nu_{as}(NO_2)$; 1259s, $\nu_s(NO_2)$; 1114s, 1051m, 997w, 872w, $\delta(NO_2)$; 722s, 628s. After removing the purple crystals, the blue crystals of $(PPN)_3[Cu_3(\mu_3\text{-}OH)(\mu\text{-}pz)_3(\eta^1\text{-}NO_2)_3](OH)(NO_3)$ **[9]** were obtained from the light green mixture solution a week later. The crystals were filtered off and dried under vacuum. The yield was approximately 10%. IR (cm^{-1}): 1436m, 1349m, 1266w, 1114s, 996m, 1054m, 689s, 721s.

1.4.2.9. Synthesis of $[PPN][Cu_3(\mu_3\text{-}OH)(\mu\text{-}4\text{-}Ph\text{-}pz)_3(\eta^1\text{-}NO_2)_3](CH_2Cl_2)_{0.5}$ [11]

Compound **[11]** was synthesized following the same procedure as that of Compound [**8**] using $(PPN)[Cu_3(\mu_3\text{-}OH)(\mu\text{-}4\text{-}Ph\text{-}pz)_3Cl_3]\cdot CH_2Cl_2$ instead of $[PPN]_2[Cu_3(\mu_3\text{-}Cl)_2(\mu\text{-}pz)_3Cl_3]$. After filtration and treatment of the filtrate with 4 mL hexane instead of Et_2O. Well-shaped crystals suitable for X-ray diffraction were obtained three days later. The yield was 80%. Anal. Calcd/found for $C_{127}H_{107}Cl_2Cu_6N_{20}O_{13}P_4$: C, 56.31/56.06; H, 3.95/4.02; N, 10.35/10.19.

1.4.2.10. Synthesis of $(PPN)_3[Cu_3(\mu_3\text{-}O)(\mu\text{-}4\text{-}Me\text{-}pz)_3(\eta^1\text{-}NO_2)_3](NO_3)$ [12]

Compound **[12]** was prepared by following the same procedure described for **[8]** by using $(PPN)_3[Cu_3(\mu_3\text{-}O)(\mu\text{-}4\text{-}Me\text{-}pz)_3Cl_3]Cl$ and $NaNO_2$. UV-vis (CH_2Cl_2, cm^{-1}): 28584, 36416, 37340, 38273.

1.4.2.11. Synthesis of $(PPN)_3[Cu_3(\mu_3\text{-}O)(4\text{-}Cl\text{-}pz)_3(\eta^1\text{-}NO_2)_3](NO_3)$ [13]

Compound **[13]** was synthesized by following the same procedure described for **[8]** by using $[(PPN)_3[Cu_3(\mu_3\text{-}O)(4\text{-}Cl\text{-}pz)_3Cl_3]Cl$ instead of $[PPN]_2[Cu_3(\mu_3\text{-}Cl)_2(\mu\text{-}pz)_3Cl_3]$. The yield was 70%. Anal. Calcd/ found for $C_{119}H_{96}Cl_3Cu_3N_{13}O_{11}P_6$: C, 59.99/58.85; H, 4.22/4.27; N, 7.78/7.66.

1.4.2.12. Synthesis of (PPN)[$Cu_3(\mu_3\text{-}O)(\mu\text{-}pz)_3(N_3)_2(\eta^2\text{-}NO_2)$] [14]

A solution obtained by mixing a MeOH solution (10 mL) of NaN_3 (0.31 mmol, 20.3 mg) and aqueous solution of $NaNO_2$ (0.28 mmol, 19.1 mg) was added under stirring to a green solution containing $[PPN]_2[Cu_3(\mu_3\text{-}Cl)_2(\mu\text{-}pz)_3Cl_3]$ (0.06 mmol, 100 mg) in 10 mL CH_2Cl_2. Color change was observed and stirring was continued for 24 h. The blue-green solution obtained was allowed to evaporate in the air yielding well-formed brown crystals, which were washed with Et_2O and dried under vacuum. Yield, 30%.

1.5. Results and discussion

1.5.1. Crystal structure description of (PPN)($C_5H_{10}NH_2$)[$Cu_3(\mu_3\text{-}OH)(\mu\text{-}Cl)(\mu\text{-}4\text{-}Ph\text{-}pz)_3Cl_3$)] [1]

Compound **[1]** consists of a nine-membered $[Cu\text{-}N\text{-}N]_3$ metallacycle where the Cu-atoms are held together by pyrazolate bridges as shown in Figure 2. A pyramidal $Cu_3(\mu_3\text{-}OH)$ moiety, with Cu-O bond lengths ranging from 1.988(1) Å to 2.044(1) Å, forms the core of complex. The Cu-O bond distances and the distance of μ_3-O from the best-fit plane of the three copper ions (ca. 0.632(5) Å) are in the range normally found for these kinds of compounds.[36,37,48,49] The three Cu-O-Cu angles are between 105.1(2)º-114.7(2)º, and the Cu···Cu intramolecular distances are within 3.231(2) - 3.381(2) Å. The μ-Cl is on the opposite side of the μ_3-OH group completing the square-pyramid coordination of two Cu atoms. The third Cu atom has distorted square-planar coordination. The Cu-(μ-Cl) distances are quite long, 2.787(2) Å and 2.795(2) Å. Another feature of this structure is the edge-to-face C-H… π interactions between the μ_3-O and the benzene ring of adjacent trimer with a distance of 3.23 Å (Figure 3).

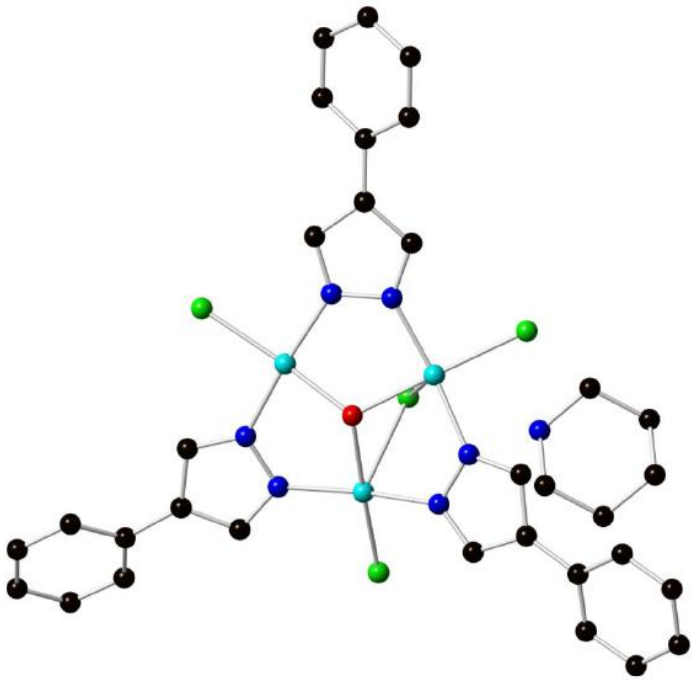

Figure 2. Molecular structure of [**1**], PPN and H are omitted for clarity.

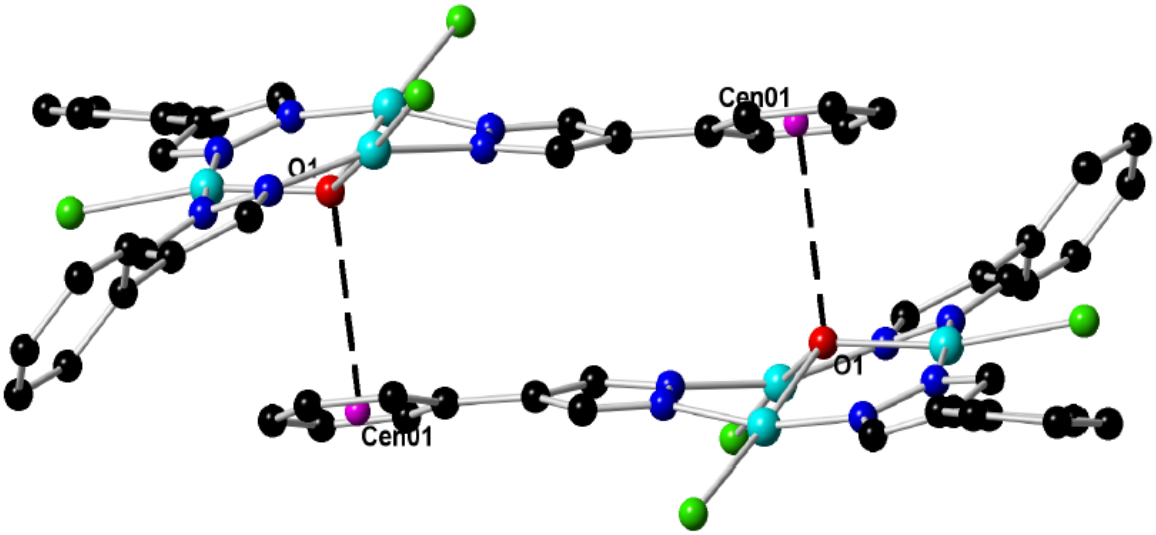

Figure 3. Edge to face π-π stacking of [**1**]. Color code: black, C; blue, N; red, O; green, Cl; cyan, Cu; purple, phenyl ring centroid.

1.5.2. Crystal structure description of (PPN)[$Cu_3(\mu_3\text{-}OH)$ (μ-4-Ph-pz)$_3Cl_3$](CH_2Cl_2)[2]

Complex **[2]** crystallizes in the monoclinic *P2₁/n* space group with the whole molecule and one CH_2Cl_2 interstitial solvent molecule in the asymmetric unit. The trinuclear complex contains a μ_3-OH group unsymmetrically bridging three copper atoms. The Cu-O bond length range from 1.949 (1) to 2.053(1) Å, Cu···Cu intramoleccular distances are within the 3.300(4)- 3.430(4) Å. The O atom is 0.152(4) Å above the the $[Cu(pz)]_3$ plane. while the three terminal chloride ligands are on the opposite side of their trans-μ_3-OH, as shown in the Figure 4. Two [$Cu_3(\mu_3\text{-}OH)$(μ-4-Ph-pz)$_3Cl_2$] units are linked via double μ-Cl bridges forming a {Cu_6} dimer-of-trimers (Figure 5). The Cu-μ-Cl bond distances are unsymmetrical, with shorter equatorial and longer axial Cu-Cl bonds ranging from 2.261(1) Å to 2.959(3) Å.

1.5.3. Crystal structure description of (PPN)[$Cu_3(\mu_3\text{-}OH)$(μ-4-Ph-pz)$_3Cl_3$]·CH_3CN [3]

Green blocks of **[3]** crystallize from the slow evaporation of CH_3CN, packing in the triclinic $P\bar{1}$ space group. In each trinuclear triangular {$Cu_3(\mu_3\text{-}OH)$(μ-4-Ph-pz)$_3Cl_3$} unit (Figure 6), the distance of capping μ_3-O_1 from the plane defined by the Cu_3 system [0.565(0) Å] as well as the Cu-O1 distances [Cu1-O1 2.029(2) Å, Cu2-O1 1.995(2) Å, Cu3-O1 2.017(2) Å] fall in the range normally found for analogous compound.[36-39] The Cu-(μ-Cl) distances range between 2.309-2.876 Å. The structure of **[3]** consists of a polymeric, one-dimensional (1D) infinite neutral chains, {(PPN)[$Cu_3(\mu_3\text{-}OH)$(μ-4-Ph-pz)$_3Cl_3$]·CH_3CN}$_n$, parallel to the crystallograp- hic *b*-axis, wherein two bridging chlorine atoms link the adjacent {$Cu_3(\mu_3\text{-}OH)$(μ-4-Ph-pz)$_3Cl$} units (Figure 7).

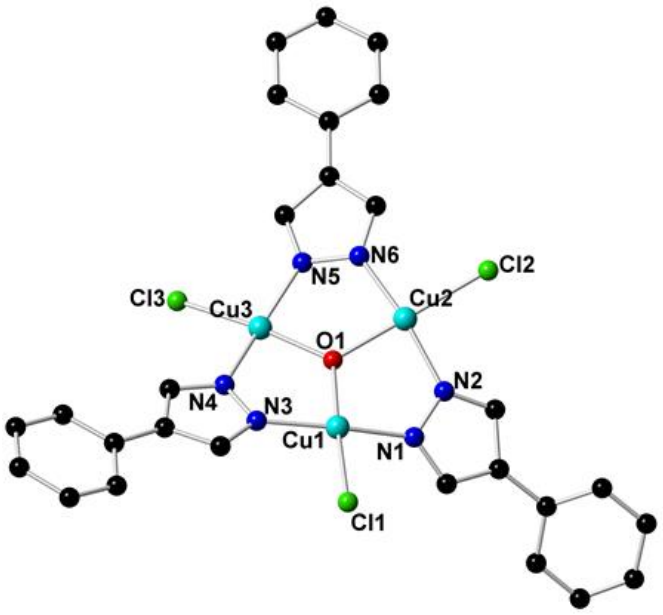

Figure 4. Crystal structure of compounds **[2]**, PPN counterion and interstitial CH_2Cl_2 are not shown for clarity.

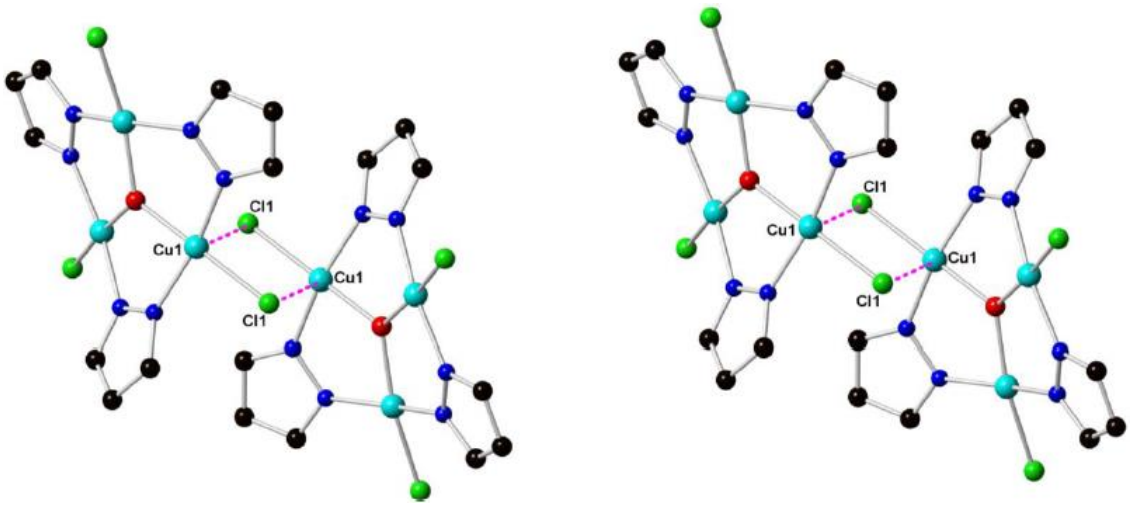

Figure 5. Packing diagram of compound **[2]**, perspective view showing the association of the two triangular units by a μ-Cl. Phenyl substitution on pyrazole rings and hydrogen atoms are omitted for clarity.

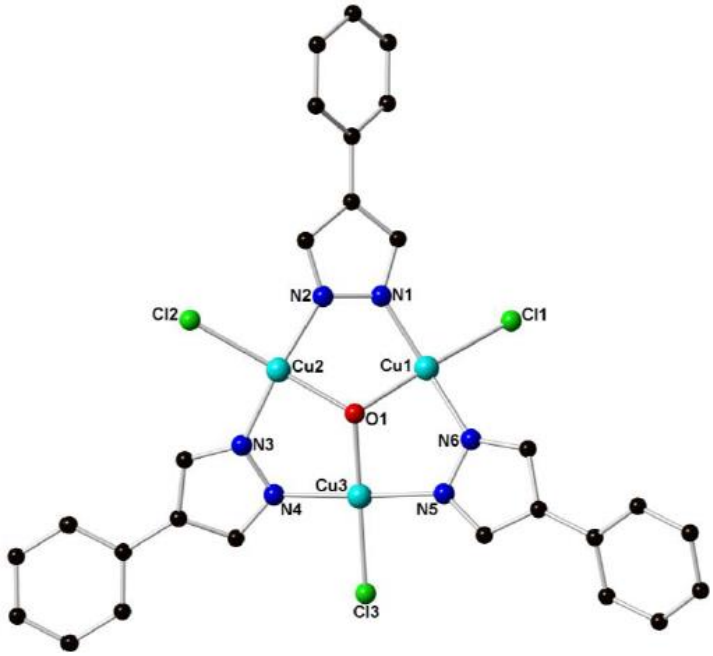

Figure 6. Crystal structure of compound **[3]**, PPN counterion and interstitial CH_3CN are not shown for clarity.

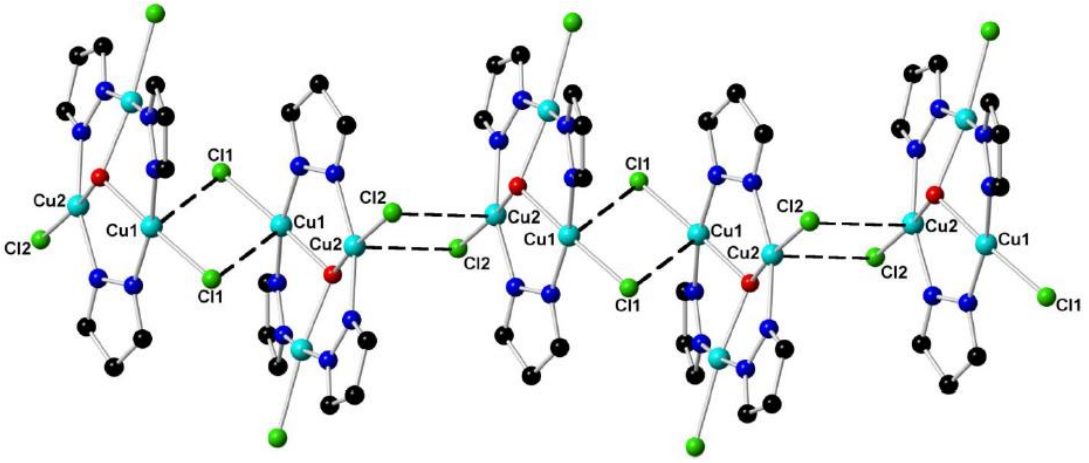

Figure 7. A review of one-dimensional polymeric chain of the unit in the compound **[3]**. Phenyl substitution on pyrazole rings, hydrogens and PPN are omitted for clarity.

Table 2. Selected bond lengths (Å) and angles (º) for compounds **[1]**, **[2]** and **[3]**.

	[1]	**[2]**	**[3]**
$Cu_3(\mu_3\text{-}O(H))$	1.988(1)-2.044(1)	1.949 (1)-2.053(1)	1.995(2)- 2.029(2)
Cu…Cu	3.231(2) -3.381(2)	3.268(1)-3.451(1)	3.256(8)-3.433(8)
Cu-N	1.940(4)-1.948(4)	1.926(7)-1.949(6)	1.919(3)-1.946(3)
Cu-Cl	2.244(2)-2.266(1)	2.229(3)-2.284(3)	2.271 (10)-2.325(9)
Cu-O-Cu	105.1(1)-114.7(1)	111.1(3)-120.2(3)	107.16(1)-117.67(1)

1.5.4. Crystal structure description of (PPN)[$Cu_3(\mu_3\text{-}OH)(\mu\text{-}pz)_3(\mu_{1,1}\text{-}N_3)_2(N_3)$] [4]

The azide anion, N_3^-, is a commonly employed pseudohalide bridging ligand for the design of coordination polymers with tunable physical and magnetic properties. Its most common coordination modes being μ-1,1 (end-on, EO) and μ-1,3 (end-to-end, EE). Orbital complementarity predict that the μ-1,3 coordination mode of azide should lead to antiferromagnetic (AF) coupling, whereas the μ-1,1 coordination mode to ferromagnetic coupling. The magnitude of magnetic coupling also depends on the detailed coordination geometries, such as the M-N_{azide}-M angles and the dihedral angle between the mean planes M–N–N–N and N–N–N–M'.

Although many different bridging groups and transition metal ions have been employed for the construction of such species, the Cu(II)-azide system is one of the most popular. A variety of copper-azide complexes with discrete or one-, two-, and three-dimensional polymeric structures have been reported, in which the azide ligand adopts various bridging modes (Scheme 10). The diversity in the structure of the Cu(II) system is a result of its flexibility in coordination numbers (ranging from 4 to 6) and geometry, along with its interesting magnetic properties.[47, 48] It is well-established that symmetric μ-1,3 Cu(II) azide bridges are strongly antiferromagnetic, whereas Cu(II)

complexes with double symmetric μ-1,1 azide bridges are strongly ferromagnetic, provided that the Cu-N_{azide}-Cu angle is smaller than 108.[52] Usually asymmetric μ-1,3 azide bridges lead to weak antiferromagnetic coupling.[53]

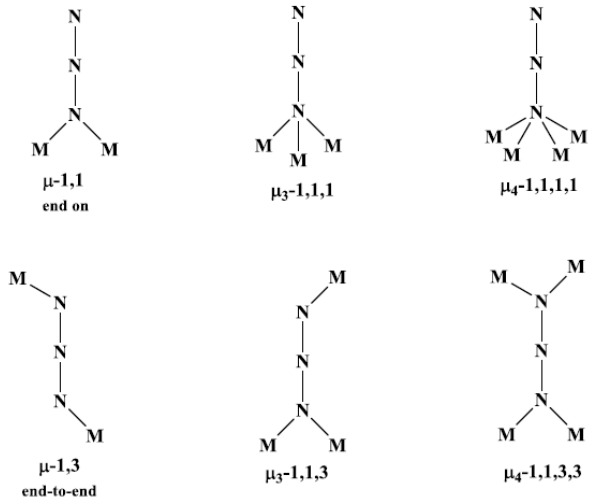

Scheme 10. Different types of bridging modes of azide (N_3^-).

The complex crystallizes in a monoclinic *P2₁/c* space group with the whole molecule in the asymmetric unit. The triangular unit consists of three copper ions, bridged by pyrazolato anions and a bridging μ_3-hydroxyl ligand. Three terminal sites are occupied by azide ligands. A perspective view of the trinuclear Cu(II) unit is shown in Figure 8. The Cu–OH distances are 1.979(2), 2.009(1), 2.024(2) Å. The capping μ_3-OH is located 0.335(2) Å from the plane containing the three copper centers. Cu1 ion is bonded to two nitrogen atoms originating from two different pyrazole ligands (Cu1–N1 1.944(4), Cu1–N12 1.937(4) Å), one nitrogen atom from N_3^- anion (Cu2–$\mu_{1,1}$-N13 = 1.985(4) Å) and one central μ_3-OH to form a 4-coordinated square planar geometry. The Cu2 ion is coordinated to two $\mu_{1,1}$-N atoms from N_3^- and two nitrogens from pyrazole ligands and one oxygen from central μ_3-OH, forming a slightly distorted square pyramid geometry. The Cu–N bond distance in the axial position (Cu2–$\mu_{1,1}$-N13i 2.340（4）Å) is also significantly

longer than the bond length in the equatorial plane (ranging from 1.942(5) - 2.003(5) Å). The Cu3 is also in a square pyramidal geometry. The only difference is the presence of an additional azide ligand coordinated through N3 in an axial position with a longer Cu-N bond distance (Cu3–$\mu_{1,1}$-N3 2.422(5) Å), and another N atom from terminal azide ligand (monodentate μ-1) with Cu3–N8 distance of 1.972(6) Å.

As shown in Figure 9, the neighboring trinuclear Cu(II) units are connected by two $\mu_{1,1}$-N_3 ligand generating an one-dimensional chain structure with Cu…Cu distances of 3.385(2)-3.469(3) Å and Cu–N_{azide}–Cu bridging angles of 105.72-114.91°. Azide ions are quasi linear with N–N–N angles in the narrow 176.8(5) - 178.1(5)° range, exhibiting unsymmetrical N–N bond lengths, with bonds involving the donor atom, N3–N4 = 1.190(6) Å, significantly longer than N4–N5 = 1.129(6) Å.[54]

1.5.5. Crystal structure description of $[Cu_3(\mu_3\text{-OMe})(\mu\text{-Cl})(\mu\text{-pz})_3(py)_2]Cl$ [5]

Complex **[5]** consists of a nine-membered $[Cu\text{-}N\text{-}N]_3$ metallacycle where the Cu-atoms are coordinated to two pyridines and two chlorines (Figure 10). The center of the metallacycle accommodates a pyramidal μ_3-OCH_3 group bridging unsymmetrically the three Cu-atoms. The Cu-OCH_3 bond lengths range from 2.100(1) Å to 2.043(1) Å. Cu-O-Cu angles from 102.69(6)º to 103.76(6)º. The O-atom is 0.880(1) Å out of the Cu_3-plane. The Cu···Cu intramolecular distances are within the 3.185(3) - 3.253(3) Å.

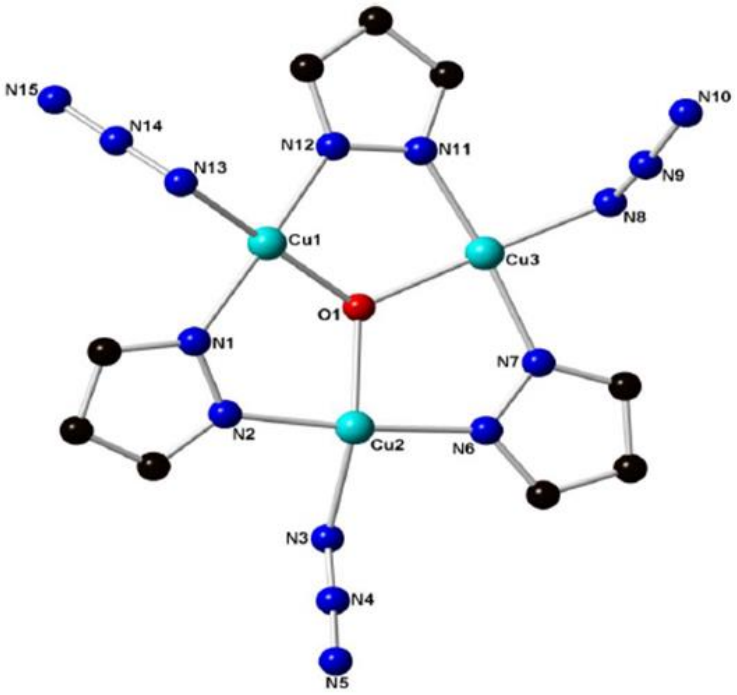

Figure 8. Crystal structure of compound **[4]**, hydrogens and PPN are omitted for clarity.

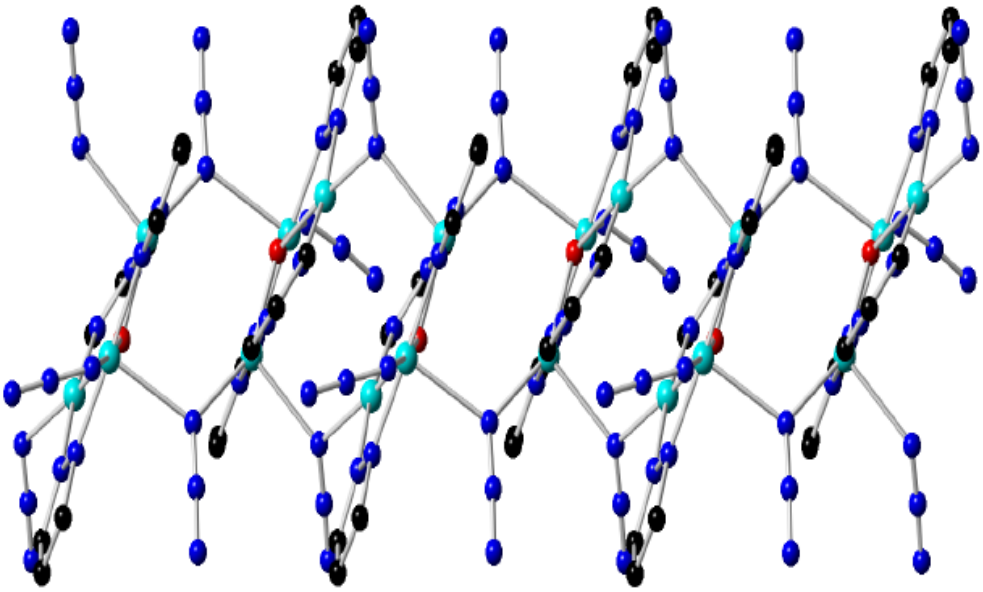

Figure 9. Packing diagram of structure **[4]** view from *b* axis.

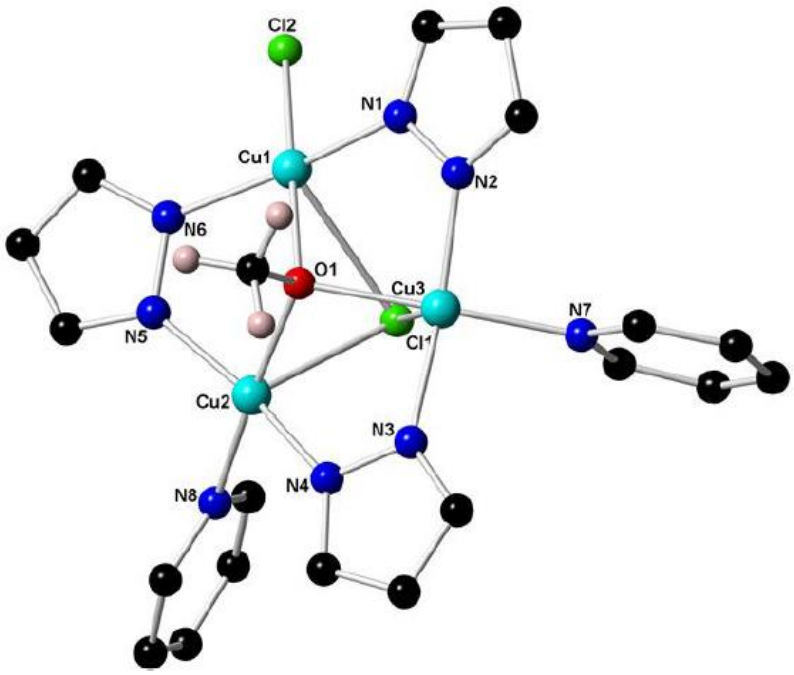

Figure 10. Crystal structure of compound **[5]**, H atoms are omitted for clarity.

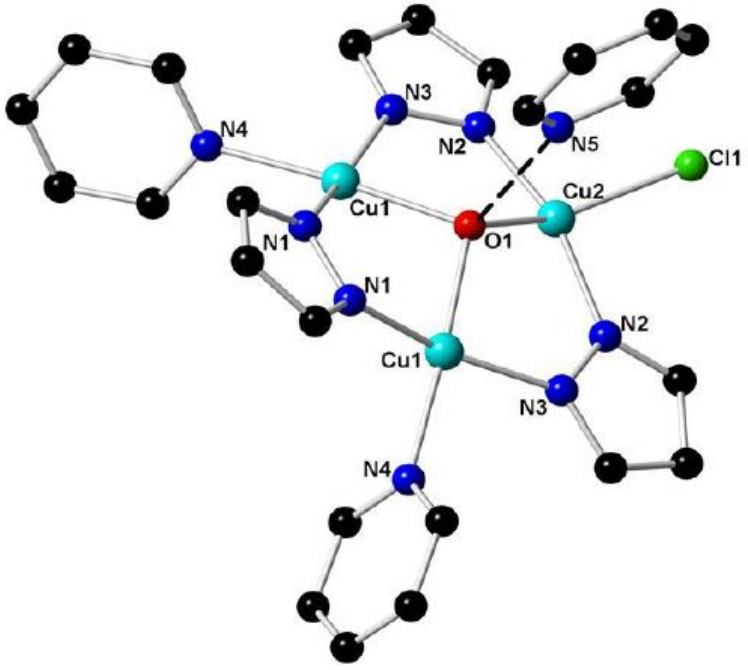

Figure 11. Crystal structure of compound **[6]**, H atoms are omitted for clarity.

Table 3. Selected interatomic distances (Å) and angles (º) for **[5]** and **[6]**.

	[5]	**[6]**
Cu–(μ_3-O)	2.100 (1) -2.043(1)	1.968(2)-2.004(4)
Cu–N_{pz}	1.937(2)-1.961(2)	1.939(2)-1.961(2)
Cu–N_{py}	2.025(2)-2.036(2)	2.026(2)
Cu–Cl	2.282(7)	2.3355(1)
Cu-μ-Cl	2.653(6)-2.680(6)	2.673(1)
Cu···Cu	3.185 (3) - 3.253(3)	3.110 (2)-3.316(1)
Cu–O–Cu:	102.67(6)-103.76(6)	101.79(1)-113.17(8)

1.5.6. Crystal structure description of $[Cu_3(\mu_3\text{-}OH)(\mu\text{-}Cl)(\mu\text{-}pz)_3(py)_2Cl]\cdot py$ [6]

Complex **[6]** crystallizes in orthorhombic *Pnma* space group. The terminal sites are occupied by two pyridines and one terminal chloride ligand (Figure 11). The Cu-N_{pz} and Cu-N_{py} bond lengths are 1.939(2)-1.961(2) Å and 2.026(2) Å, respectively. The center of this metallacycle accommodates a triply bridging hydroxide. The O-atom is 0.671(2) out of the Cu_3-plane. Cu-O-Cu angle and Cu-O distances are within 101.79(1)º-113.17(8)º and 1.968(2)-2.004(4) Å, respectively. One additional chloride cap unsymmetrically the trimer on one side at distance of 2.336(1) Å from the Cu_3 plane, completing the distorted square pyramidal coordination geometry. The (μ_2-Cl)-Cu distance is 2.673(1) Å. Cu···Cu distances vary between 3.110(2) and 3.316(1) Å. Complex **[6]** contains one non-coordinating pyridine molecule to form a H-bond to hydroxyl, O-H ··· N= 2.706 Å, ∠O-H···N = 171.94º.

1.5.7. Crystal structure description of $Cu_3(\mu_3\text{-}OH)(\mu\text{-}4\text{-}Cl\text{-}pz)_3(py)_3(ClO_4)_2]\cdot(CH_2Cl_2)\cdot((CH_3)_2(CO)$ [7]

Complex **[7]** contains a μ_3-OH group bridging unsymmetrically three copper atoms, the average Cu–OH bond length is 2.000(1) Å and the O-atom is 0.465(3) Å above the $[Cu(pz)]_3^-$plane (Figure 11). Three terminal py ligands are on the opposite side of the Cu_3-plane than their *trans*-μ_3-OH, with their planes orthogonal to the Cu_3-plane. The Cu···Cu distances and the Cu–N bond lengths, are within 3.336(1) - 3.339(2) Å and 1.952(1) - 1.960(1) Å, respectively. One Cu ion exhibits an octahedral coordination geometry with two nitrogen atoms from 4-Cl-pzH, one nitrogen from pyridine ligand and a capping ligand μ_3-OH forming the basal plane, while two oxygen atoms from two triflate anions are coordinated in the apical positions. The basal Cu-N (1.952 (9)-2.022(1) Å) and Cu-O (1.998(1) Å) distances are slightly shorter than the basal Cu-O_{CF3SO3} one, while the long apical Cu-O_{CF3SO3} distance (2.628(1) Å) is a manifestation of the typical Jahn-Teller elongation, indicative also of a very weak axial coordination. The two remaining copper atoms are in square-pyramidal N_3O_2 -coordination environments with a weak interaction involving one triflate anion and one acetone, if the long Cu···O interactions of 2.367(1) in Cu···$OC(CH_3)_2$ are taken into account (Figure 13).

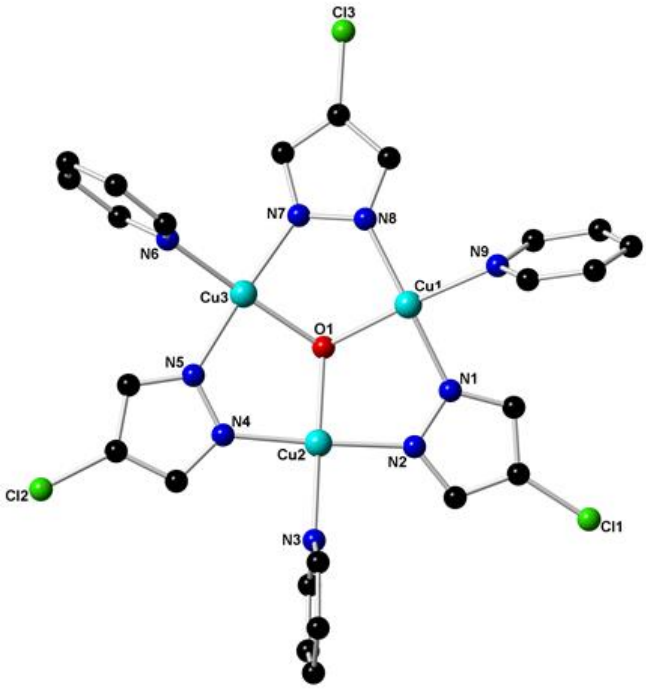

Figure 12. Crystal structure of $Cu_3(\mu_3\text{-}OH)(\mu\text{-}4\text{-}Cl\text{-}pz)_3(py)_3(ClO_4)_2$] **[7]**, showing the atom-labeling scheme, triflate anions were omitted for clarity.

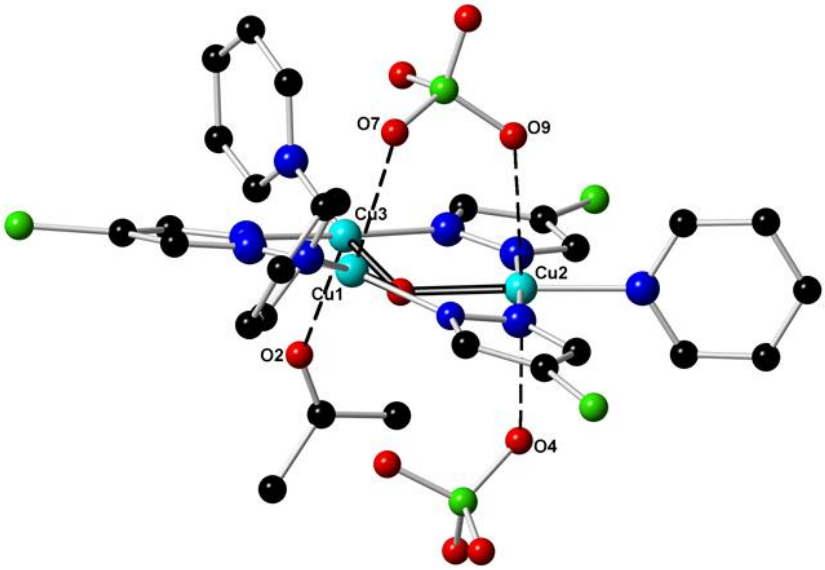

Figure 13. Crystal structure of $Cu_3(\mu_3\text{-}OH)(\mu\text{-}4\text{-}Cl\text{-}pz)_3(py)_3(ClO_4)_2$] **[7]**, showing the $Cu_3\cdots(\mu_3\text{-}CF_3SO_3)$ interaction and interaction with a coordinating acetone molecule.

1.5.8. Crystal structure description of $(PPN)_2[Cu_3(\mu_3\text{-}O)(\mu\text{-}pz)_3(\eta^1\text{-}NO_2)_2(\eta^2\text{-}NO_2)]$ [8], $(PPN)_3[Cu_3\ (\mu_3\text{-}OH)(\mu\text{-}pz)_3(\eta^1\text{-}NO_2)_3](OH)(NO_3)$ [9] and $(PPN)_2[Cu_3(\mu_3\text{-}O)(\mu\text{-}pz)_3(\eta^1\text{-}NO_2)_2Cl]$ [10]

Compound **[8]** was obtained from a metathetical reaction of the chloro-terminated complex $[Cu_3(\mu_3\text{-}O)(\mu\text{-}pz)_3Cl_3]^{2-}$ with excess $NaNO_2$ in CH_2Cl_2 and was recrystallized from CH_2Cl_2/Et_2O at ambient temperature, resulting in blue-green X-ray quality crystals of $[PPN]_2[Cu_3(\mu_3\text{-}O)(\mu\text{-}pz)_3(NO_2)_3]$ **[8]** with monoclinic, $P2_1/c$ space group. It consists of a nine-membered $[Cu\text{-}N\text{-}N]_3$ metallacycle where the Cu-atoms are held together by *trans* pyrazolato bridges, accommodating an almost planar $Cu_3(\mu_3\text{-}O)$ core (Figure 14). Complex **[8]** contains two η^1-O and one η^2-O,O nitrite ligands, with a C_2 axis going through the nitrogen of the $\eta^2\text{-}NO_2$ ligand, Cu- and μ_3-O-atoms. The Cu-O distances involving the η^2-nitrite, 2.349(3) Å, are intermediate to those of the bonded (2.015(2) Å) and non-bonded (2.653(4) Å) Cu-O distances to the η^1-O nitrite.

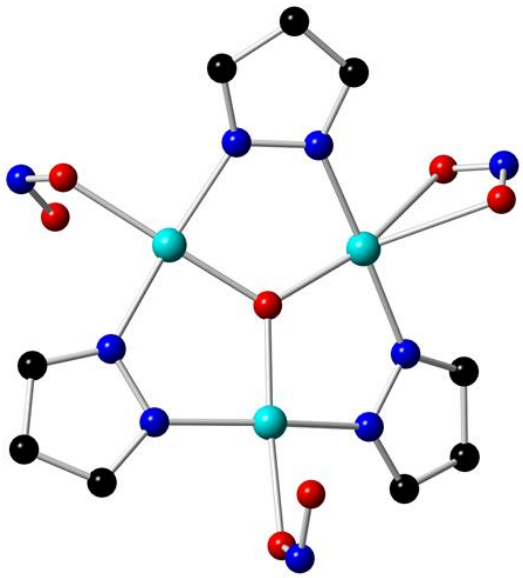

Figure 14. Crystal structure of compound **[8]**, hydrogen atoms and PPN^+ are omitted for clarity. Color codes: black, C; blue, N; red, O; cyan, Cu.

In the infrared spectrum of compound **[8],** the asymmetric nitrite stretches, $\nu_{as}(NO_2)$, are identified with strong bands at 1439 cm^{-1} and 1377 cm^{-1}, whereas the symmetric O-N-O stretch, $\nu_{sym}(NO_2)$, is assigned to a band at 1259 cm^{-1}. The assignments agree with those reported for other nitrito complexes in the literature.[55,56] ^{15}N-labeling studies of an η^2-NO_2 complex have revealed that the IR-active O-N-O bending vibration of nitrite, $\delta(NO_2)$, occurred at 877 cm^{-1}.[56] A similar weak band is observed at 872 cm^{-1} for **[8]**. It is worth noting that the differences between η^1- and η^2- binding modes do not have significant manifestation in their vibrational spectrum.

The asymmetric unit of compound **[9]** consists of one third of the Cu_3-trimer, one [PPN] cation and one third of a distant nitrate anion. A C_3-axis, perpendicular to the Cu_3-plane, goes through the □$_3$-O, generating an equilateral Cu_3-triangle, with three η^1-O nitrite ligands coordinated to the Cu-centers at a Cu-O bond length of 1.954(2) Å (Table 5). The source of the nitrate counter ion is presumed to be nitrite, which is known to oxidize to nitrate, even under mild conditions.[57]

In the IR spectrum of compound **[9],** the asymmetric nitrite stretches occur at 1437, 1379 and 1267 cm^{-1}. The assignments agree with those reported for other nitrito complexes in the literature.[55,56] Similar weak bands are observed at and 877 cm^{-1} for **[9]**.

Complex **[10]** crystallizes in the monoclinic space group *P2/c*. The terminal sites are occupied by two □□-ONO□ and one terminal chloride ligand (Figure 16). The Cu…Cu intramolecular distances are within the 3.263(6)-3.264(9) Å range. Table 4 lists the important bond lengths and angles for **[8]**, **[9]**, **[10]** and **[11]**.

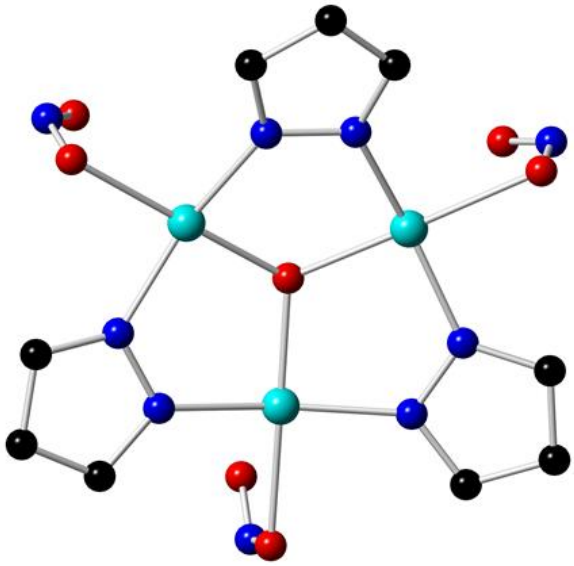

Figure 15. Crystal structure of **[9]**, hydrogen atoms and PPN are omitted for clarity. Color codes: black, C; blue, N; red, O; cyan, Cu.

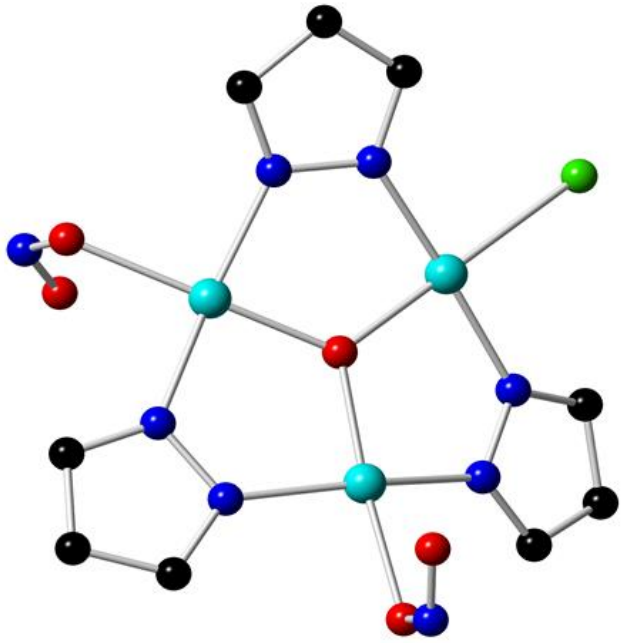

Figure 16. Crystal structure of **[10]**, hydrogen atoms and PPN are omitted for clarity. Color codes: black, C; blue, N; red, O; cyan, Cu.

Table 4. Selected interatomic distances (Å) and angles (º) of compound **[8]**, **[9]**, **[10]** and **[11]**.

	[8]	**[9]**	**[10]**	**[11]**
Cu…Cu	3.248 (1)-3.261(2)	3.338(1)	3.263(6)-3.264 (9)	3.355(7)-3.403(7)
Cu–(μ_3-O/OH)	1.874(2)- 1.880(1)	1.954(2)	1.881(2)-1.889(4)	1.982(3)-2.005(4)
Cu–N	1.947(2)-1.959(2)	1.942(5)	1.945(4)-1.963(3)	1.925(3)-1.942(3)
Cu–O(NO)	2.015(2)-2.653(4)	2.156(5)	2.035(3)	2.028(4)-2.140(4)
Cu–O–Cu	119.85(5)-120.30(1)	117.33(1)	119.85(1)-120.29(2)	114.53(2)-117.89(2)
Cu–Cl			2.362(4)	

1.5.9. Crystal structure description of (PPN)[$Cu_3(\mu_3$-OH)(μ-4-Ph-pz)$_3(NO_2)_3$]·0.5(CH_2Cl_2) [11]

Compound **[11]** crystallizes in the triclinic $P\bar{1}$ space group with a whole molecule in the asymmetric unit. Three nitrite ligands are η^1-O-coordinated to Cu-centers with Cu-O_{ONO} bondining distances of 2.028(4), 2.062(4) and 2.140(4) Å and non-bonded Cu…O distances of 2.488(5), 2.475(4) and 2.548(6) Å. Of the three nitrito ligands, one is *syn* to the μ_3-OH group while the other two are *anti*. The μ_3-OH groups from adjacent Cu_3-units form strong H-bonds with the bound O of the nitrito ligand (O(H)···O: 2.771(7) Å) (Figure 18).

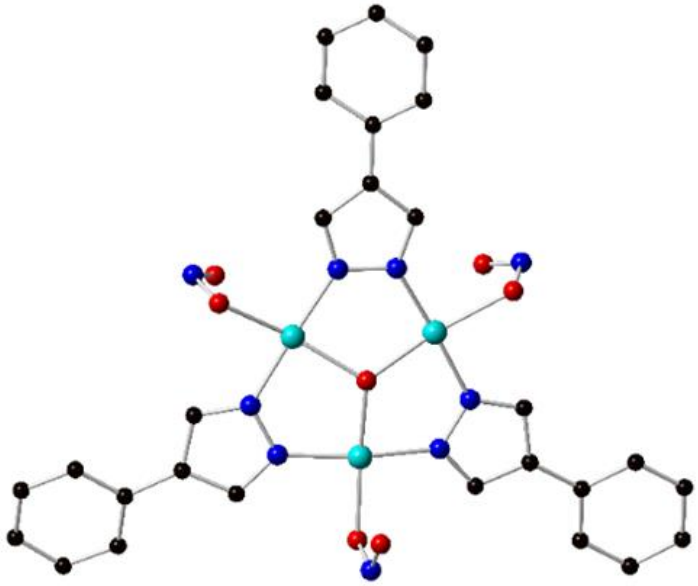

Figure 17. Crystal structure for **[11]**, PPN and H atoms have been omitted for clarity. Color codes: black, C; blue, N; red, O; cyan, Cu.

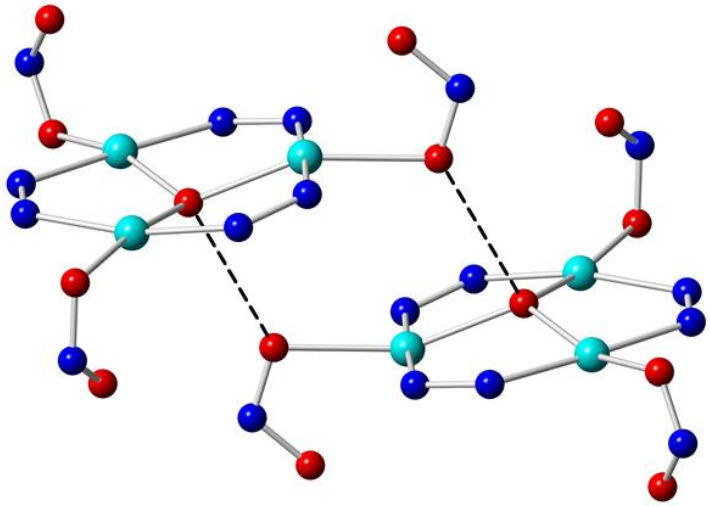

Figure 18. H-bonded dimeric structure of **[11]**. Phenyl substitution on pyrazole rings, H atoms and PPN counterions are omitted for clarity. Color codes: blue, N; red, O; cyan, Cu.

1.5.10. Crystal structure description of $(PPN)_3[Cu_3(\mu_3\text{-}O)(\mu\text{-}4\text{-}Me\text{-}pz)_3(\eta^1\text{-}NO_2)_3](NO_3)$ [12] and $(PPN)_3[Cu_3(\mu_3\text{-}O)(\mu\text{-}4\text{-}Cl\text{-}pz)_3(\eta^1\text{-}NO_2)_3](NO_3)$[13]

Compounds **[12]** and **[13]** crystallize in the trigonal R_3 space group, and the asymmetric unit consists of a third of the Cu_3-trimer and one [PPN] along with a distant nitrate anion. Since nitrite to nitrate oxidation is known to occur even under mild conditions, it is hardly surprising that a nitrate is found in the minor product of the reaction. All the terminal sites in **[12]** and **[13]** are occupied with η^1-O nitrite ions (Figure 19 and 20). All the Cu ions are tetra-coordinated, displaying a square-planar geometry. Table 6 lists important bond lengths and angles for **[12]** and **[13]**, respectively.

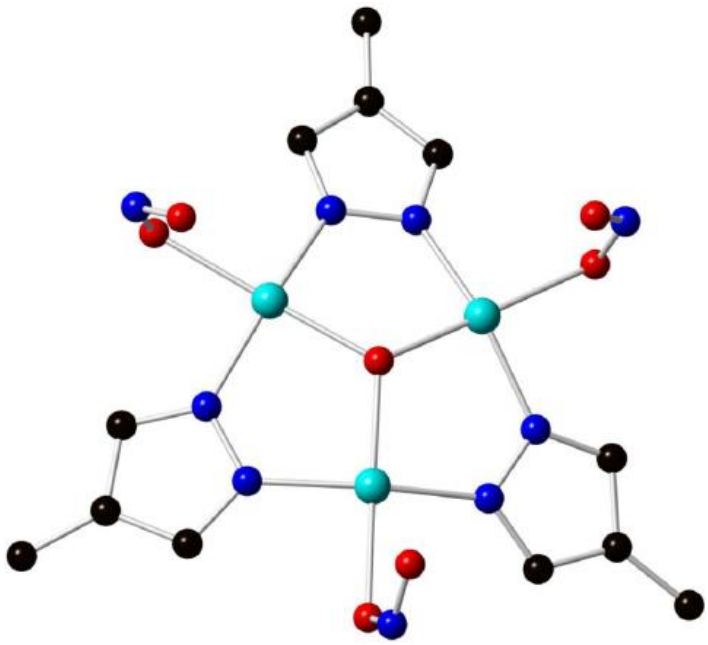

Figure 19. Crystal structure of **[12]**, hydrogen atoms and PPN are omitted for clarity. Color codes: black, C; blue, N; red, O; cyan, Cu.

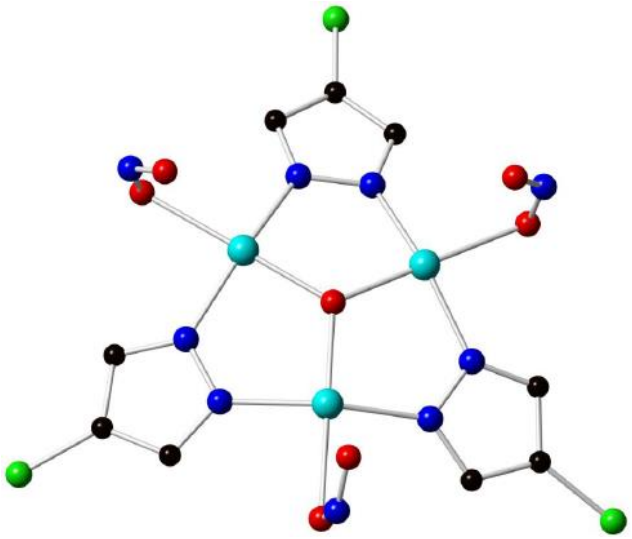

Figure 20. Crystal structure of **[13]**, hydrogen atoms and PPN are omitted for clarity. Color codes: black, C; blue, N; red, O; green, Cl; cyan, Cu.

Table 5. Selected bond lengths (Å) and angles (deg) for **[12]** and **[13]**.

Bond	**[12]**	**[13]**
Cu- (μ_3-O)	1.960(2)	1.919(2)
Cu-O(NO)	2.075(5)	2.164(8)
Cu-N	1.936(6)	1.957(6)
Cu…Cu	3.341(1)	3.306(3)
Cu-O-Cu	116.99 (3)	119.02(3)

1.5.11. Crystal structure description of [PPN][$Cu_3(\mu_3\text{-}O)(\mu\text{-}pz)_3(N_3)_2(\eta^2\text{-}NO_2)$] [14]

The compound **[14]** was prepared by treating $[PPN]_2[Cu_3(\mu_3\text{-}Cl)_2(\mu\text{-}pz)_3Cl_3]$ with stoichiometric (1:5:5) amount of $NaNO_2$ and NaN_3. Single-crystal X-ray diffraction analysis reveals that compound **[14]** crystallizes in the monoclinic space group $P2_1/n$. There are two crystallographically independent Cu^{2+} ions (Cu1 and one-half Cu2) with a two-fold axis bisecting the molecule,

generating a trinuclear unit. The azide bridges the Cu atoms in an asymmetrical end-on fashion. The Cu1 ion is four-coordinated with μ-O1, two nitrogens (N1, N7) from pyrazole rings and one nitrogen(N2) from end-on azide to form a distorted square planar. The average bond length of Cu-N (1.909 Å) is slightly shorter than those associated with Cu2 (1.944 Å). While Cu2 coordinates with μ-O1, two nitrogens (N6, N6A) from pyrazole rings and two Oxygen atoms (O2, O2A) from η^2-NO_2 to form trigonal bipyramidal geometry. The average bond lengths of Cu2-N_{pz} and Cu2-O1 are 1.944 and 1.863 Å, respectively.

Azide ions are quasi linear with the N-N-N being 178.6(2)º and exhibit unsymmetric N-N bond lengths, with bonds involving the donor atoms, N(2)-N(3) = 1.151(2) Å being relatively longer than N(3)-N(4) = 1.112(7) Å (Figure 21).

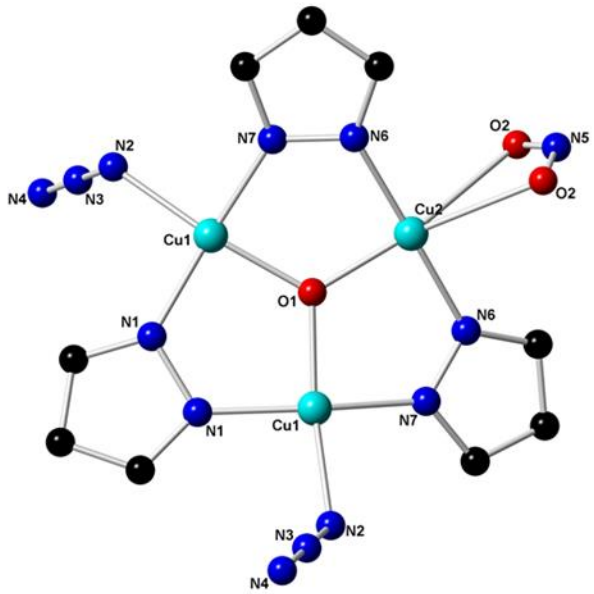

Figure 21. Crystal structure of **[14]**, H atoms and PPN are omitted for clarity. Color codes: black, C; blue, N; red, O; cyan, Cu.

1.6. Redox activity of $[Cu_3(\mu_3\text{-}O)]$-pyrazolate complexes

Cu(II)-pz complexes with $Cu_3(\mu_3\text{-}O)$ are redox active, as has been shown by the reversible one-electron wave in the cyclic voltammogram. The chemical oxidation of all Cu^{II} complexes by either $(NH_4)_2Ce(NO_3)_6$ (CAN) or benzoyl peroxide provides the one-electron oxidized mixed valent (MV) complex, formally-$Cu^{III}Cu_2^{II}$ in bulk. The analysis of the Intervalence Charge Transfer (IVCT) band in the NIR-region of the absorption spectra gives information regarding the extent of electron localization/delocalization and classification under the Robin-Day formulation.

When the MV $[Cu_3(\mu_3\text{-}O)]$-complex is unstable, it can be generated in situ by the addition of a base, as shown in Scheme 11. Compounds (PPN)$[Cu_3(\mu_3\text{-}OH)\ (\mu\text{-}4\text{-}Ph\text{-}pz)_3Cl_3](CH_2Cl_2)$ **[2]**, [PPN] $[Cu_3(\mu_3\text{-}OH)(\mu\text{-}pz)_3(N_3)_3]$ **[4]**, $[Cu_3\,(\mu_3\text{-}OH)(\mu_2\text{-}Cl)(\mu\text{-}pz)_3(py)_2Cl]\cdot py$ **[6]** are deprotonated to form the $Cu_3(\mu_3\text{-}O)$ core by adding base and counterion, the IVCT bands are recorded by UV-vis-NIR spectroscopy during the chemical oxidation of these copper pyrazolates complexes.

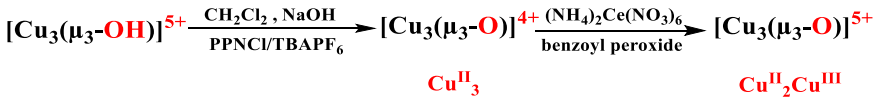

Scheme 11. Chemical oxidation of $Cu_3(\mu_3\text{-}O)$-containing complexes.

1.6.1. UV-vis-NIR spectroscopy of trinuclear Cu(II)-pz complexes

1.6.1.1. UV-vis-NIR spectroscopy of $[Cu_3(\mu_3\text{-}O)\ (\mu\text{-}4\text{-}Ph\text{-}pz)_3Cl_3]^-$ $[2]^-$

Compound **[2]** has μ_3-OH group, which is redox inert. The oxidized $[Cu_3(\mu_3\text{-}O)(\mu\text{-}4\text{-}Ph\text{-}pz)_3Cl_3]^-$ $[2]^-$ was obtained by stoichiometric addition of NaOH and $(NH_4)_2Ce(NO_3)_6$ (CAN) in CH_2Cl_2 (Scheme 11). The UV absorption of $[2]^-$ exhibited a new weak band at 9433 cm^{-1} which can be

attributed to an IVCT transition, characteristic of mixed-valent compounds (Figure 22). All crystallization efforts have failed, so far, to yield X-ray quality crystals of the oxidized products.

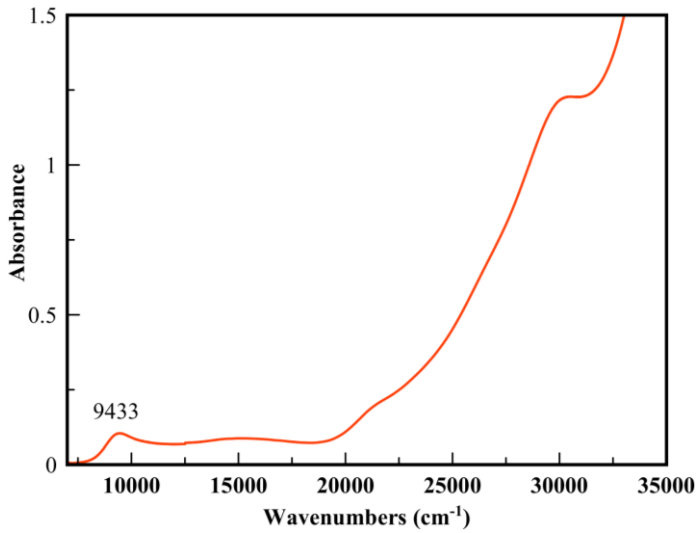

Figure 22. The red trace represents the spectrum of oxidized $[Cu_3(\mu_3\text{-}O)(\mu\text{-}4\text{-}Ph\text{-}pz)_3Cl_3]^-$ **[2]$^-$.**

1.6.1.2. UV-vis-NIR spectroscopy of $[Cu_3(\mu_3\text{-}O)(\mu\text{-}pz)_3(N_3)_3]^-$ [4]$^-$

By a similar procedure to the one described in Scheme 11, the green solution of $[PPN][Cu_3(\mu_3\text{-}OH)(\mu\text{-}pz)_3(N_3)_3]$ **[4]** turned reddish-brown upon stoichiometric addition (one equivalent) of NaOH and benzoyl peroxide. Repetitive UV-Vis-NIR scans were run to determine the stability of mixed-valence complex over a period of 2 h. The reddish color disappeared gradually while the green color was reestablished. Chemical oxidation of the homovalent precursor of $[Cu_3(\mu_3\text{-}O)(\mu\text{-}pz)_3(N_3)_3]^{2-}$, $[4]^{2-}$ by a Ce (IV) reagent produces **[4]$^-$** which is unstable, reacting readily with moisture or solvent. Formation of **[4]$^-$** has been demonstrated by the appearance of the IVCT band in the NIR region at 8630 cm^{-1} (Figure 23). Analysis of the band by the Hush method results in a parameter $\Gamma = 0.52$, classifying **[4]$^-$** as a Robin-Day type-III, strongly delocalized system.

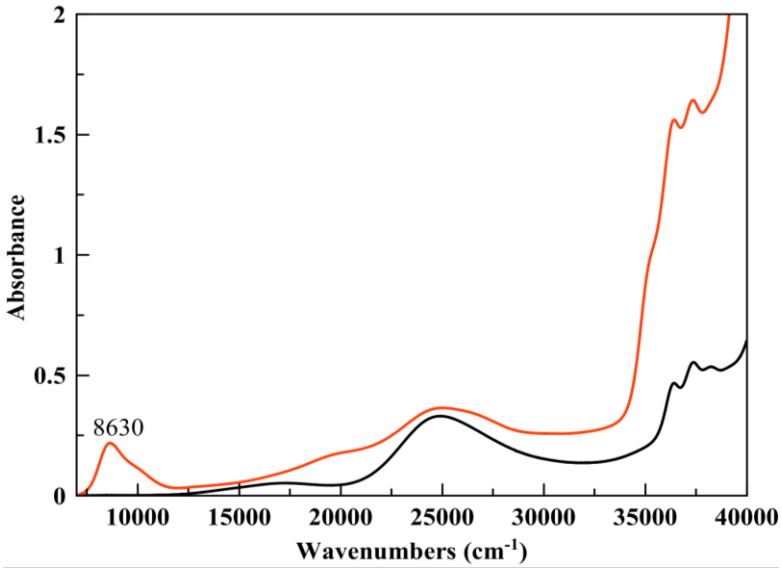

Figure 23. In situ UV-vis-NIR spectra recorded during the oxidation of **[4]**$^{2-}$ in CH_2Cl_2 at room temperature. The black trace and red trace represent the spectra of **[4]**$^{2-}$ and the oxidized species **[4]**$^{-}$, respectively.

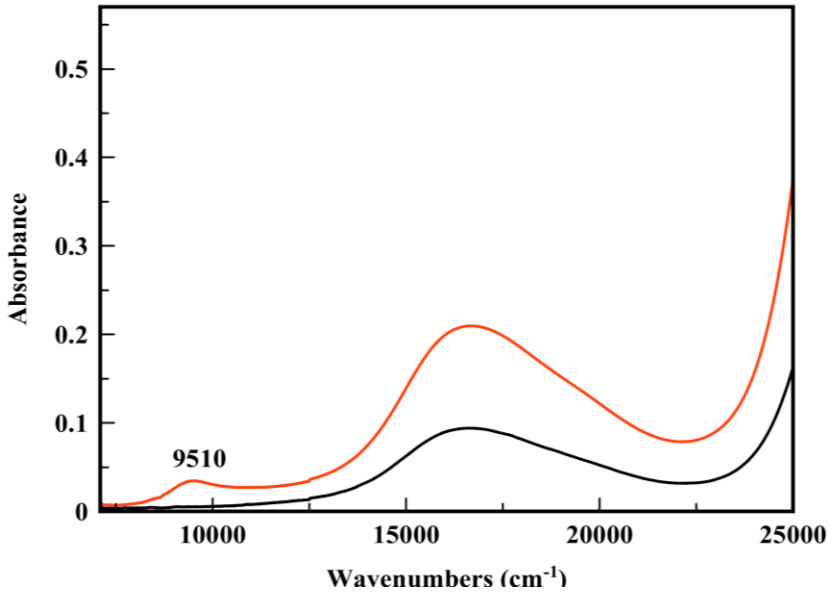

Figure 24. In situ UV-vis-NIR spectra recorded during the oxidation of $[Cu_3(\mu_3\text{-}O)(\mu\text{-}Cl)(\mu\text{-}pz)_3(py)_2Cl]^+$ **[6]**$^+$ in CH_2Cl_2 at room temperature. The black trace and red trace represent the spectra of $[Cu_3(\mu_3\text{-}O)(\mu_2\text{-}Cl)(\mu\text{-}pz)_3(py)_2Cl]$ **[6]** and the oxidized species, respectively.

Following the procedure as shown in Scheme 11, $[Cu_3(\mu_3\text{-}OH)(\mu\text{-}Cl)(\mu\text{-}pz)_3(py)_2Cl](py)$ **[6]** was deprotonated by adding NaOH and $TBAPF_6$ in 10 mL CH_2Cl_2 under stirring. Chemical oxidation

by benzoyl peroxide or CAN results in formation of the formally $Cu^{II}_2Cu^{III}$-compound, accompanied by visible color change from dark blue to light blue with the appearance of new absorption band at 9510 cm^{-1} in the NIR (Figure 24), which is assigned to an IVCT band, characteristic of mixed-valent species.

1.6.1.3. UV-vis-NIR of $[Cu_3(\mu_3\text{-}O)(\mu\text{-}pz)_3(\eta^1\text{-}NO_2)_2(\eta^2\text{-}NO_2)]$ $[8]^{2-}$ and $[8]^-$

Chemical oxidation by a stoichiometric amount of benzoyl peroxide in CH_2Cl_2 results in formation of the formally $Cu^{II}_2Cu^{III}$-compound, **[8]**$^-$, accompanied by visible color change from greenish blue to reddish brown with the appearance of new absorption bands at 20000 cm^{-1} in the visible and 9191 cm^{-1} in the near-IR part of the electronic spectrum (Figure 26). The latter is assigned to an IVCT band, characteristic of mixed-valent species. Analysis of this band by the Hush method results in a parameter Γ = 0.63, classifying **[8]**$^-$ and a Robin-Day type-III, strongly delocalized system.[24, 25] In ambient temperature solution, **[8]**$^-$ decomposes within minutes to a mixture containing an Cu^{II} trinuclear complex and nitrate anions.

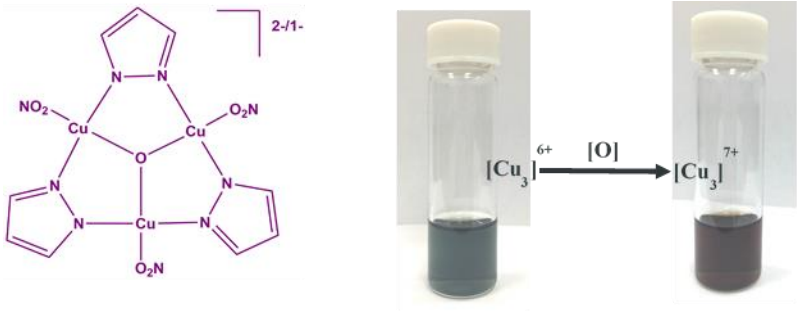

Figure 25. The color change of Chemical oxidation of Compound [**8**] with benzoyl peroxide.

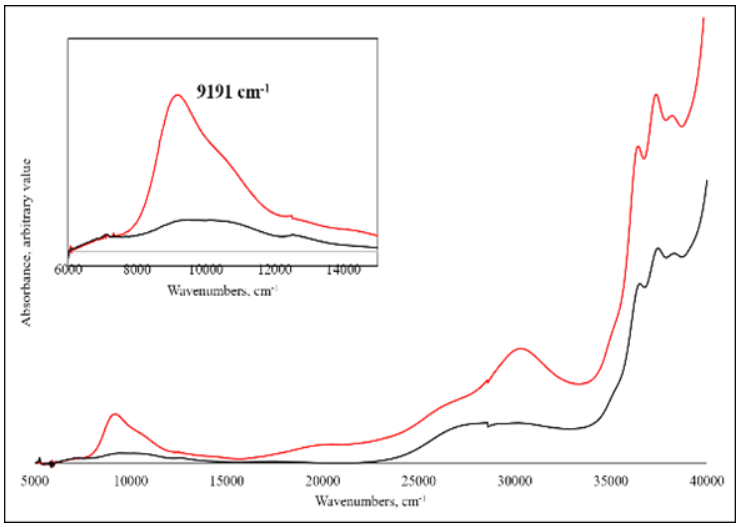

Figure 26. UV-vis-NIR spectra of **[8]** (black) and **[8]**$^{-}$ (red). Inset: IVCT band.

1.6.2. Electrochemistry

Compound **[8]** undergoes electrochemically a reversible one-electron oxidation at $E_{1/2}$ = –0.133 V (*vs*. Fc^{+}/Fc) to yield a mixed-valence compound, [Cu_3^{7+}] (Figure 27). We have previously described the solution characterization of a series of [$Cu_3(\mu_3\text{-}O)(\mu\text{-}4\text{-}R\text{-}pz)_3X_3]^z$ complexes and shown that substitution at the bridging pyrazole 4-position (R) and at the terminal ligand positions (X) influence the redox potential, revealing a trend that follows the order of electron withdrawing/releasing properties of the substituents.[15i] Compound **[8]** has the lowest oxidation potential (Table 6), an expected result given the position of the O-bound nitrite higher in the spectrochemical series.

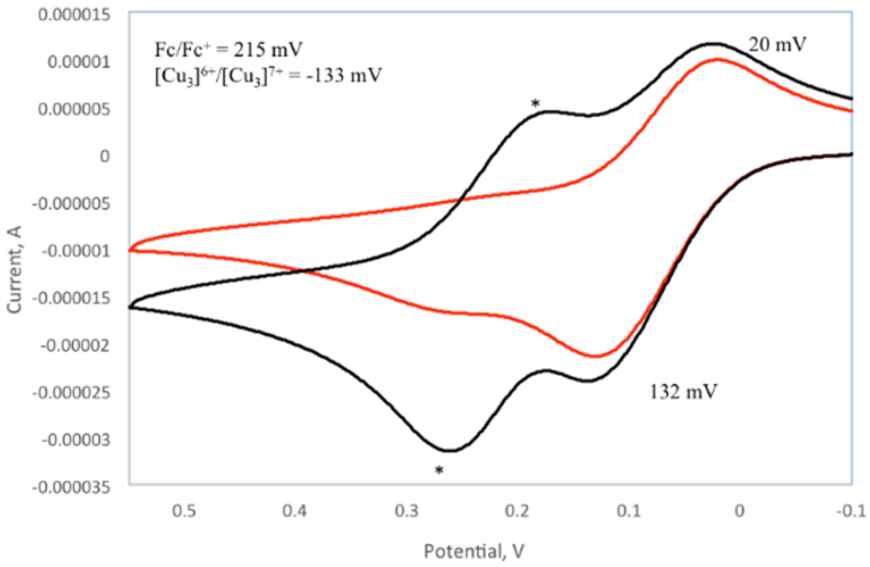

Figure 27. Cyclic voltammograms of [**8**] in CH_2Cl_2 with 0.1 M Bu_4NPF_6 as the electrolyte. Values on the figure are reported vs. Fc^+/Fc. Red trace is without the ferrocene standard.

Table 6. $E_{1/2}$ values of the [Cu_3^{6+}/Cu_3^{7+}] couple with various R and X *vs*. Fc/Fc+. (*only EPA values are given, as they have irreversible oxidations).

R	X	$E_{1/2}$ (V, *vs*. Fc^+/Fc)	Ref
H	NO_2	-0.133	This work
H	Cl	-0.013	[27]
H	CF_3CO_2	+0.131	[27]
Cl	Cl	+0.142	[40]
Br	Cl	+0.142	[40]
H	NCS	+0.253 (E_{pa})*	[40]
CHO	Cl	+0.280	[40]
H	py	+0.400	[40]
NO_2	Cl	+0.449	[40]
H	CH_3CO_2	+0.476 (E_{pa})*	[40]

1.6.3. NO release from trinuclear copper-pyrazolate complexes

1.6.3.1. Detection of NO generated from $(PPN)_2[Cu_3(\mu_3\text{-}O)(\mu\text{-}pz)_3(\eta^1\text{-}NO_2)_2(\eta^2\text{-}NO_2)]$ [8] and thiophenol in varying stoichiometry

A solution of $(PPN)_2[Cu_3(\mu_3\text{-}O)(\mu\text{-}pz)_3(\eta^1\text{-}NO_2)_2(\eta^2\text{-}NO_2)]$ in CH_2Cl_2 (9.24 mmol, 15 mg) was prepared in a small vial. This vial was placed inside a larger vial containing a solution of CoTPP (9.24 mmol, 6.2 mg) in 2 mL CH_2Cl_2 and was capped with a septum. A solution of PhSH (27.72 mmol, 2.88 µL) in 2 mL CH_2Cl_2 was injected to the solution of $(PPN)_2[Cu_3(\mu_3\text{-}O)(\mu\text{-}pz)_3(\eta^1\text{-}NO_2)_2(\eta^2\text{-}NO_2)]$ via a syringe. The UV-vis spectrum of the CoTPP solution was recorded at 2 h and spectra changes were observed due to NO binding to CoTPP (Figure 28). The trinuclear copper nitrite complex is essential for NO generation.

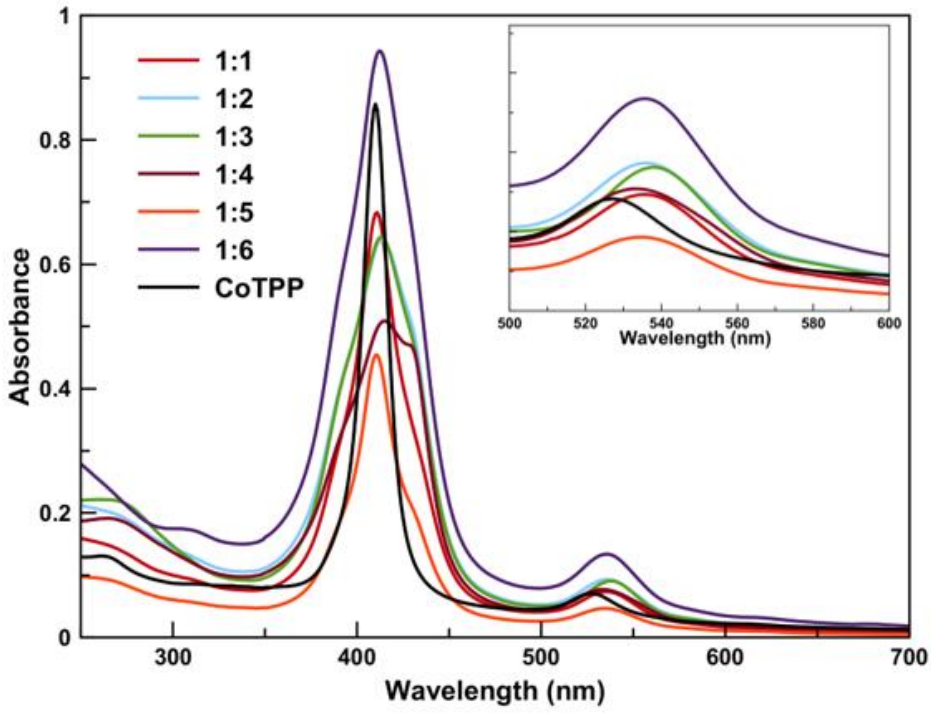

Figure 28. UV-Vis detection of NO(g) formation in the experiment with varying stoichiometry. CoTPP was equimolar to $(PPN)_2[Cu_3(\mu_3\text{-}O)(\mu\text{-}pz)_3(\eta^1\text{-}NO_2)_2(\eta^2\text{-}NO_2)]$ **[8]**.

1.6.3.2. Detection of NO generated from (PPN)[$Cu_3(\mu_3\text{-}OH)(\mu\text{-}4\text{-}Ph\text{-}pz)_3(\eta^1\text{-}ONO)_3$] [11] and thiophenol

A similar procedure was followed for the detection of NO generated from (PPN)[$Cu_3(\mu_3$-OH)(μ-4-Ph-pz)$_3(\eta^1$-ONO)$_3$] **[11]** and thiophenol in varying stoichiometry. As shown in Figure 29, The UV-vis spectra of the resultant CoTPP solutions were monitored over a period of 2 h and spectra changes were observed because of NO binding to CoTPP.

1.6.3.3. Detection of NO generated from (PPN)$_2$[$Cu_3(\mu_3\text{-}O)(\mu\text{-}pz)_3(\eta^1\text{-}NO_2)_2(\eta^2\text{-}NO_2)$] [8] or (PPN)[$Cu_3(\mu_3\text{-}OH)(\mu\text{-}4\text{-}Ph\text{-}pz)_3(\eta^1\text{-}ONO)_3$][11] and six equiv. acetic acid.

NO was detected by UV-vis analysis of Co(TPP) when 6 equiv. acetic acid was added to **[8]** or **[11]** in CH_2Cl_2 (Figure 30).

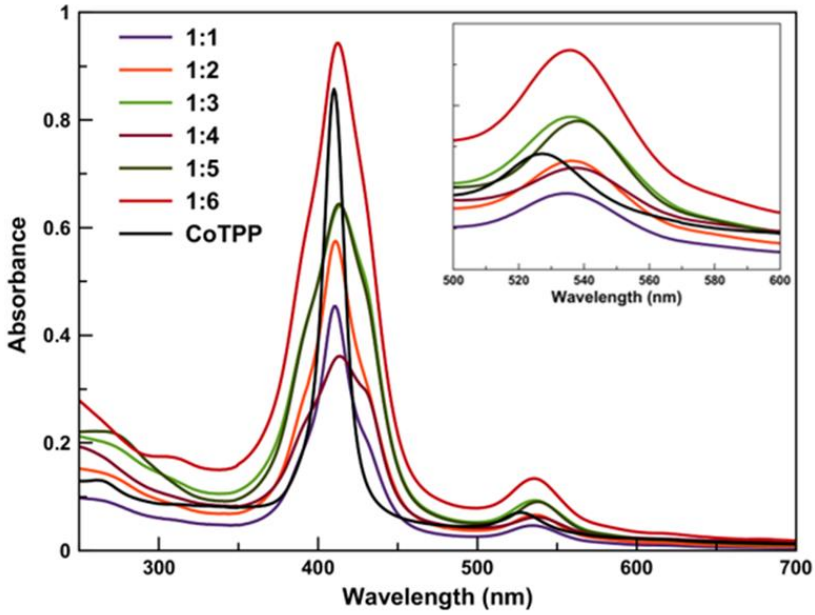

Figure 29. UV-Vis detection of NO(g) formation in the experiment with different stoichiometries. The CoTPP was equimolar to (PPN)[$Cu_3(\mu_3$-OH)(μ-4-Ph-pz)$_3(\eta^1$-ONO)$_3$] **[11]**

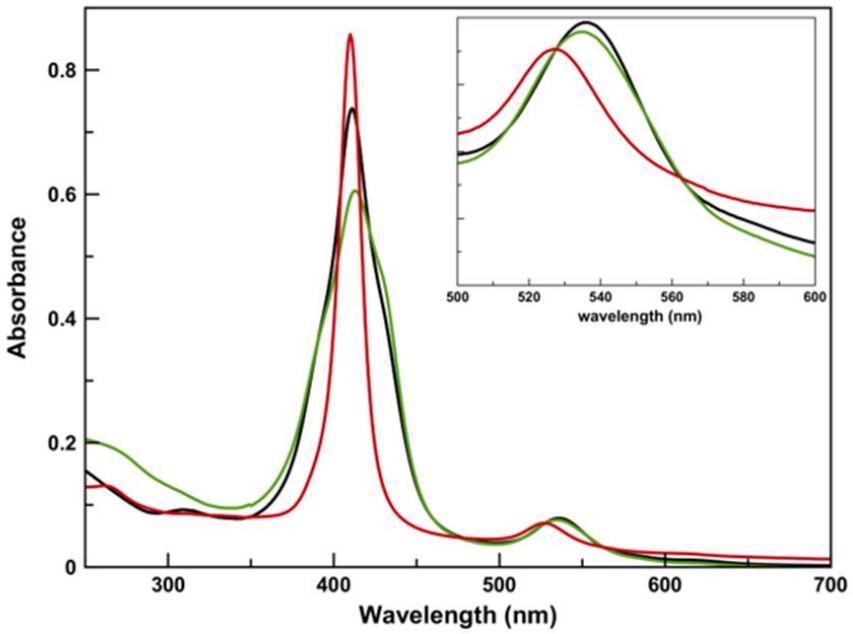

Figure 30. Absorption spectra in CH_2Cl_2 for CoTTP (red), CoTPP(NO) formed by the mixture of [8] and HAc (black) and CoTPP(NO) from **[11]** (green) and HAc.

1.7. Conclusion

To identify the suitable SBU for the construction of MOF, 14 new triangular Copper pyrazolate complexes with suitable ligands in μ_3- and terminal positions have been successfully synthesized and characterized in this project. Various pyrazole substitutions and terminal ligands were tried, simple pyrazole (pzH), 4-Cl-pzH, 4-Me-pzH and 4-Ph-pzH were used for preparing trinuclear copper-pyrazolate complexes.

By employing 4-Ph-pzH, (PPN)[$Cu_3(\mu_3$-OH) (μ-4-Ph-pz)$_3Cl_3$](CH_2Cl_2) **[2]** and (PPN)[$Cu_3(\mu_3$-OH)(μ-4-Ph-pz)$_3Cl_3$]·CH_3CN **[3]** were prepared. These two trimers differ by the interstitial solvent content (CH_2Cl_2 for [2] *Vs* CH_3CN for **[3**] and intermolecular interactions. The structure of **[2]** is observed as a Cu_6 unit, in which two [$Cu_3(\mu_3$-OH)(μ-4-Ph-pz)$_3Cl_3$] units are linked via double μ-Cl bridges, while **[3]** is a polymeric, 1D infinite neutral chain with CH_3CN.

Simple pyazole was used to prepare complexes with -NO_2, -N_3 and py-terminal ligands. The complexes were obtained by simple metathesis reactions of $[PPN]_2[Cu_3(\mu_3\text{-}Cl)_2(\mu\text{-}pz)_3Cl_3]$ and Na salts (NaN_3 and $NaNO_2$) or pyridine.

We show here that the one-electron oxidation of the all-Cu^{II} complex $[Cu_3(\mu_3\text{-}O)(\mu\text{-}pz)_3(NO_2)_3]^{2-}$, **[8]$^{2-}$**, is achieved at an even more cathodic redox potential, allowing the in the *in situ* spectroscopic-characterization of the mixed-valent complex, $[Cu_3(\mu_3\text{-}O)(\mu\text{-}pz)_3(NO_2)_3]^{-}$, **[8]$^{-}$**, the easiest accessible $Cu^{II}_2Cu^{III}$ species known to date. The structural characterization of **[8]$^{2-}$** revealed a new coordination mode of the nitrite to a Cu^{II}-center.

Compounds $(PPN)_2[Cu_3(\mu_3\text{-}O)(\mu\text{-}pz)_3(\eta^1\text{-}NO_2)_2(\eta^2\text{-}NO_2)]$**[8]** and $(PPN)[Cu_3(\mu_3\text{-}OH)(\mu\text{-}4\text{-}Ph\text{-}pz)_3(NO_2)_3]\cdot 0.5\ (CH_2Cl_2)$ **[11]** release NO almost quantitatively upon the addition of PhSH or acetic acid. The system has been established to be catalytic in the presence of excess nitrite. The complexes have been characterized by a string of spectroscopic and electrochemical techniques.

Compound $(PPN)[Cu_3(\mu_3\text{-}OH)(\mu\text{-}pz)_3(\mu_{1,1}\text{-}N_3)_2(N_3)]$**[4]** forms an one dimensional (1D)-chain, as the neighboring trinuclear Cu(II) units are connected by two $\mu_{1,1}$-N_3 ligand. As in the case of py-terminal ligands studied previously, the redox-active $Cu_3(\mu\text{-}O)$ core can only form in solution by adding excess base, by analyzing of IVCT band, classifying **[4]$^{-}$** can be classified as a Robin-Day type-III, strongly delocalized system.

Except 4-Ph-pz, all Cu_3 complexes with 4-R substitution have been able to form $[Cu_3(\mu_3\text{-}O)]$ compounds in the solid state when the terminal ligand is Cl/Br. Compounds $(PPN)[Cu_3(\mu_3\text{-}OH)(\mu\text{-}4\text{-}Ph\text{-}pz)_3Cl_3](CH_2Cl_2)$ **[2]**, $(PPN)[Cu_3(\mu_3\text{-}OH)(\mu\text{-}pz)_3(\mu_{1,1}\text{-}N_3)_2(N_3)$ **[4]**, $[Cu_3(\mu_3\text{-}OH)\ (\mu_2\text{-}Cl)(\mu\text{-}pz)_3(py)_2Cl]\cdot py$ **[6]** were deprotonated in solution to form the $Cu_3(\mu_3\text{-}O)$ core by adding a base and

a counterion. Oxidation of these compounds was also achieved in solution; the formation of the oxidized compound was indicated by the formation of the IVCT bands at 9433 cm^{-1}, 8630 cm^{-1}, and 9510 cm^{-1} for **[2]**, **[4]** and **[6]** respectively, during the chemical oxidation of these copper pyrazolate complexes either by CAN or $(PhCO)_2O_2$.

These are the first examples of a polynuclear NO release system up to now. Both complexes **[8]** and **[11]** release NO almost quantitatively upon the addition of PhSH or acetic acid. The system has been established to be catalytic in the presence of excess nitrite. The complexes have been characterized by a string of spectroscopic and electrochemical techniques.

Chapter 2. Polynuclear Copper-pyrazolate complexes

Multinuclear transition metal ion complexes often have interesting properties, such as magnetic, electrochemical, and catalytic functions. The N-donor ligands have coordination plasticity and large affinity for transition metals, and their employment has provided structures of various nuclearities and dimensionalities, which have been shown to be of interest in catalysis, bio-inorganic chemistry and molecular magnetism.

2.1. Hexanuclear Copper-pyrazolate complexes

There have been several reports concerning multinuclear Cu(II) complexes supported by pyrazolato (pz^-) bridging ligands. In this context, we have investigated a family of redox-active Cu_6-pyrazolato complexes with trigonal prismatic shapes,[39,58] including one with a μ_6-F central ligand.[59] In connection with our earlier work, $[\{Cu_3(\mu_3\text{-}OCH_3)(\mu\text{-}C_3H_2N_2Cl)_3\}_2(\mu\text{-}C_3H_2N_2Cl)_3(\mu_6\text{-}Cl)]$ **[15]** has been prepared recently; it contains an encapsulated μ_6-Cl ligand at the center of the hexanuclear complex.

2.1.1. Synthesis of $[\{Cu_3(\mu_3\text{-}OCH_3)(\mu\text{-}C_3H_2N_2Cl)_3\}_2(\mu\text{-}C_3H_2N_2Cl)_3(\mu_6\text{-}Cl)]$ [15]

The complex was formed in an one-pot reaction when $CuCl_2 \cdot 2H_2O$ (0.06 mmol, 10.2 mg), 4-Cl-pzH (0.09 mmol, 8.9 mg) and triethylamine (0.08 mmol, 11.3 ml) were stirred in 10 ml CH_2Cl_2 for 24 h at ambient temperature. The green solution was transferred to a test tube after filtration. A 4 ml 1:1 mixture of CH_2Cl_2 : MeOH (v/v) was layered over the CH_2Cl_2 layer, 1,2-di(4-pyridy-l)ethylene (bpe) (0.01mmol, 1.9 mg) in 4 mL MeOH was added as the third layer on top of the lower two. Suitable crystals for X-ray diffraction were obtained one week later. Yield: 29%. Analysis calculated/found for $C_{29}H_{24}Cl_{10}Cu_6N_{18}O_2$: C, 25.15/25.22; H, 1.75/1.76; N, 18.22/18.17.

2.1.2. Results and Discussion

The crystal structure of this compound (Figure 31) consists of two trinuclear $[Cu_3(\mu_3\text{-OMe})(\mu\text{-4-Cl-pz})_3]^{2+}$ (OMe is a methoxide, 4-Cl-pz = 4-chloropyrazolato ligand) units bridged by three μ-4-Cl-pz⁻ ligands; the complete molecule adopts .2. point group symmetry. The six Cu^{II} ions form a trigonal prismatic array and a chloride ion is located at the center of the cage, coordinating to the two $\{Cu\}_3$ units in a μ_6 mode. All six Cu(II) atoms are five-coordinate with distorted square pyramidal N_3OCl coordination sets with the Cl atom occupying the apical position. Each Cu_3 triangle is capped by an OMe group with the O atom 0.847 (1) Å above the Cu_3-plane, a somewhat smaller deviation from the Cu_3 plane than the one found in the previously reported structure of $[\{Cu_3(\mu_3\text{-OMe})(\mu\text{-pz})_3\}_2(\mu\text{-pz})_3(\mu_6\text{-Cl})]$, where μ_3-bridging methoxy groups are located ca 1.0 Å above this plane.[60] The distance between two Cu_3 planes is 3.3858 (2) Å. The six Cu—O bond lengths range from 2.033 (2)–2.044 (2) Å, while the Cu–O–Cu angles are in the 102.70 (1)–105.62(1) range. The Cu…Cu distances within each triangle, 3.180 (9)–3.253 (9) Å, are slightly shorter than those between the triangles, 3.356 (2)–3.401 (2) Å. The μ_6-Cl ligand is located close to the center of the trigonal prism defined by the six Cu atoms and non-equidistant from the three pairs of Cu^{II} ions. The longest Cu—Cl distance of 2.622 (1) Å (Cu2) is longer than the sum of the ionic radii (2.38 Å), indicating that the two $[Cu_3(\mu_3\text{-OMe})(\mu\text{-4-Cl-pz})_3]^{2+}$ units are not templated by the encapsulated chloride. The other two Cu—Cl bond lengths are 2.424 (2) (Cu1) and 2.4859 (1) Å.

Differences in structural parameters between the four known $\{Cu_6\text{-pyrazolato}\}$ complexes with trigonal prismatic shape are compiled in Table 7. The inter-trimer and intratrimer Cu…Cu distances are shorter in the title compound than those in the $[Cu_6Cl]$ compound reported earlier with 4-Hpz as a ligand,[60] indicating the effect of electron-withdrawing Cl-substitution of the pyrazolato ligands. The Cu—N distances of the pyrazolato ligands connecting the two trimers are longer compared to

those in {Cu_6-μ_6-F}[59] or {Cu_6-μ_6-Cl}.[60] However, the Cu—N distances are similar to those in the empty Cu_6-pyrazolato cage.[39]

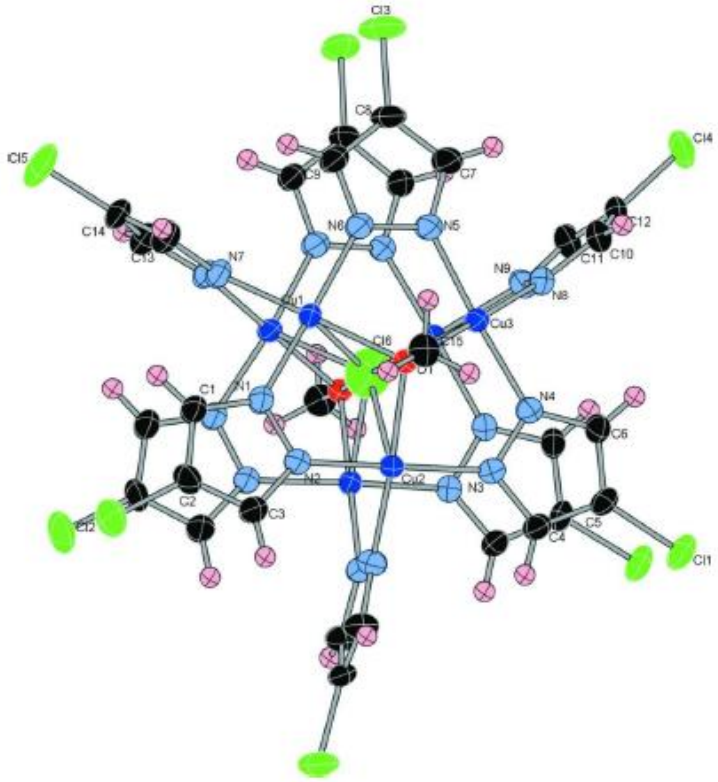

Figure 31.The molecular structure of [15], showing the atom-labeling scheme. H atoms are not shown for clarity. Displacement ellipsoids are drawn at the 40% probability level. Non-labeled atoms are related to the labeled atoms by the symmetry operation (-x, y, -z). Color codes: black, C; light blue, N; red, O; green, Cl; dark blue, Cu.

In the trigonal prismatic molecules, the six pyrazolato ligands of the eclipsed {Cu_3-pyrazolato} trimers exhibit weak π–π stacking interactions, with centroid-to-centroid distances of 3.848 (6) and 3.606 (6) Å. These distances are comparable to the ones found in the Cu_6-pyrazolato complex with no encapsulated anion, where the pyrazolato ring centroids are 3.741 (6), 3.700 (6) and 3.680 (6) Å apart. While conventional hydrogen bonds are absent in the structure, there are three weak intermolecular C-H…Cl interactions observed in the crystal structure (Figure 32 and Table 8).

Individual {Cu6-μ_6-Cl} molecules are stacked in rods parallel to [110] that, in turn, are arranged in a pseudohexagonal packing (Figure 33).

Table 7. Comparison of Selected Structural Parameters (Å) in Compound **[15]**.

	{Cu_6}, PPN[a]	{Cu_6Cl}[b]	{Cu_6Cl}[c]	{Cu_6F}[d]
Cu…Cu (inter-trimer)	2.975(3), 2.999, 3.028 (3)	3.356(1)–3.401 (1)	3.621 (1), 3.675 (1)	3.281(2), 3.335 (2), 3.289 (2)
Cu…Cu (intra-trimer)	3.206(4)–3.279 (5)	3.180 (9)–3.253 (9)	3.209 (1), 3.233 (1)	3.234(2)–3.289 (2)
Cu…X		2.424(2), 2.4858 (14), 2.6221 (13) (X = Cl)	2.604 (1), 2.623 (2) (X = Cl)	2.383(5)–2.605 (5) (X = F)
Cu-(μ_3-OR)	1.883(1)–1.894 (5)	2.003 (2)–2.044 (2)	2.083(4), 2.085(6) (R = Me)	2.048(3)–2.096 (5) (R = H)
Cu—N (inter-trimer)	2.003(7)–2.056 (6)	2.003 (3)–2.004 (3)	1.990(5)–1.992 (7)	2.018(6)–2.047 (6)
Cu—N (intra-trimer)	1.934(7)–1.964 (7)	1.923 (3)–1.954 (3)	1.931(5)–1.941 (5)	1.942(5)–1.979 (6)

Notes: (a) ref [39]; (b) This work; (c) ref [61]; (d) ref [59]

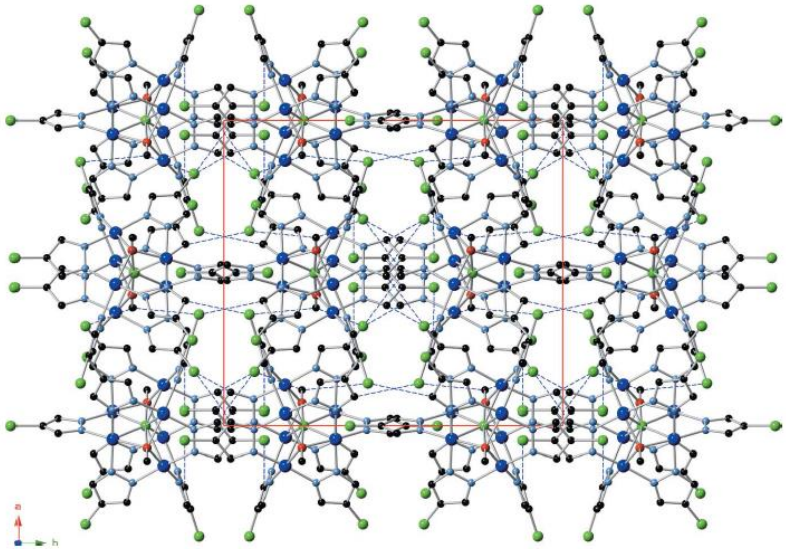

Figure 32. Crystal packing diagram of [15] viewed along [001], showing hydrogen bonds as blue dashed lines.

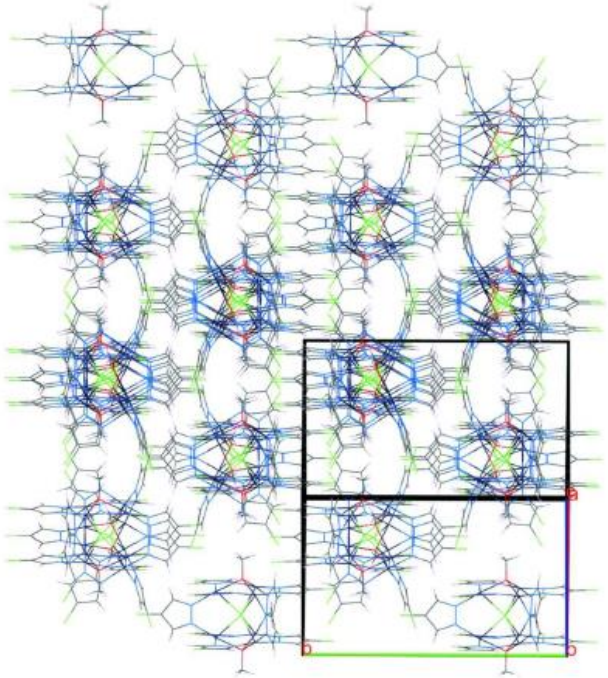

Figure 33. Crystal packing diagram of [15] viewed along [110], highlighting the pseudo-hexagonal rod packing of {Cu_6} molecules.

Table 8. Hydrogen Bond Geometry of [15] (Å, °)

D – H…A	D – H	H…A	D…A	D–H…A
C1–H1…Cl4^{i}	0.93	2.75	3.586(4)	149
C6–H6…Cl3^{ii}	0.93	2.81	3.466(4)	129
C15–H15A…Cl3^{iii}	0.96	2.82	3.651(4)	146

Symmetry codes: (ii) *x*−1/2, *y*+1/2, −*z*+1/2; (iii) −*x*+1/2, *y*−1/2, *z*; (iv) −*x*+1/2, −*y*+1/2, *z*+1/2.

2.2. Heptanuclear Copper-pyrazolate complexes

2.2.1. Synthesis

2.2.1.1. Synthesis of [{$Cu_3(\mu_3\text{-}OH)(\mu\text{-}4\text{-}Ph\text{-}pz)_3(4\text{-}Ph\text{-}pzH)(Cl)_2\}_2$][$Cu(CH_3CNHpz)_2$ ($\mu\text{-}Cl_2$)] [16] and $[PPN]_2$ [{$Cu_3(\mu_3\text{-}OH)(\mu\text{-}4\text{-}Ph\text{-}pz)_3Cl_3\}_2${$CuCl_2(4\text{-}Ph\text{-}pzH)_2$}] [17]

$CuCl_2{\cdot}2H_2O$ (0.6 mmol, 102.3mg), 4-Ph-pzH (0.9 mmol, 129.8 mg), NaOH (0.13 mmol, 52 mg), PPNCl (0.1 mmol, 57.4 mg) were added to 15 mL CH_3CN under stirring, the reaction mixture was stirred overnight, a small amount of a grey solid was filtered off and the solvent volume was reduced to 4 mL under reduced pressure. Suitable crystals for X-ray diffraction were grown by slow evaporation. Yield: 25%. Minor product is $[PPN]_2$[{$Cu_3(\mu_3$-OH)(μ-4-Ph-pz)$_3Cl_3\}_2${$CuCl_2$(4-Ph-pzH)$_2$}] **[17].**

2.2.1.2. Synthesis of $[PPN]_2$[{$Cu_3(\mu_3\text{-}OH)(\mu\text{-}4\text{-}Ph\text{-}pz)_3Cl_3\}_2${$Cu(\mu\text{-}Cl)_2(4\text{-}Ph\text{-}pzH)_4$}]·$(CH_3CN)_2$ [18]

$CuCl_2{\cdot}2H_2O$ (0.15 mmol, 25.6 mg), 4-Ph-pzH (0.2 mmol, 28.8 mg), NaOH (0.25 mmol, 10 mg), PPNCl (0.025 mmol, 14.4 mg) were added to 15 mL CH_3CN under stirring, the reaction mixture was stirred overnight, a small amount of a grey solid was filtered off and the solvent volume was

reduced to 4 mL under reduced pressure. Suitable crystals for X-ray diffraction were grown by slow evaporation. Yield: 72%.

2.2.2. Description of crystal structure

2.2.2.1. Crystal structure description of [{$Cu_3(\mu_3\text{-}OH)(\mu\text{-}4\text{-}Ph\text{-}pz)_3(4\text{-}Ph\text{-}pzH)(Cl)_2\}_2$] [$Cu(CH_3CN\ Hpz)_2(\mu\text{-}Cl_2)$] [16]

The Cu_4 atom is coordinated by two nitrogens from pyrazoles, two nitrogens from acetone and two μ_2-Cl atoms, forming a slightly distorted octahedron coordination geometry as a result of the John-Teller effect. The Cu- μ-Cl distance is 2.911(2) Å, Cu_1 and Cu_2 atoms are in square-planar geometries, Cu_3 are in square –pyramidal N_3ClO-coordination environments. Cu···Cu distances within triangular units are 3.243(1)-3.442(1) Å. The Cu4 weakly interacts with a chloride atom of the central of $Cu(CH_3CNHpz)_2Cl_2$ unit. Therefore, the coordination of the central mononuclear octahedral $Cu(CH_3CNHpz)_2Cl_2$ unit, in which a copper atom is occupying the inversion center of the heptanuclear assembly joining together two trinuclear units. The coordination environment of Cu(4) is completed by two chloride ions, axially bond through weak Cu-Cl interactions, generating octahedral trans-CuN_4O_2 units (Figure 34).

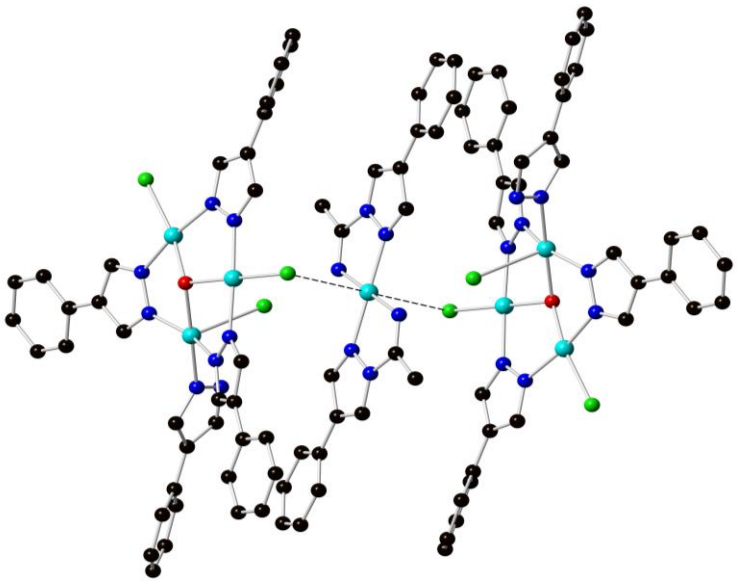

Figure 34. Molecular structure of [**16**] showing its polymeric character in different angles. H atoms and PPN counterions are omitted for clarity. Color codes: black, C; blue, N; red, O; green, Cl; cyan, Cu.

2.2.2.2. Crystal structure description of $[PPN]_2[\{Cu_3(\mu_3\text{-}OH)(\mu\text{-}4\text{-}Ph\text{-}pz)_3Cl_3\}_2\{CuCl_2(4\text{-}Ph\text{-}pzH)_2\}]$ [17]

The molecular structure of **[17]** consists of two trinuclear units of $[Cu_3(\mu_3\text{-}OH)(\mu\text{-}4\text{-}Ph\text{-}pz)_3Cl_3]^-$ weakly "bridged" by the copper atom of a $Cu(\mu\text{-}Cl)_2(4\text{-}Ph\text{-}pzH)_2$ fragment, which sits on the crystallographic center of symmetry (Figure 35). The copper center (Cu4) of this neutral moiety possess a N_2Cl_2 square-planar coordination sphere. Two pyrazole ligands trans-coordinated at a Cu^{II}-N distance of 2.007(3) Å and two chlorides trans-coordinated at a Cu^{II}-Cl distance of 2.338(2) Å. The Cu3- (μ_2-Cl4) distance is 2.964(2) Å, the broad range in Cu-Cl distance because of the hydrogen bond [μ_3-O…Cl] of 3.163(4) Å. In the triangular unit, Cu1 and Cu2 atoms adopt square-planar geometries with four-coordination mode, Cu3 atom exhibits square–pyramidal N_2Cl_2O-coordination environments, two nitrogens, belonging to two 4-phenyl-pyrazoles, one capping μ_3-O ligand and one terminal chloride define the equatorial plane of the square pyramid, while the bridging chloride atom occupies the apical position with Cu…Cl = 2.964(3) Å.

2.2.2.3. Crystal structure description of $[PPN]_2[\{Cu_3(\mu_3\text{-}OH)(\mu\text{-}4\text{-}Ph\text{-}pz)_3Cl_3\}_2\{Cu(\mu\text{-}Cl)_2(4\text{-}Ph\text{-}pzH)_4\}](CH_3CN)_2$ [18]

The crystal structure of **[18]** (Figure 36) is formed by repeating heptanuclear units consisting of two trinuclear $[Cu_3(\mu_3\text{-}OH)(\mu\text{-}4\text{-}Ph\text{-}pz)_3Cl_3]^-$ and one neutral mononuclear *trans*-$[CuCl_2(4\text{-}Ph\text{-}pzH)_4]$ complex, the latter located on a crystallographic inversion center. In the solid state, the trinuclear and mononuclear components are connected via long Cu–Cl interaction, as follows: The two trinuclear anions, containing 4-coordinate, distorted square planar Cu-centers and a pyramidal μ_3-OH (the O-atom is 0.478(1) Å away from the Cu_3-plane), have their Cu_3-planes approximately parallel to each other and are connected, via two long Cu(1)-Cl(2) contacts of 3.021(2) Å, into a $\{Cu_3\}_2$ assembly; the μ-Cl atoms occupy one equatorial and one axial position with a Cu(1)-Cl(2)-Cu(2) angle of 101.05(4)º. Then, the 6-coordinate mononuclear centers act as bridges between $\{Cu_3\}_2$ units, with a Cl…Cu distance of 2.744(2) Å, thus generating 1D chains running parallel to the crystallographic *a*-axis. The PPN counter ions and the interstitial MeCN solvent molecules occupy positions of no chemical significance separating the polymeric chain. The heptanuclear species are further connected by intermolecular by two long μ_3-OH···Cl(1) H-bonds (O···Cl 3.145(2) Å). The *trans*-$[CuCl_2(4\text{-}Ph\text{-}pzH)_4]$ complex shows a pronounced Jahn-Teller effect with long Cu-Cl bonds of 2.792(1) Å, but shorter than the corresponding bonds of 2.817– 2.839 Å reported for other *trans*-$[CuCl_2(pz^*H)_4]$ complexes (pz*H = pzH, 3-^{t}Bu-pzH and 3-Ph-pzH).[62–65] Considering all the long Cu–Cl contacts, the heptanuclear repeat unit of complex **[18]** contains one 4-coordinate, four 5-coordinate and one 6-coordinate Cu-centers. Table **10** summarizes selected interatomic distances and angles for **[18]**.

gg

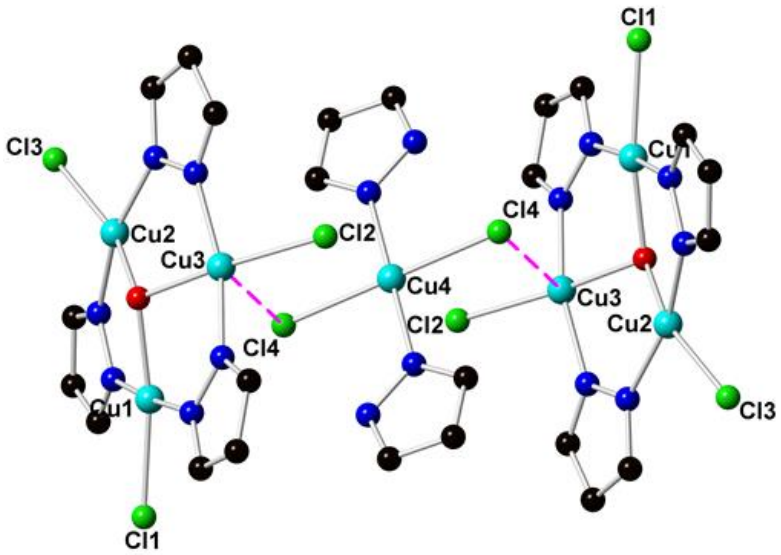

Figure 35. Crystal structure of [**17**]. Substitutions at 4 position on the pyrazole ring, PPN counterion and H atoms on **[17]** are omitted for clarity.

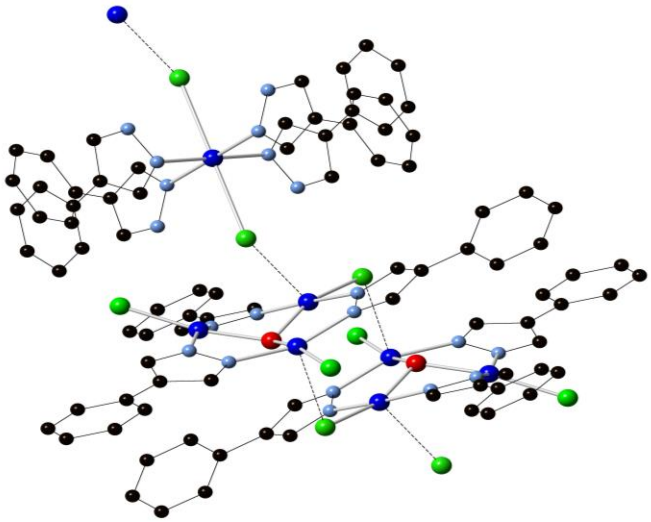

Figure 36. Molecular structure of **[18]** showing its polymeric character. Color coding: Cu, blue; O, red; N, light blue, C, gray and Cl, green. Hydrogen atoms are omitted for clarity.

Table 9. Selected Interatomic distances and angles for **[18]**.

	Distances, Å		Angles, °
Cu···Cu (inter-trimer)	3.244(1), 3.417(1), 3.451(1)	Cu-O-Cu	108.4(1)–118.3(1)
Cu–N (trimer)	1.948(3) –1.957(3)	Cu1-Cl1-Cu2	101.05(4)
Cu–Cl (trimer)	2.251(2) – 2.307(1)	Cu1-Cl4-Cu4	141.7(4)
Cu4–Cl4	2.791(2)		
Cu1-Cl4	2.744(2)		
Cu-(μ3-OH)	1.993(2) - 2.013(2)		

2.3. Conclusion

In this part, Cu_6-pyrazolato with trigonal prismatic shapes, including an an encapsulated μ_6-Cl central ligand was successfully synthesized. We have prepared two Cu_7-systems consisting of three weakly-interacting through Cl-bridging atoms -- two trinuclear Cu_3-pyrazolato metallacycles and a mononuclear Cu-pyrazole unit. The molecular structure of **[17]** consists of two trinuclear units of $[Cu_3(\mu_3\text{-OH})(\mu\text{-4-Ph-pz})_3Cl_3]^-$ weakly "bridged" by the copper atom of a $Cu(\mu\text{-Cl})_2(4\text{-Ph-pzH})_2$ fragment, which sits on the crystallographic center of symmetry. While the crystal structure of **[18]** is formed by repeating heptanuclear units consisting of two trinuclear $[Cu_3(\mu_3\text{-OH})(\mu\text{-4-Ph-pz})_3Cl_3]^-$ and one neutral mononuclear *trans*-$[CuCl_2(4\text{-Ph-pzH})_4]$ complex, the latter located on a crystallographic inversion center.

Chapter 3. Metal-Organic Frameworks based on Copper-Pyrazolato Complexes

3.1. Introduction

3.1.1. Definition of MOFs

Metal-organic frameworks (MOFs), also known as porous coordination polymers (PCPs), are compounds consisting of metal ions or metal clusters coordinated to predefined polydentate organic linkers to form three-dimensional extended structures. Metal organic frameworks have attracted significant attention in recent years not only because of their intriguing structural architectures and topologies, but also for their novel properties.[66,67] The adjustable pore size, high void volume, large surface area, ultrahigh porosity, and tunable functionality make MOFs useful materials for CO_2 capture,[68,69] gas separation and strorage,[70] catalysis,[9] magnetism,[71] ion exchange,[72] and drug delivery applications.[73]

The structure, function and porosity of a MOF can be modified by using a suitable geometry of the subunits of MOF, called Secondary Building Units (SBU), that are either organic or metal-containing. Reticular synthesis, as it was first described by Yaghi et al., is the use of predesigned combination of SBUs and linkers to obtain desired framework structures.[66] For example, using a tetrahedral SBU and a linear linker can be used to prepare diamondoid (dia) framework structures. These clusters used as SBUs can be of any shape such as triangles, squares, tetrahedral or octahedral (Figure 37), which can be linked to form periodic structures.[74] Secondary Building Units are essential to the design of directionality for the construction of MOFs and to the achievement of robust frameworks.

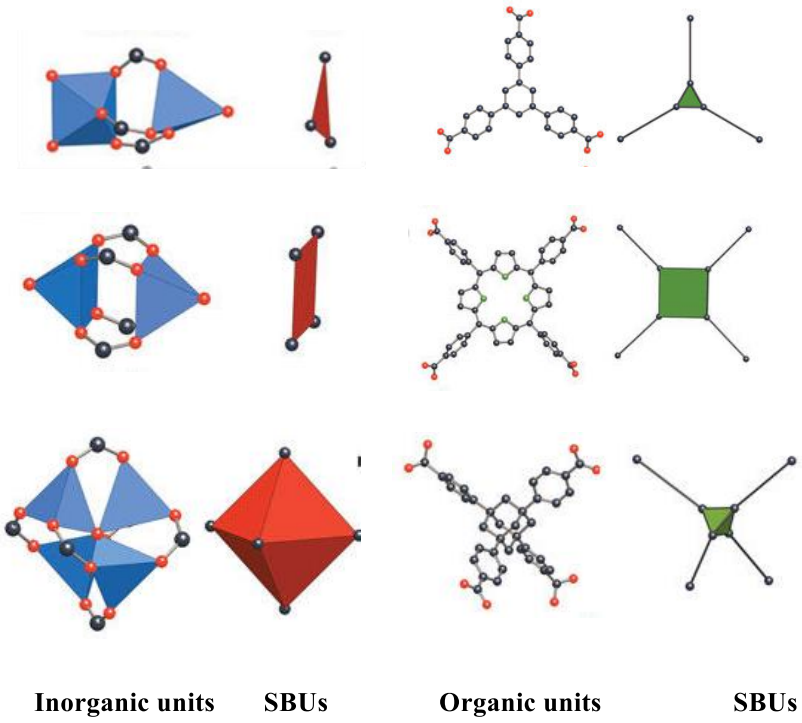

Figure 37. Examples of SBUs from carboxylate MOFs. C, black, O, red: N, green. Modified from Yaghi et al.[1]

With the availability of various linkers and SBUs, controlling various parameters one can target a specific MOF with desired functionality. Parameters that can influence property and function are described below.

3.1.2. Important parameters for rational design of MOFs

Variation of process (T, P, time) and compositional parameters (pH, solvent, molar ratio of reactants, ligands substituents, concentration, counterions), listed in Scheme 12, allows some control over the synthesis of MOFs.

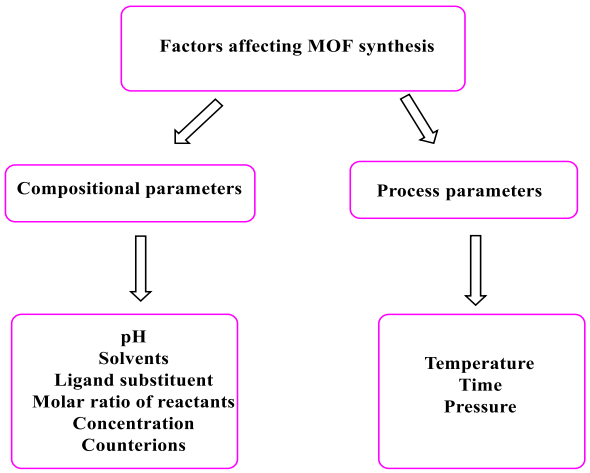

Scheme 12. Various parameters controlling the formation of MOFs.

3.1.2.1. Effect of pH

The pH of a reaction mixture has a remarkable influence in the assembly of supramolecular architectures. It not only affects its charge, but also the ligand coordination ability and the metal-to-ligand ratio. The influence of pH a MOF synthesis has been investigated by many research groups.[75–77] Wu and co-workers proposed that high pH leads to higher dimensionality in their systems. Hydrothermal reaction of copper(II), benzoic acid and 4'4-bipyrdine (bpy) at different pH conditions (Figure 38) yielded the 0D $[Cu(H_2O)(PhCOO)_2(bpy)_2](PhCOOH)_2 \cdot (bpy)$ complex at pH = 5.5, the 1D chain $\{[Cu_3(H_2O)_4\ (PhCOO)_6\ (bpy)_{4.5}].(bpy)(H_2O)_5\}$ at pH = 7, and the 2D layer structure $[Cu_3(OH)_2(H_2O)_2\ (PhCOO)_4(bpy)_2]$ at pH = 8. The role of pH in determining the above structures is attributed to its control on the extent of deprotonation of the organic acid.[78]

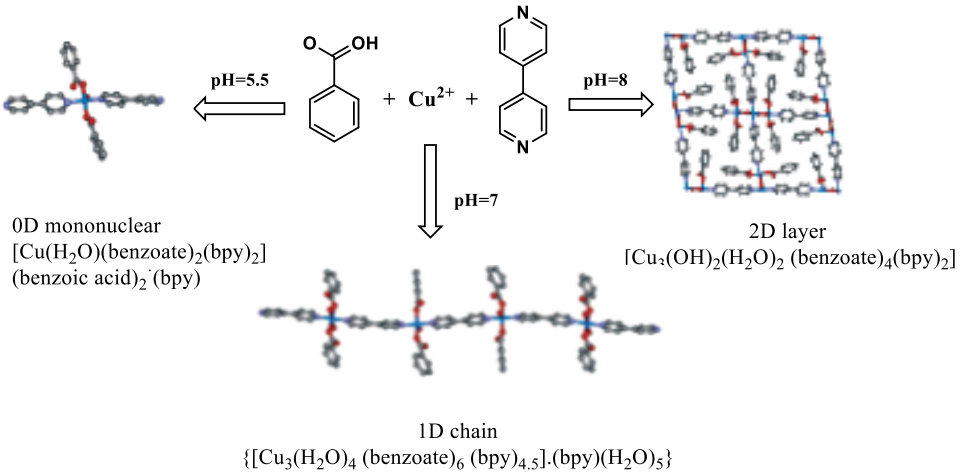

Figure 38. Systematic illustration of the assemble tendency of three Cu(II)-compounds under different pH values. Modified from zZheng et al.[14]

3.1.2.2. Effect of temperature

Temperature is also key parameter for the preparation of MOFs. Hydrothermal synthesis of MOFs is an effective approach in comparison with conventional and non-conventional synthetic methods. Thermodynamic reasoning argues against the formation of polymeric products at increasing temperature. However, the experimental evidence from several hydrothermal syntheses is that high temperature favors the construction of high dimensional MOFs.[79,80] This is because the reactants dissolve better under hydrothermal conditions (a closed system at temperature above 100 ºC and pressures above 1 atm).

3.1.2.3. Effect of solvent

Reaction solvents can regulate the formation of different coordination environments. Some solvents may become incorporated in the as-synthesized MOF, either as space-fillers in the lattice voids, or as coordinated entities to the metal ions.[81] As shown in Figure 39, Banerjee et al. synthesized two structurally different fluorinated MOFs, $[Cu_2(hfbba)_2(3\text{-mepy})_2]$ $(DMF)_2(3\text{-mepy})]$ (F-MOF-4) and

$[Cu_2(hfbba)_2(3\text{-mepy})_2]$ (Cu-F-MOF-4B) hfbba = 4, 4'-(hexafluoroisopropylidine)bis(benzoic acid), 3-mepy = (3-mepy-3-methyl pyridine) using DMF and DEF solvents, respectively, under the same reaction conditions, underlining that different solvents caused divergent MOF architecture: F-MOF-4 exhibits formation non-interdigitated square shaped pores and Cu-F-MOF-4B shows the formation of square-shaped pores with interdigitated layered structure. Depending their structural variety, gas adsorption is also different in these two MOFs.[82]

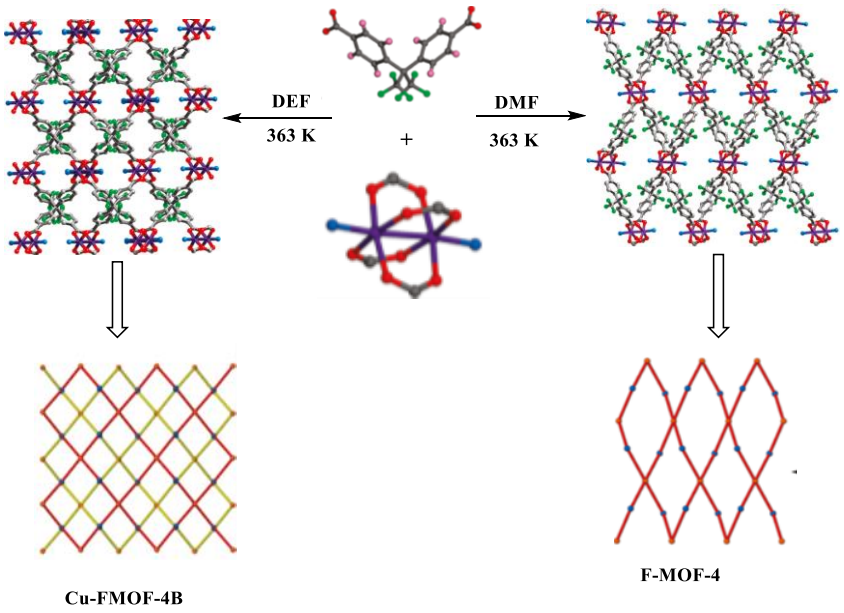

Figure 39. Formation of two isomeric frameworks. Figure modified from Pachfale et al.[18]

3.1.2.4. Coordination geometry of metal ions

Metal ions act as nodes in MOF structures and therefore play a central role in the synthesis of MOFs. Typical metal coordination geometries are shown in Scheme 13.

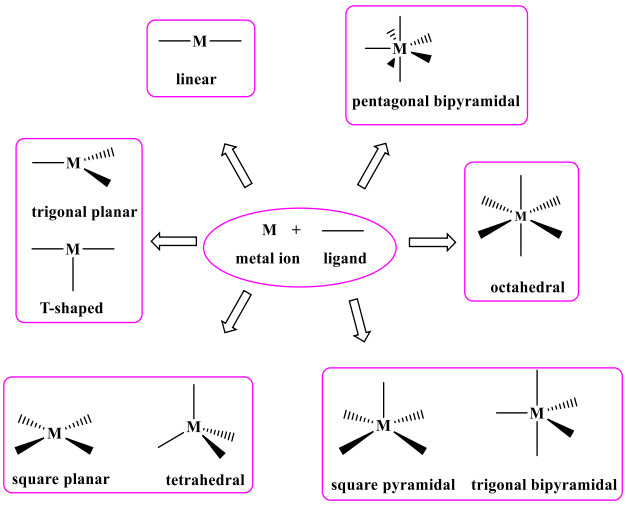

Scheme 13. Typical coordination geometries of transitional metal ions.

3.1.3. Porosity in MOFs

One of the most interesting properties of MOFs is their permanent porosity. MOFs can have high surface area and large pore volumes. The surface areas of permanently porous MOFs range from 100 m^2/g to greater than 7000 m^2/g and pore sizes range from a microporous (< 2 nm) to a mesoporous (2 – 50 nm) scale. The pore size and shape of MOFs can be easily modified by changing the nature of the organic linker or the connectivity of the inorganic moiety. As a result of the extraordinary property, MOFs can be used in adsorption (both in gas and liquid phases). It is essential to understand the applicability of porous MOF composites through adsorption phenomena.

A common strategy to increase porosity in MOFs consists of targeting a framework topology and elongating the linkers to generate additional pore space. This approach has shown suceess in a number of MOF systems. The expansion of organic linkers provides the possibility of preparing MOFs with new functionalities. The classical way to incorporate functional groups into MOF is the modification of the organic ligands with specific substituents before synthesizing the MOF (direct synthesis). Yaghi's research group has illustrated strategies to incorporate diverse

functionalities into MOFs. The first example of MOFs was the IRMOF series (IR stands for isoreticular, meaning it is a series of MOFs with the same topology), where the MOFs were modified with the incorporation of various organic functional groups, such as $-NH_2$, -Br, $-C_2H_4$, $-C_4H_4$, $-OC_3H_7$, $-OC_5H_{11}$, and their pore size was expanded with long molecular struts like biphenyl, pyrene and terphenyl without changing the topology.[83] As shown in Figure 40, a family of stable porous materials incorporating octaconnected linkers (ranging from ranging from 19 to 30 Å in dimension) and Cu(II) cation has been reported. The pores of these MOFs can be altered systematically by elongation of the ligands allowing a strategy of selective pore extension along one dimension. These materials show remarkable gas adsorption properties with high working capacities for CH_4 (0.24 g g^{-1} , 163 cm^3 cm^{-3} at 298 K, 5–65 bar) for the most porous system.[84]

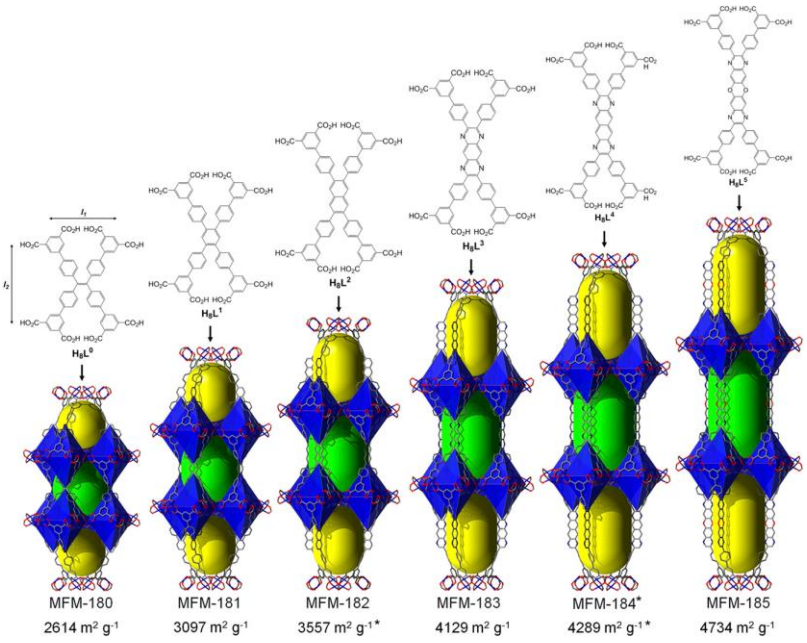

Figure 40. Chemical structures for the octacarboxylate linkers H8L0 to H8L5 used for the synthesis of MFM-180 to MFM-185, representation of the cage assembly in MFM-180, MFM-181, MFM-182, MFM-183, MFM-184 (* predicted structure) and MFM-185, and corresponding BET surface areas. Figure reproduced from Moreau et al.[84]

3.1.4. Separation of CO_2 from gas mixtures

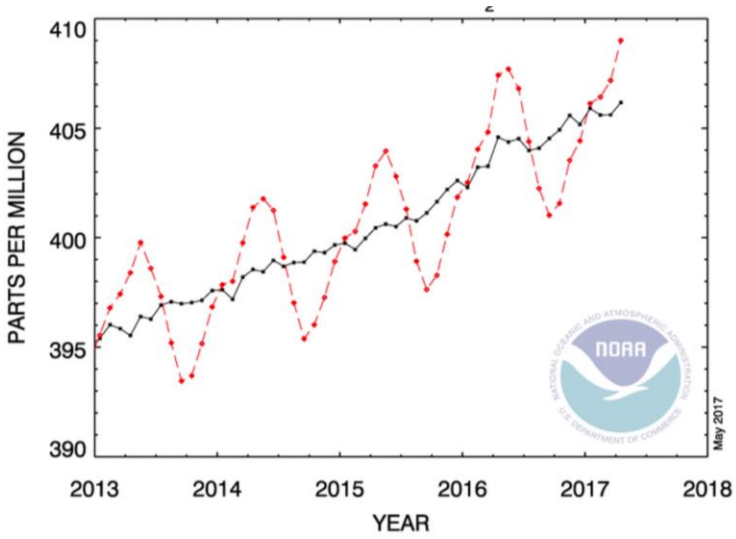

Figure 41. This graph shows carbon dioxide concentrations in the atmosphere as measured at the Mauna Loa observatory in Hawaii. Figure reproduced from Tom Yulsman.[85]

In recent year, carbon dioxide (CO_2) emission has become a major concern as the amount of the emitted gas significantly increase annually (Figure 41).[85] Consequently, this phenomenon contributes to global warming. Many options for CO_2 separation has been proposed. The main types of technology for CO_2 capture from flue gases are the following: absorption, adsorption, membrane separation and cryogenic distillation, etc (Figure 42).

The adsorptive separation process involves both adsorption and desorption. Physical adsorption is a process in which molecules (adsorbates) are bound on the surface of a highly porous solid (adsorbent). The desorption is the reverse process of adsorption, during which a bound molecule is released from the adsorbent. The operation of physical absorption is based on Henry's law. Carbon dioxide is absorbed under a high pressure and a low temperature, and desorbed at reduced pressure and increase temperature. Once captured, the CO_2 is then released by changing the adsorption

conditions. Pressure Swing Adsorption (PSA) is one of the most common regeneration techniques. Desorption is performed by reducing the total pressure in the adsorption column, since the adsorption capacity decreases with pressure. In the Temperature Swing Adsorption (TSA) process, the regeneration is carried out by heating the adsorbent material, reducing its adsorption capacity. The problems associated with the methods are in the thermal energy requirement (for TSA) and bed pressurization (for PSA). In the TSA technique has low thermal conductivity of the adsorbent bed, which causes difficulty in desorbing impurities and regenerating the adsorbent. TSA presents drawbacks, as heating and cooling the adsorbent are time consuming tasks (long time of desorption cycles).

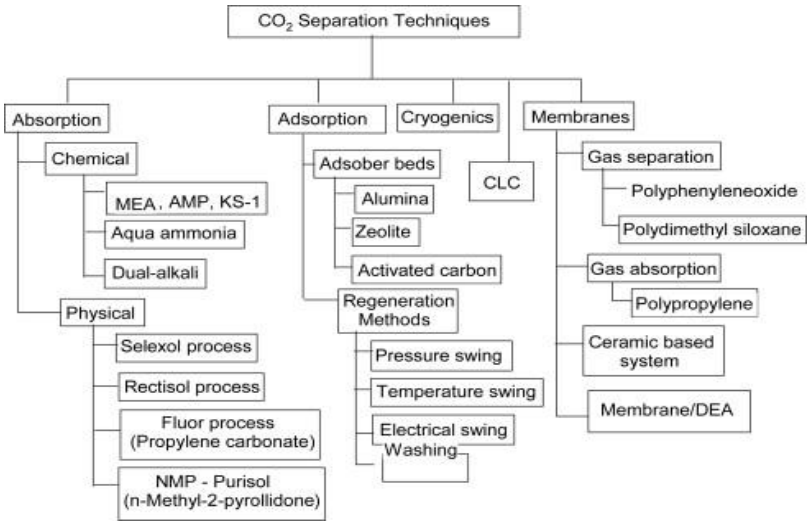

Figure 42. The technology option for CO_2 separation. Redrawn from Olajire et al.[21]

Departing from traditional temperature- and pressure -triggers to control adsorption and desorption, a process that can increase the temperature of the adsorbent very fast is Electric Swing Adsorption, where a low voltage electric current is employed to heat the adsorbent by the direct Joule effect. ESA is an attractive area and has been tested on MOFs or zeolites. A MOF that has either ligand- or metal-based redox activity can undergo various redox processes. In this case, which can generation of different redox states via ex situ oxidation and reduction of the materials. A further

issue relates to how redox activity might be exploited for industrial-scale gas separations processes (e.g., CO_2 separation from flue gas).

3.1.5. Classification of adsorption isotherms

When a gas comes into contact with a solid surface, molecules of the gas will adsorb to the surface in quantities that are a function of their partial pressure in a bulk. The measurement of the amount of gas adsorbed over a range of partial pressures at a single temperature results in a graph known as an adsorption isotherm. The IUPAC classification of adsorption isotherms is illustrated in Figure 43. The six types of isotherm are characteristic of adsorbents that are microporous (type I), nonporous or microporous (type II, III and VI) or mesoporous (types IV and V). These isotherms can have different shapes depending on the type of adsorbent, the type of adsorbate and intermolecular interaction between the gas and the surface. Type I isotherms characterize microporous adsorbents having relatively small external surfaces. Type II and III describe adsorption on microporous adsorbents with strong and weak adsorbate-adsorbent interactions, respectively. Type IV and V represent adsorption isotherms with hysteresis, and characterize mesoporous adsorbents, which arises from capillary condensation in mesopores. And type VI has steps, the isotherm represents stepwise multilayer adsorption on a uniform non-porous surface.

The adsorption hysteresis in Figure 44 (IV and V) are classified and it is widely accepted that there is a correlation between the shape of the hysteresis loop and the texture (e.g., pore size distribution, pore geometry, and connectivity) of a mesoporous material. Type H1 is often associated with porous materials consisting of well-defined cylindrical-like pore channels or agglomerates of approximately uniform spheres. Porous adsorbents, such as inorganic oxide gels and porous glasses, tend to give H2 kind of hysteresis and their pore size and shape are not well-defined. Type H3 loops

result from aggregates of plate-like particles giving rise to slit-shaped pores. Type H4 is also associated with narrow slit-like pores, but the Type I character is indicative of micro-porosity. The dashed curves in the hysteresis loops reflect low-pressure hysteresis, which may be associated with the change in volume of the adsorbent.

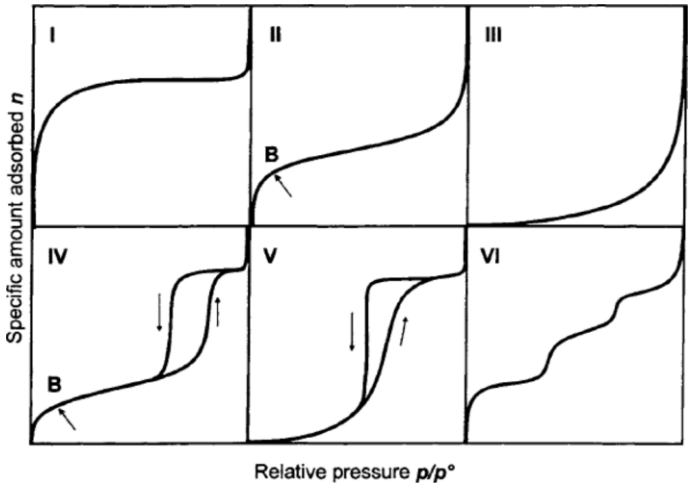

Figure 43. The IUPAC classification of adsorption isotherms showing both the adsorption and desorption pathways. Note the hysteresis in types IV and V. Figure reproduced from Alothman et al.[22]

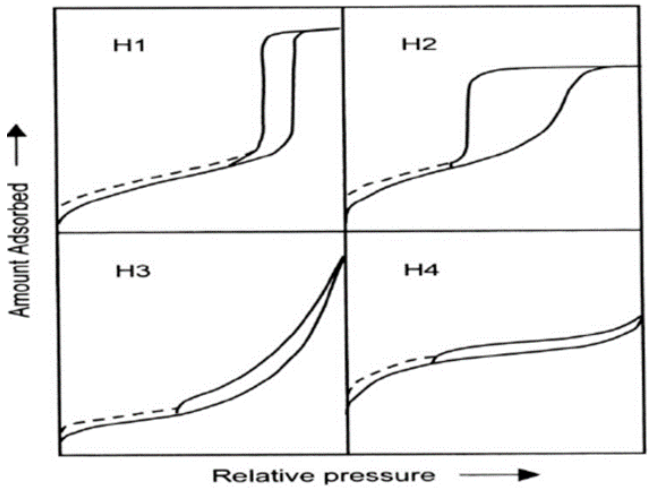

Figure 44. Four types of hysteresis loops identified by IUPAC. Figure reproduced from Althoman et al.[22]

3.1.6. CO_2 gas adsorption in MOFs

Several methods have been investigated for the disposal of carbon dioxide, such as carbon capture and sequestration(CCS) technologies.[86,87] Along with those traditional methods, the use of MOFs for the removal of CO_2 by adsorption is considered to be the most promising future cost-effective and efficient technology for the selective CO_2 removal.[88] In other words, MOFs have been considered as an ideal platform for the development of next-generation CO_2 capture materials. An appropriate CO_2 capture adsorbent should satisfy (i) low- cost raw materials, (ii) fast kinetics, (iii) low heat capacity, (iv) high CO_2 adsorption capacity and high CO_2 selectivity. Metal organic frameworks have attracted significant interest in the recent years due to their remarkable high surface area, controllable pore structures and tunable pore surface properties, which can easily be tuned by changing either the metallic clusters or the organic ligands.

Considerable techniques have been developed to enhance the capacity and selectivity for CO_2 adsorption. To make a MOF suitable for selective CO_2, the first requirement is to have pores with dimensions comparable to the kinetic diameter of CO_2. Because CO_2 has a quadruple moment, MOFs functionalized with -NH_2,[89] NO_2,[90] -CONH-,[91] -OH-,[92] -CN-,[93] -SO_3H,[94] or pyridine [95] show enhanced CO_2 adsorption. The grafting of functional groups with a high affinity for CO_2 onto the surfaces of porous materials through ligand modification, or coordination to unsaturated metal centers have been employed as strategies to enhance the capacity and selectivity for CO_2 adsorption. For example, because of the presence of pyridine nitrogen, the CO_2 uptake of bio-MOF-11 is 264 mg g^{-1} at 1 bar and 273 K,[89] compared to the lower adsorption capacities of traditional materials, such as Norbit RB_2 (110 mg g^{-1}) and zeolite 13-X (207 mg g^{-1}), at similar conditions.[96]

Second, designing frameworks containing open metal sites to enhance the capacity of CO_2 adsorption. Carbon dioxide adsorption has been investigated in large-pore sorbents [Cr_3F-

$(H_2O)_2O(bdc)]_3$ (MIL-100) and $[Cr_3F(H_2O)_2O(bdc)]_3$ (MIL-101), which exhibit higher capacities for CO_2 at relatively high pressure at 300 K, due to the presence of coordinatively unsaturated Cr^{3+} sites acting as CO_2 traps (i.e., O=C=O…Cr^{3+}).[97] The influence of the metal center on the capacity and selectivity of CO_2 adsorption has been studied in the microporous metal-organic framework $[Ni_2(dhtp)]$ (H_4dhtp = 2,5-dihydroxyterephthalic acid). As shown in Figure 45, this framework is characterized by a honeycomb structure with large micropores of 11-12 Å diameter, and a high concentration of open metal sites. These sites play a major role in the adsorption of CO_2. It shows distinct end-on CO_2 coordination to coordinatively unsaturated nickel sites giving rise to high CO_2 adsorption capacity at sub-atmospheric pressures and ambient temperatures (Figure 46). Infrared studies confirmed an end-on coordination mode for CO_2, with the increased ionic character of Mg^{2+}–O interaction.[98]

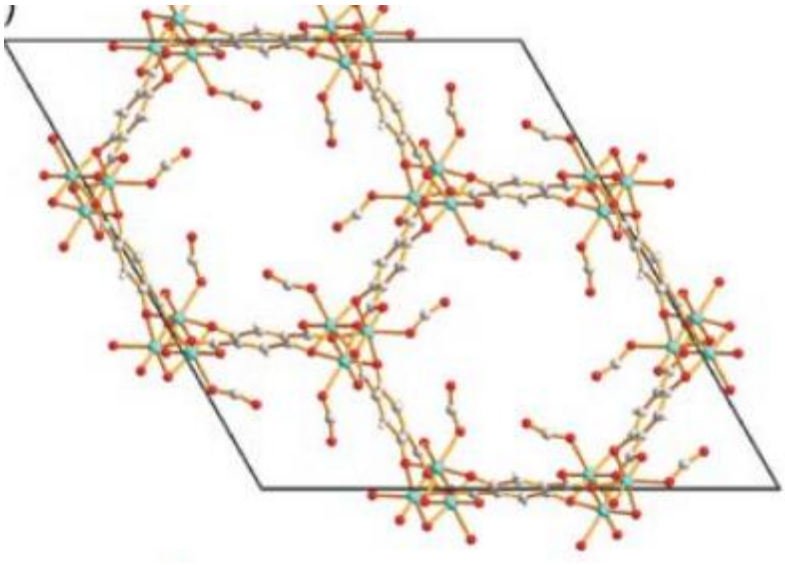

Figure 45. Crystal structure of $[Ni_2(dhtp)]$ with adsorbed CO_2 at the metal atom. Packing showing the end-on coordination of the CO_2 molecules. Figure reproduced from Dietzel et al.[35]

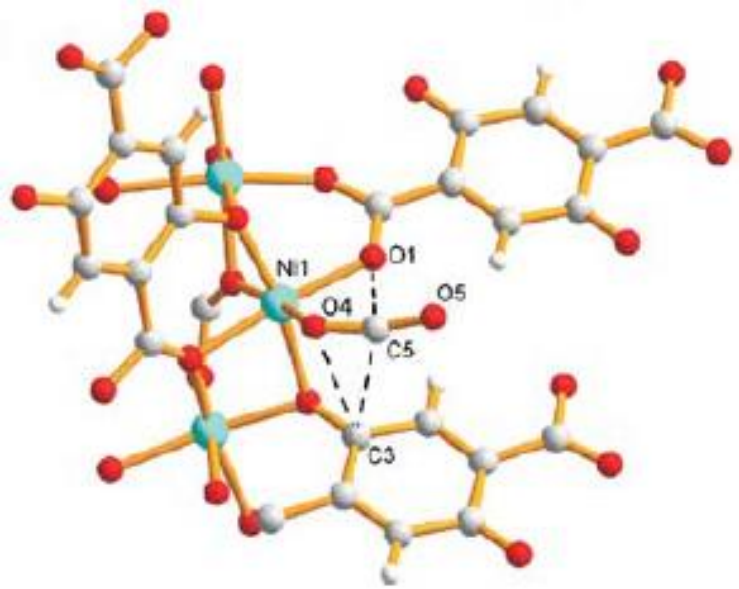

Figure 46. Crystal structure of [Ni_2(dhtp)] with adsorbed CO_2 at the metal atom. Local environment of the adsorbed CO_2 molecule. Figure reproduced from Dietzel et al.[35]

3.1.7. Statement of problem

MOFs have been considered to be the most promising future cost-effective and efficient technology for the selective CO_2 adsorption.[99,100] Several methods have been investigated for the disposal of carbon dioxide, such as carbon capture and sequestration (CCS) technologies.[87] A variety of these candidate materials with permanent porosity have been successfully synthesized. However, their regeneration cost is still high, due to the use of temperature swing adsorption (TSA), pressure/vacuum cycle or some combination of these processes. Departing from traditional temperature- and pressure-triggered regeneration techniques on MOFs, and designing reversible redox- or photo-active MOFs that will vary their structural and porous features is challenging. On the other hand, it will reduce the cost and energy required for regeneration by applying voltage or UV irradiation.

Recently, substantial progress has also been made in the field of porous MOFs by using excellent pyridyl N,N'-donor spacer ligands.[101] The exo-bidentate pyridyl derivates, 1,2-di(4-pyridy l)ethylene (bpe) and 4,4'-azopyridine (abp) possess several peculiar characteristics when employed in the construction of porous frameworks: (i) abp and bpe can be used as photoswitchable tailor-made spacers, good candidates for coordination polymers with photo-dimerization reactions.[102] (ii) Abp containing the -N=N- (azo) functional group play an important role in selective adsorption, due to the ability of the polar azo group to act as Lewis basic sites to interact with CO_2 moleclules effectively.[90,103] (iii) Introduction of stimuli-responsive functional groups in a pyridyl N,N'-donor linker can also play a crucial role in altering the porosity of the resulting MOFs.[104] (iv) As a conjugated bipyridine ligand, bpe can act as an electron acceptor through alkylation.[105] (v) 4'4-azopyrdine was found to be reducible in situ to a flexible ligand 1,2-bis(4-pyridyl)hydrazine.[106,107] In this project, we will concentrate on two synthetic goals: the introduction of MOF components that will allow the reversible photochemical or electrochemical modification of structure and sorption properties of MOFs.

3.1.8. Redox and photochemical modification on MOFs

3.1.8.1. Photo-active modification of CO_2 adsorption on MOFs

Metal organic frameworks (MOFs) can be designed, synthesized and functionalized to include photo-switchable linkers, such as azobenzene, diarylethene, spyropyran, etc. Typical chromophores as functional groups can undergo photochemical reactions (*cis-trans* isomerization or cycloaddition) upon UV irradiation or heating.[108] The rationale of this strategy is that MOFs containing photo-responsive components will be able to change the pore shape or size by a photo-chemical reaction. A MOF designated as PCN-123 (PCN stands for porous coordination network) has been synthesized from 2-(phenyldiazenyl)terephthalate and $Zn(NO_3)_2 \cdot 6H_2O$ in (N,N-diethylformamide

(DEF) via a solvothermal reaction. The functional group (the acid form of ligand) undergoes trans-to-cis conformational change by irradiation with visible light, as shown in Figure 47. Carbon dioxide adsorption has been measured to study the effect of the trans-cis isomerization of the ligand. Upon UV irradiation, the total uptake of CO_2 decreased as consequence of the change of conformation of azobenzene groups inside the pores of the MOF (Figure 49). This demonstrates that the selectivity and regeneration efficiency of the sorbent can be modulated by an external stimulus.[109]

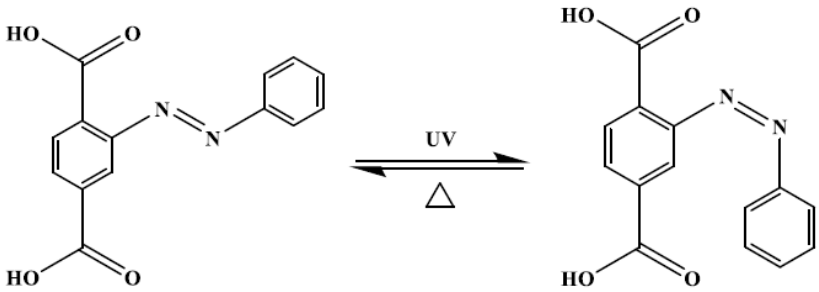

Figure 47. Reversible trans-cis isomerization of the ligand of PCN-123. Redrawn from Park et al.[39]

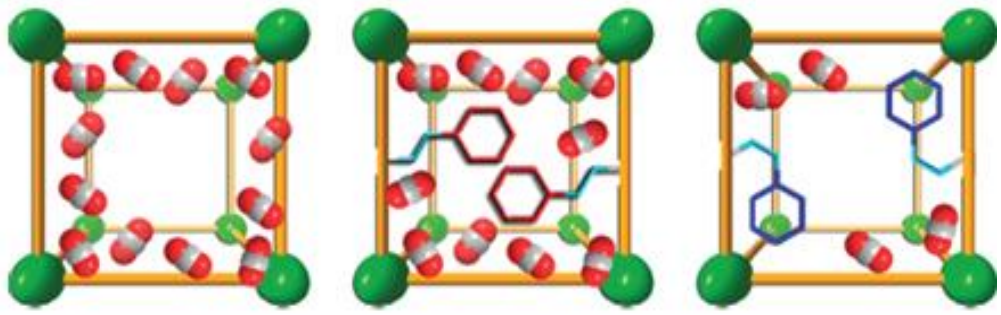

Figure 48. Schematic illustration showing suggested CO_2 uptake in showing in MOF-5, PCN-123 trans, and PCN-123 cis. Figure reproduced from Park et al.[39]

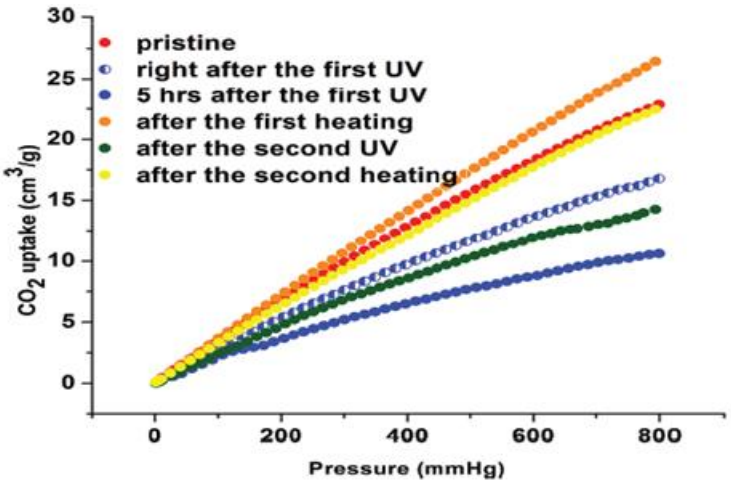

Figure 49. CO_2 adsorption isotherms of PCN-123, reversible conformational change at 295 K. Figure reproduced from Park et al.[39]

3.1.8.2. Redox-active modification of CO_2 adsorption on MOF

Metal organic frameworks (MOFs) are also able to alter their framework charge by redox reactions. Redox modification of a MOF will result in modulation of its affinity for sorbate molecules and change its overall sorption capacity. The enhancement in selective gas adsorption can also be achieved by chemical reduction of MOFs by incorporating a flexible redox-active ligand or metal. A new microporous framework, [Zn(NDC)(DPMBI)] (Figure 50), (where NDC = 2,7-naphthalene dicarboxylate and DPMBI = N, N'-di-(4-pyridylmethyl)-1,2,4,5-(benzenetetracarboxydiimide) reacts with a single-electron reductant, sodium naphthalenide (NaNp), to form monoradical anion of the pyromellitic diimide ligand in the framework [Zn(NDC)(DPMB-I)]·Na_x (where *x* represents the Na+/Zn^{2+} molar ratio of 0.109, 0.233, 0.367 and 0.378 from ICP-AES, Table 10). As shown in Figure 51, the CO_2 uptake in the reduced materials relative to the neutral framework is enhanced up to a Na^+/Zn^{2+} molar ratio of 0.367; however, beyond this concentration the surface area and CO_2 uptake decreases because of pore obstruction.[110]

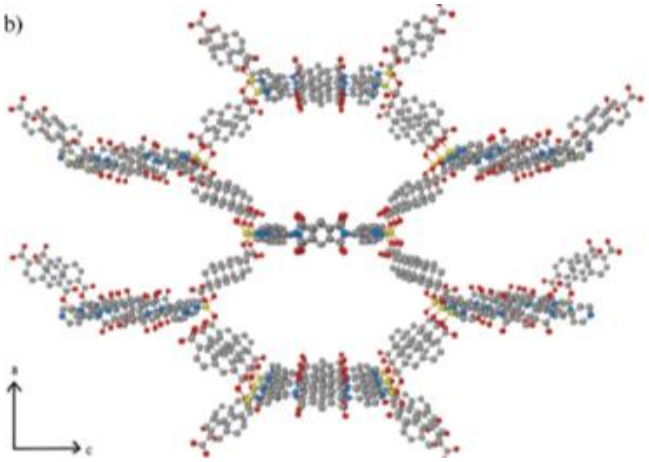

Figure 50. The extended crystal structure of a single Zn(NDC)(DPMBI) framework viewed down the b axis where hydrogen atoms. Figure reproduced from leong et al.[40]

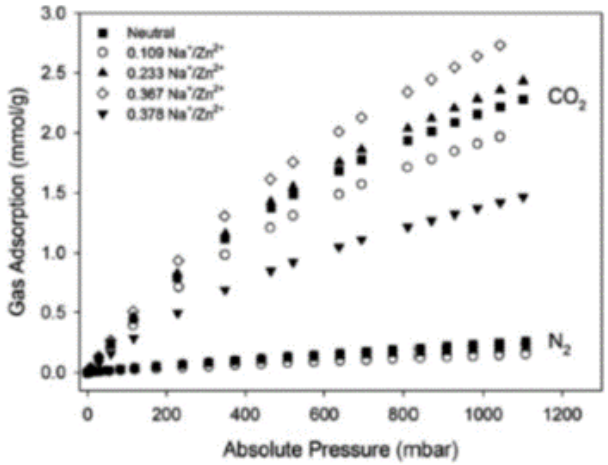

Figure 51. CO_2 and N_2 adsorption isotherms for Zn(NDC)(DPMBI) and its reduced species at 298 K. Figure reproduced from leong et al.[40]

Table 10. BET surface areas measured at 77 K and CO_2 adsorption data at 298 K and 1 atm for [Zn(NDC)(DPMBI)] and its reduced species.

Molar ratio Na^+/Zn^{2+}	BET surface area (m^2g^{-1})	CO_2 uptake (mmol g^{-1})
0.378	345.2±0.1	1.42
0.367	653±3	2.74
0.233	539.9±0.6	2.37
0.109	546.2±0.2	1.97
-	608.2±0.7	2.23

3.2. Synthesis and characterization of network of trimers containing triangular copper pyrazolate SBUs.

3.2.1. Synthesis

3.2.1.1 Synthesis of $[Cu_6(\mu_3\text{-}OMe)_2(\mu_4\text{-}Cl)(\mu\text{-}4\text{-}Ph\text{-}pz)_8Cl]_2[bpe]\{Cu_6\text{-}bpe\text{-}Cu_6\}$ [19]

$CuCl_2 \cdot 2H_2O$ (0.12 mmol, 20.5 mg), 4-Ph-pzH (0.12 mmol, 17.3 mg), NaOH (0.16 mmol, 6.4 mg) were stirred in 5mL CH_2Cl_2 for 2 hours at ambient temperature. The green solution was transferred to a test tube after filtration. A 4 mL 1:1 mixture of CH_2Cl_2: MeOH was layered over the CH_2Cl_2 layer, and a third layer of 1,2-di(4-pyridyl)ethylene (bpe) (0.02 mmol, 3.8 mg) in 5mL of MeOH was layered on top. Green crystals suitable for X-ray diffraction appeared gradually on the tube wall over two weeks.

3.2.1.2. Synthesis of $[Cu_6(\mu_3\text{-}OMe)_2(\mu4\text{-}Cl)(\mu\text{-}4\text{-}Ph\text{-}pz)_8Cl]_2[abp]\{Cu_6\text{-}abp\text{-}Cu_6\}$ [20]

A procedure similar to that used for **[19]** was followed but using piperidine (0.16 mmol, 16 µL) and abp instead of NaOH and abp, respectively.

3.2.2. Results and discussion

Complex **[19] and [20]** crystalize in triclinic p-1 space group. Both compounds are first examples of two trigonal prismatic Cu_6-units connected by a linker. The trigonal hexanuclear centers themselves are unique in a sense that they have two "clipping" pyrazolato ligands. The X-ray crystal structure of **[19]** consists of two $[Cu_6(\mu_3\text{-}OMe)_2(\mu_4\text{-}Cl)(\mu\text{-}4\text{-}Ph\text{-}pz)_8Cl]$ units bridged by a bpe ligand (Figure 52). Each trinuclear unit accommodates a μ_3-OMe as the capping ligand and it sits 0.845(3)-0.725(3) Å above the Cu_3-plane, the two μ_3-O atoms are 5.828(5) Å apart. The inter-trimer Cu···Cu distances are 3.554(9), 3.555(9) and 5.845(1) Å, while the intra-trimer Cu···Cu are in the range of 3.191(7) to 3.384(8) Å. The Cu-N_{bpe} and Cu-N_{pz} bond lengths are 2.032(4), 1.915(4)-1.991(4) Å respectively. In each trinuclear unit, two copper atoms are in a square pyramidal N_3OCl coordination environment if taking into account the interactions with Cl at 2.591(1)-2.680(2) Å, while the third copper is in N_2ClO distorted square planar coordination sphere (Figure 53).

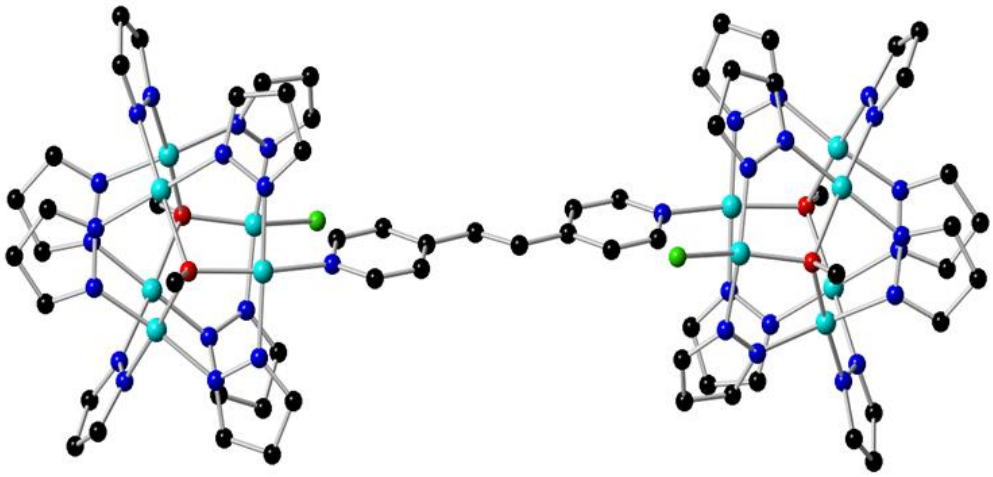

Figure 52. Crystal structure of $[\{Cu_6(\mu_3\text{-}OMe)_2(\mu_4\text{-}Cl)(\mu\text{-}4\text{-}Ph\text{-}pz)_8Cl\}_2(bpe)]$ [**19**]. H atoms were omitted for clarity.

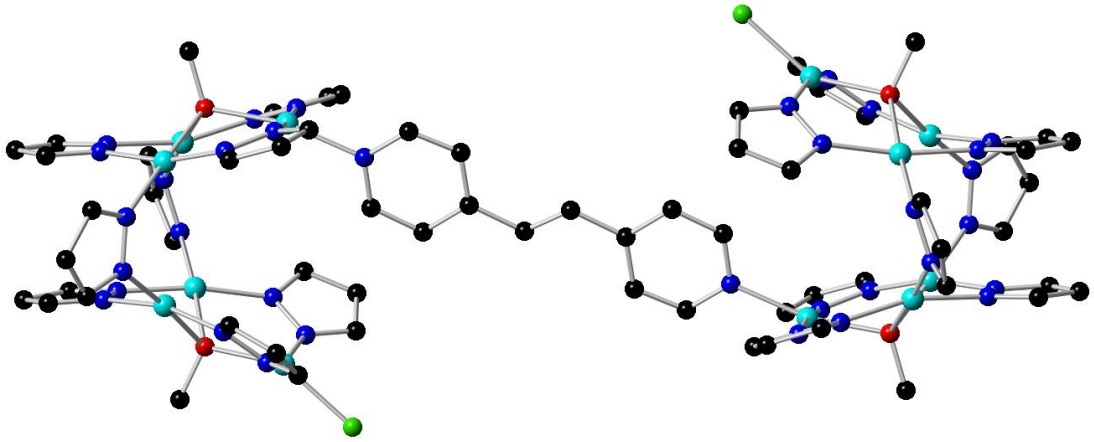

Figure 53. Crystal structure of [{$Cu_6(\mu_3\text{-}OMe)_2(\mu 4\text{-}Cl)(\mu\text{-}4\text{-}Ph\text{-}pz)_8Cl\}_2$(bpe)] **[19]** from different angles.

An isostructural dimer [$Cu_6(\mu_3\text{-}OMe)_2(\mu_4\text{-}Cl)(\mu\text{-}4\text{-}Ph\text{-}pz)_8Cl]_2$[abp]{$Cu_6$-abp-$Cu_6$} **[20]** was prepared using abp as the linker instead of bpe in a similar procedure. In these two complexes, we will focus on studying their photochemical reactivity and spectroscopic properties to facilitate analyzing similar features in their polymeric, 3D-MOF analogues.

3.3. Synthesis and characterization of dimers-of-trimers of copper-pyrazolate complexes

The simple dimer-of-trimer complex is synthesized as model of the photochemical reaction with UV light, 4,4'-azopyridine (abp) is used as photo-responsive linker that can undergo photo-chemical reactions to switch their conformation upon UV irradiation.

3.3.1. Synthesis of [{$Cu_3(\mu_3\text{-}OH)(\mu\text{-}4\text{-}Cl\text{-}pz)_3(py)_2\}_2(\mu\text{-}abp)](ClO_4)_4$ [21]

4,4-azobis(pyridine) (0.017 mmol, 3.1 mg) in 4mL CH_2Cl_2 was placed in the test tube, then a 4 mL 1:1 mixture of CH_2Cl_2 and acetone was layering as the blank solvent. Then $Cu(ClO_4)_2 \cdot 6H_2O$ (0.1 mmol, 37.1 mg), 4-Cl-pzH (0.1 mmol, 10.3 mg), NaOH (0.17 mmol, 6.7 mg), py (0.07 mmol, 5.4 µL) were stirred in 4 mL acetone for 24 h. The bright blue solution after filtration was added as

third layer on top of the lower two after filtration. Blue crystals were gradually obtained on the walls of the tube in the one week.

3.3.2. Crystal structure description of [{$Cu_3(\mu_3$-OH)(μ-4-Cl-pz)$_3$(py)$_2$}$_2$(μ-abp)](ClO$_4$)$_4$ [21]

Complex **[21]** crystalizes in orthorhombic *Fddd* space group. As shown in Figure 54, it is a dimer–of– trimers containing two [{$Cu_3(\mu_3$-OH)(μ-4-Cl-pz)$_3$(py)$_2$}$^{2+}$ units bridged by 4,4-azobis(pyridine) (abp), each triangular unit has two pyridines at terminal sites. Two triflate anion (for charge balance per Cu_3 unit) are coordinated on the opposite external faces of trimers. The distance of capping μ_3-O from the plane defined by the Cu_3 system [0.46(5) Å] as well as Cu-O1 bod distances [Cu1-O1 1.989(5) Å, Cu2-O1 2.000(5) Å, Cu3-O11.989(5) Å] fall in the range normally found for analogous compounds. Similar compound [{$Cu_3(\mu_3$-OH)(μ-pz)$_3$ (py)$_2$}$_2$ (μ-4,4'-bpy)](CF$_3$SO$_3$)$_4$ have been reported in the literature.[16]

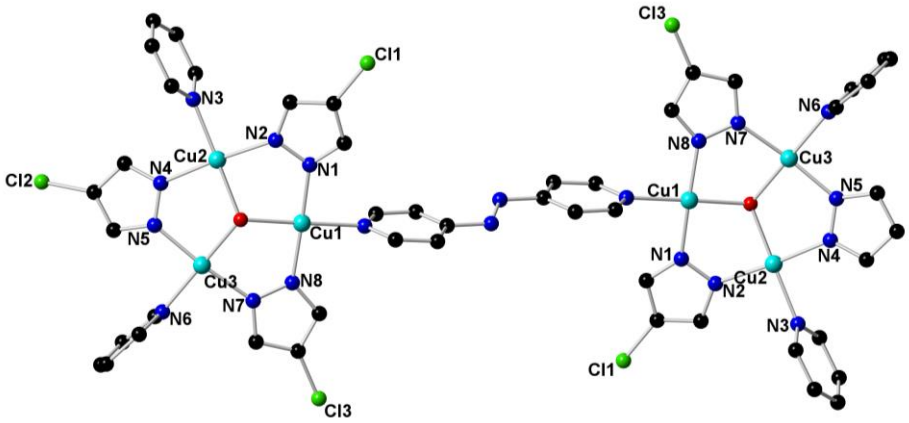

Figure 54. Structure of [{$Cu_3(\mu_3$-OH)(μ-4-Cl-pz)$_3$(py)$_2$}$_2$(μ-abp)](ClO$_4$)$_4$ **[21]**, H atoms and ClO$_4$ ions are omitted for clarity.

3.3.3. Preliminary results of photo-chemical reaction of dimer–of –trimers.

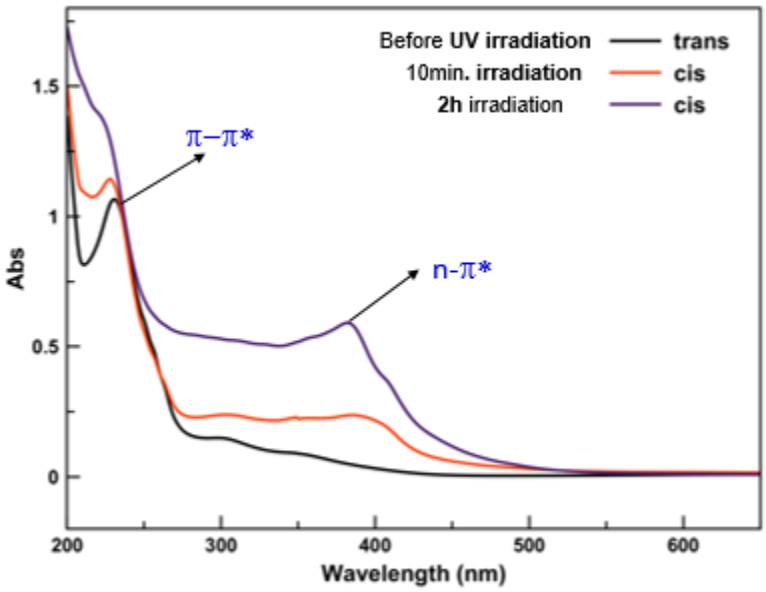

Figure 55. UV irradiation of [{$Cu_3(\mu_3\text{-}OH)(\mu\text{-}4\text{-}Cl\text{-}pz)_3(py)_2\}_2(\mu\text{-}abp)](ClO_4)_4$ **[21]** at 254 nm in CH_3CN.

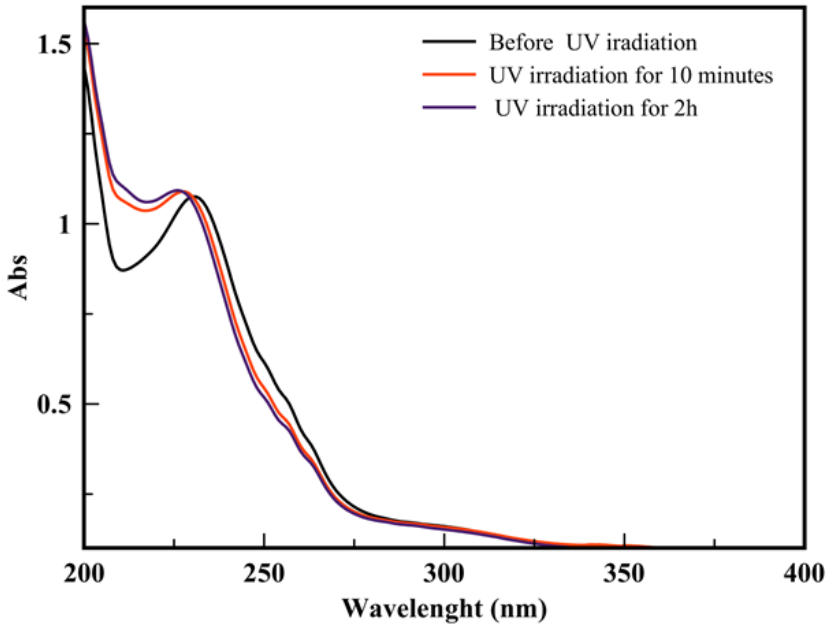

Figure 56. UV irradiation of [{$Cu_3(\mu_3\text{-}OH)(\mu\text{-}4\text{-}Cl\text{-}pz)_3(py)_2\}_2(\mu\text{-}abp)](ClO_4)_4$ [**21**] at 365 nm in CH_3CN.

To identify how the MOFs respond to UV-irradiation, model compounds were first chosen, which was then followed by the irradiation of MOFs. The model compound was irradiated at two wavelengths (254 and 365 nm) for 10 minutes and the change in the absorption spectra indicates a structural change (Figure 55 and 56). We are attempting to structurally characterize irradiation products.

3.4. Synthesis of 1D chain based on the trinuclear $[Cu_3(\mu_3\text{-}OH)(\mu\text{-}pz)_3]^-$ moiety

3.4.1. Experiment

3.4.1.1. Synthesis of $\{[Cu_3(\mu_3\text{-}OH)(\mu\text{-}Cl)(\mu\text{-}pz)_3Cl(tmpy)(CH_3CN)]\}_n$ [22] and $\{[Cu_3(\mu_3\text{-}OH)(\mu\text{-}Cl)(\mu\text{-}pz)_3Cl]_2(tmpy)_2](CH_3CN)_2\}_n$ [23]

$[PPN]_2[Cu_3(\mu_3\text{-}O)(\mu\text{-}pz)_3Cl_3]$ (0.013 mmol, 20 mg) and 4,4′-Trimethylenedipyridine (tmpy, 0.006 mmol, 1.2 mg) were added to 10 mL CH_3CN under stirring. The reaction mixture was filtered after 24 h and slow evaporation of the filtrate in air yielded well-formed light blue stable crystals of **[22]**, suitable for a single crystal X-ray diffraction (SC-XRD) determination. After removal of the crystals of **[22]**, the mother liquor was allowed to further concentrate by evaporation, finally yielding a second crop of dark blue crystals of **[23]**. The crystals of **[23]** quickly turned into powder upon loss of solvent by standing in the air. The SC-XRD determination of [**23]** was carried out at low temperature (200 K) with a crystal covered in mineral oil. Yield: 60%. Elemental analysis calcd (%) for $C_{28}H_{32}Cl_2Cu_3N_{10}O_2$: C, 38.10; H, 3.78; N, 16.17. Found: C, 37.19; H, 3.81; N, 15.75.

3.4.1.2. Synthesis of {[$Cu_3(\mu_3\text{-}OH)(\mu\text{-}Cl)(\mu\text{-}pz)_3Cl(tmpy)](CH_3CN)\}_n$ [24]

Complex **[24]** was synthesized in a similar way as described for **[22]**, by changing the molar ratio to 2:1.5, instead of 2:1. Yield: 40%. Elemental analysis calcd (%) for $C_{44}H_{48}Cl_4Cu_6N_{16}O_2$: C, 39.11; H, 3.58; N, 16.60. Found: C, 38.74; H, 3.67; N, 16.56.

3.4.2. Results and discussion

Synthesis of complexes **[22]**– **[24]**: Compound **[22]** and **[23]** were obtained with molar ratio of tmpy to $[PPN]_2[Cu_3(\mu_3\text{-}O)(\mu\text{-}pz)_3Cl_3]$ of 1:2 in CH_3CN. When the molar ratio was changed to 1.5:2 compound **[24]** was synthesized under identical conditions. All three compounds were crystallized from the mother liquor and have the same chemical formula but different 3D structures.

The organic ligands (linkers) can exhibit different conformations to produce diverse structures.[111,112] Among the N-donor bridging ligands, 4,4'-trimethylenedipyridine (tmpy) has been used as a flexible N-donor ligand for the construction of several coordination polymers with various network topologies and structure motifs.[113,114] The flexible nature of the $-(CH_2)_3-$ spacer allows it to rotate freely and adopt TT, TG, GG, or GG' conformations (T = trans and G = gauche) with respect to the relative orientations of CH_2 groups, that display quite different N-to-N distances (Scheme 14).[115] Obviously, this kind of conformational freedom allows supramolecular isomerism, including different supramolecular arrays,[116] interpenetrated[117] and helical[118] structures.

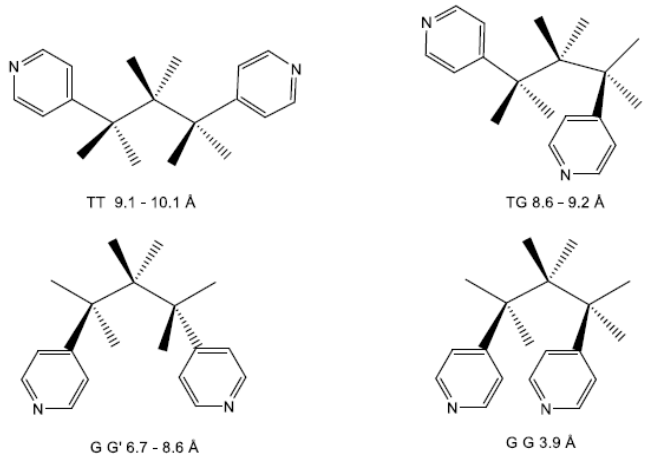

Scheme 14. Representation of the conformational isomers of the tmpy ligand.

3.4.2.1 crystal structure description of {[$Cu_3(\mu_3\text{-}OH)(\mu\text{-}Cl)(\mu\text{-}pz)_3Cl(tmpy)(CH_3CN)]\}_n$ [22]

Compound **[22]** crystallizes in the orthorhombic *Pnma* space group. The asymmetric unit consists of one-half formula unit, the other half generated by a mirror plane bisecting the trinuclear motif perpendicularly to the Cu_3-plane. As shown in Figure 57, Cu2 ion connect two Cu1 ions (Cu1, $Cu1^i$) through μ-OH bridge to form the trinuclear Cu_3 cluster in **[22]**. The distance between μ_3-OH and Cu^{2+} [Cu1-O1 1.975(4), Cu2-O1 1.966(6) Å] are in the range commonly found in [$Cu_3(\mu_3$-OH)] compounds reported in the literature.[14,22,49,119] The capping oxygen is 0.53(6) Å out of [$Cu_3(pz)_3$] plane, a value comparable to those found in the analogous derivatives. Three Cu ions form an isoscleles triangle [Cu1…Cu2 3.387 (1), Cu1…$Cu1^i$ 3.094 (1) Å. In each trinuclear unit, the two symmetry equivalent Cu ions exhibit a square pyramidal coordination geometry with μ_3-OH, pyrazolate nitrogens [Cu1-N1 1.962(5), Cu1-N4 1.978(5) Å], and tmpy nitrogen [Cu1-N3 2.013(5) Å] in the equatorial positions, while the coordinated μ-Cl [Cu1-Cl1 2.635(2) Å] occupies the axial sites. Cu2 adopts distorted square planar coordination geometry with μ_3-OH, two nitrogens from pyrazolate ligands [Cu2-N2 1.954(6), Cu2-$N2^i$ 1.954(6) Å]. This Cu2 atom bears a Cl ligand

[Cu2-Cl2 2.267(3) Å] end-capping the polymer and preventing further polymerization to an additional dimension.

Compound **[22]** is a 1D chain based on trinuclear Cu_3 clusters running along the crystallographic *a* axis bridged by tmpy ligands (Figure 58). The tmpy ligand in the TT conformation presents an N…N distance of 9.520 Å with Cu…Cu separation of 12.682 Å and Cu-tmpy-Cu angle is 119.42°. The tmpy spacers link adjacent trinuclear [$Cu_3(\mu_3$-OH)(μ-Cl)(μ-pz)$_3$Cl] SBUs generating a zigzag, parallel, 1D coordination polymer, which are shown in Figure 58. On dimensional parallel chains of **[22]** do not interact with each other (Figure 59). Two similar structures of {[$Cu_3(\mu_3$-OH)(μ-pz)$_3$(py)(μ-4,4'-bpy)] (CF_3-$SO_3)_2$ ·0.5$H_2O\}_n$[42] and [$Cu_3(\mu_3$-OMe)(μ-pz)$_3$($Me(CH_2)_4COO)_2$(μ-4,4'-bpy)] have been reported by employing 4'4-bipyridine as organic linker instead of tmpy ligand. Other studies of coordination polymers constructed by the interaction of metal cations with the flexible tmpy have been reported.[120] Among these previously known coordination polymers, zigzag chains similar to those that have been found in [Ag(bpp)](ClO_4), [Ag(bpp)](PF_6)[121] and [Cu_2(maa)$_4$(tmpy)] (Hmaa = 2-methylacrylic acid).[122] In the former two polymers the tmpy ligands display a TT conformation and have large N-to-N separations of 9.57 and 9.70 Å, respectively. The third polymer is the only one to have the tmpy ligand in TG conformation with N-to-N distance of 8.979 Å.

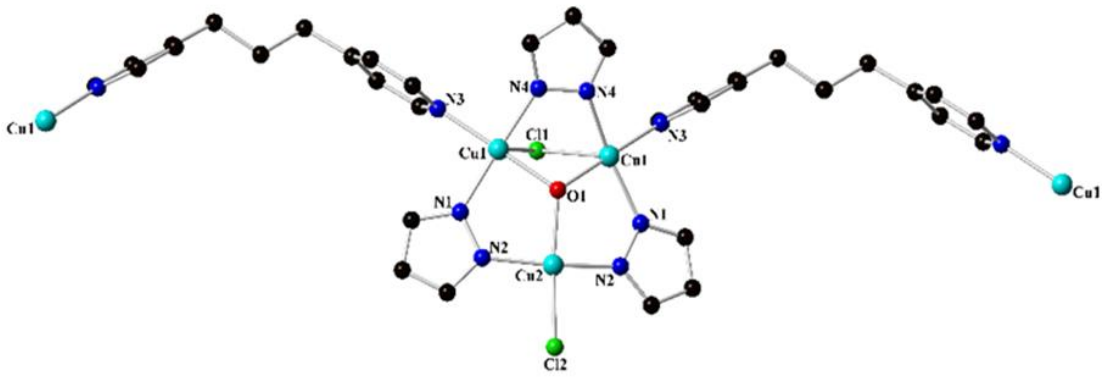

Figure 57. Coordination environment of Cu^{II} in complex [22] with partial atom labeling. H atoms have been omitted for clarity. Color codes: black, C; blue, N; red, O; green, Cl; cyan, Cu.

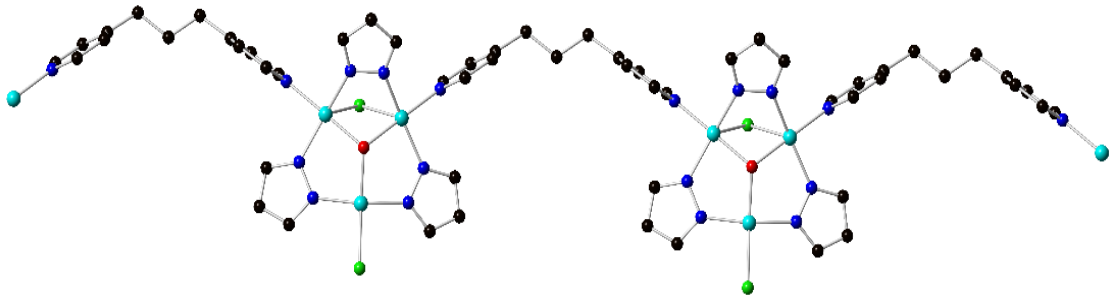

Figure 58. The zigzag $\{[Cu_3(\mu_3\text{-}OH)(\mu\text{-}Cl)(\mu\text{-}pz)_3Cl(tmp)]\}_n$ chain in complex [22]. Color codes: black, C; blue, N; red, O; green, Cl; cyan, Cu.

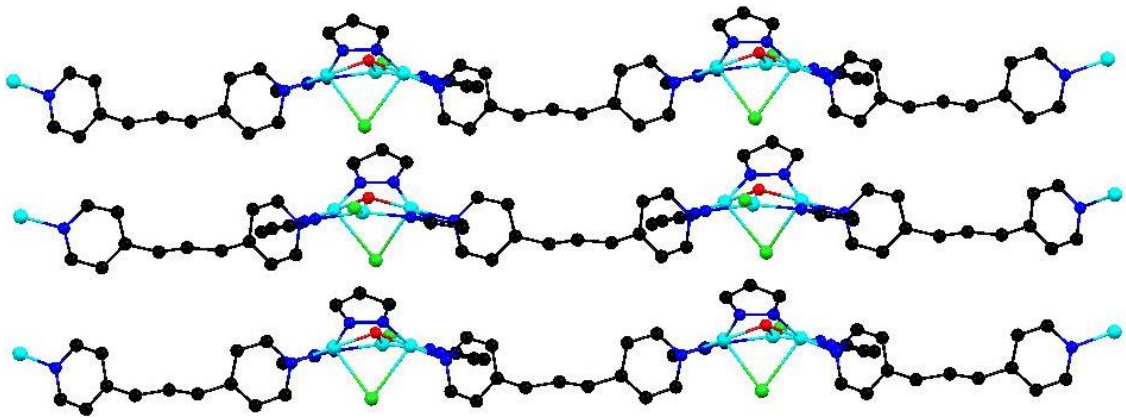

Figure 59. Side view of stacking of layers in [22], hydrogen atoms are omitted for clarity. Color codes: black, C; blue, N; red, O; green, Cl; cyan, Cu.

3.4.2.2 Crystal structure description of $\{[Cu_3(\mu_3\text{-}OH)(\mu\text{-}Cl)(\mu\text{-}pz)_3Cl]_2(tmpy)_2](CH_3CN)_2\}_n$ [23]

Compound **[23]** crystallizes in the monoclinic space group $P2_1/n$, where the asymmetric unit consists of trinuclear unit $[Cu_3(\mu_3\text{-}OH)(\mu\text{-}Cl)(\mu\text{-}pz)_3Cl]$, one tmpy ligand and two acetonitrile molecules. In each trinuclear triangular $[Cu_3(\mu_3\text{-}OH)(\mu\text{-}Cl)(\mu\text{-}pz)_3Cl]$ fragments, the distance of capping μ_3-O1 from the plane defined by the Cu_3 centre is 0.63(3) Å, slightly more pyramidal than compound **[22]** as well as Cu-O bond distances [Cu1-O1 1.985(3), Cu2-O1 2.005(3), Cu3-O1 2.029(3) Å] fall in the range normally found for analogous compounds.[49,56–58] These are considerably longer than **[22]**. Copper distances vary between 3.191(9) and 3.378(1) Å (Cu1-Cu2 3.378(1), Cu2-Cu3 3.191(9), Cu1-Cu3 3.320(1) Å). The Cu1 adopts a square planar coordination geometry determined besides μ-Cl1and μ_3-O1, by N1 and N6 pyrazolate nitrogens [Cu1-Cl1 2.273(15), Cu1-N11.958(4), Cu1-N6 1.936(4) Å]. The Cu2 coordinates with μ_3-O, two nitrogen atoms from pyrazolate rings (N2, N3), and one nitrogen atom N8 from tmp ligand [Cu2-N2 1.957(4), Cu2-N3 1.955(4) Cu2-N8 2.017(5) Å], the weak Cu2…Cl1 bond (2.894 (2) Å) is at axial site, which make the coordination geometry around Cu2 close to a distorted square-pyramid. The coordination environment of Cu3 is similar to Cu2. The weak Cu3…Cl2 (2.577(1) Å) bond is shorter than the Cl1 atom associated with Cu2.

As shown in Figure 60, compound **[23]** self-assembles forming hexanuclear cluster generated by two trinuclear moieties doubly bridged by Cl atoms, [Cu1-Cl1 2.273(2) Å, Cu2-Cl1 2.894(2) Å]. The crystal structure determination evidences that two Cu_3 planes of **[23]** are parallel to each other. This hexanuclear arrangement is very similar to the one found in the $[\{Cu_3(\mu_3\text{-}OH)(\mu\text{-}pz)_3(Cl)(Hpz)_3\}_2(\mu\text{-}Cl)_2]\cdot H_2O$ in which $[Cu_3(\mu_3\text{-}OH)(\mu\text{-}pz)_3Cl$

$(Hpz)_2]^+$ units are connected to each other through two symmetric chloride bridges [Cu-Cl 2.709(5) Å].[123] All the flexible tmpy ligands in **[23]** adopt a symmetrical TT conformation with average N…N separation of 9.487(6) Å and the corresponding distances between the neighboring two Cu atoms bonded to the same tmpy is 12.577Å, which also conforms to the requirements of this conformation. The Cu-tmpy-Cu angle is 121.88° which is larger than in **[22]**.

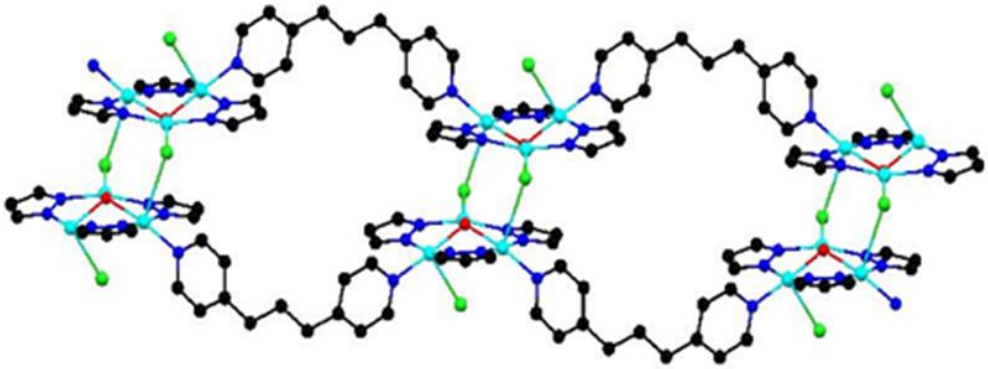

Figure 60. Arbitrary view of the crystal packing of **[23]** showing the hexanclear SBUs constructed by weak Cu…Cl interactions. Hydrogen atoms are not shown for clarity.

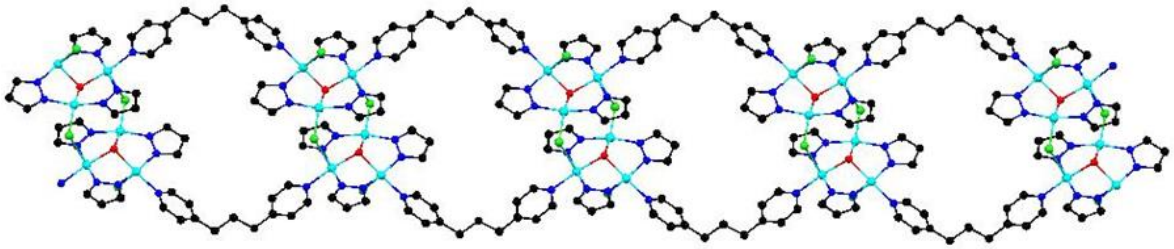

Figure 61. The 2D framework constructed by hexanuclear secondary building blocks of **[23]**, H atoms and solvent molecules are omitted for clarity.

Finally, crystal packing diagrams show that the adjacent wave-like Cu_3-tmpy 1D chain extends into a 2D framework via weak Cu-Cl bond. The asymmetric μ-Cl bridge gives rise to a Cu…Cu separation distance of 3.970 (3) Å [Cu2-Cl1 2.894(2), Cu1-Cl1 2.273(2) Å, Cu1-Cl1-Cu2 99.69°]. These hexanuclear clusters act as 4-connecting nodes to construct 2D framework, which is shown in Figure 61.

3.4.2.3 Crystal structure description of $\{[Cu_3(\mu_3\text{-}OH)(\mu\text{-}Cl)(\mu\text{-}pz)_3Cl(tmpy)](CH_3CN)\}_n$

Compound **[24]** crystallizes in the monoclinic *C2/c* space group and features a 2-fold interpenetrating 2D framework. It has a similar asymmetric unit as that described in **[23]**, except that there is one acetonitrile molecule instead of two in **[23]**. The Cu1 is coordinated by two pyrazolate nitrogens aotms [Cu1-N1 1.959(2), Cu1-N6 1.950(2) Å], one nitrogen atom pertaining to the tmpy linker [Cu1-N8 2.023(2) Å], capping ligand μ_3-OH occupying the equatorial plane [Cu1-O1 2.014(2) Å], Cl1 and Cl2 weakly coordinated to Cu1 with the bond length of 2.861 and 2.876 Å form as distorted octahedral geometry. The Cu2 a distorted square planar coordination sphere. Cu2 is coordinated by μ-Cl1 [2.278(8) Å], μ_3-O1 [Cu2-O1 1.981(2) Å], pyrazolate nitrogens N2 and N3 [Cu2-N2 1.941(2), Cu2-N3 1.929(2) Å]. The Cu3 shows a distorted square pyramidal coordination geometry with Cl2 atom in axial position [Cu3-Cl2 2.569(8) Å] and μ_3-OH, pyrazolate N4 and N5 and the tmp nitrogen N7 lying in the square plane [Cu3-N4, 1.967(2), Cu3-N5 1.962(2), Cu3-N7 2.012 (2) Å]. Only in compound **[24]**, all the tmpy ligands in TG[124] conformation present a N-to-N distance of 9.083 Å.

The supramolecular assembly of **[24]** is also very similar to that found in **[23]**. The SBU of **[24]** can be better described as a hexanuclear complex formed by two trinuclear moieties

joined through two monodentate asymmetrically bridging Cl ions (Figure 62). In comparison with compound **[23]**, The μ-Cl bridges give rise to a shorter Cu…Cu separation distance of 3.833 (1) Å [Cu1-Cl1 2.861 (6) Å, Cu2-Cl1 2.278(8) Å, Cu1-Cl1-Cu2 95.79°]. Each hexanuclear Cu_6 cluster is linked to four further Cu_6 clusters through four tmby ligands to form 2D double-interpenetrated structure (Figure 63). Small channels, running along the *a* axis, are occupied by disordered acetonitrile molecules, (solvent accessible voids constitute up to 2.4% of cell volume, larger than in compound **[23]** (0.3%)). Weak C-H…π interactions are found between the carbon atom of acetonitrile and centroid of pyrazolate ring. The distance in the edge-to-face π-π stacking is 3.611(2) Å, as shown in Table 11.

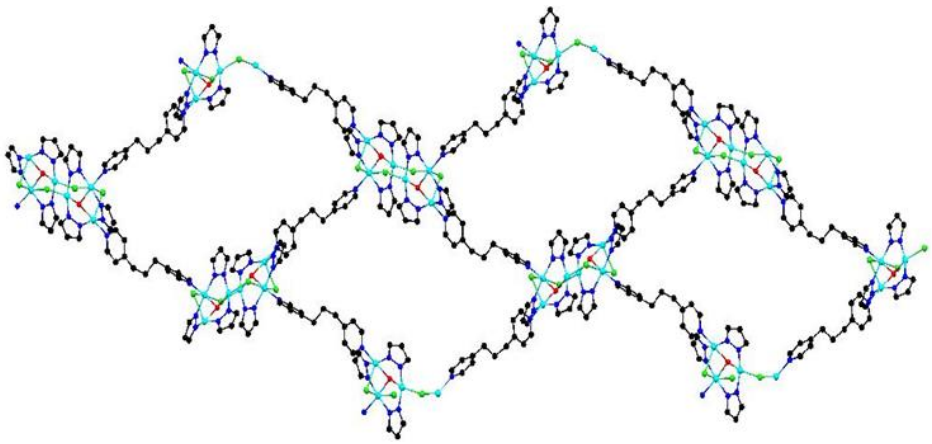

Figure 62. View of the 2D coordination network of **[24]**. All hydrogen atoms are omitted for clarity.

Table 11. X-H…Cg interactions (Distances and Angles) found in compound **[24]**.

X-H…Cg	D (H…Cg)	D (X…Cg)	∠X-H…Cg
C(24)-H(24B)…Cg(8)	2.72 Å	3.61(2) Å	151°
O(1)-H(1)…Cg(6)	2.59 Å	3.426(2) Å	140

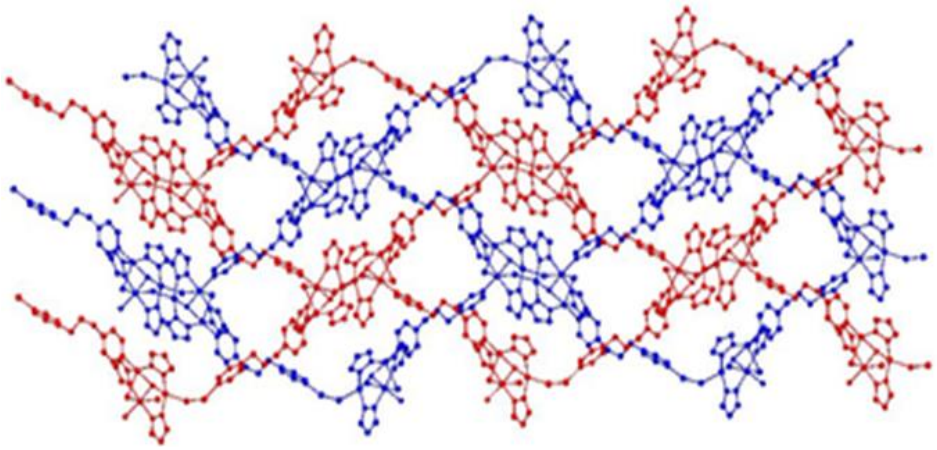

Figure 63. Two identical interpenetrating 2D undulating sheets of **[24]** shown in blue and red color. All hydrogen atoms are omitted for clarity.

Table 12. The conformation of the tmpy linker in complexes **[22]**-**[24]**.

No.	Formula	Structure	Conformation of the tmpy linker	N-to-N/Å
[22]	$\{[Cu_3(\mu_3\text{-}OH)(\mu\text{-}Cl)(\mu pz)_3Cl(tmpy)(CH_3CN)]\}_n$	1D Zigzag chain	TT	9.520
[23]	$\{[Cu_3(\mu_3\text{-}OH)(\mu\text{-}Cl)(\mu\text{-}pz)_3Cl]_2(tmpy)_2](CH_3CN)_2\}_n$	2D	TT	9.488
[24]	$\{[Cu_3(\mu_3\text{-}OH)(\mu\text{-}Cl)(\mu\text{-}pz)_3Cl(tmpy)](CH_3CN)\}_n$	2D Interpenetrated	TG	9.083

3.4.3. Investigation the flexibility of Cu-MOFs under high pressure

While structural, electronic, spectroscopic and thermodynamic properties of coordination polymers (CPs) and MOFs are studied rather routinely, their mechanical properties, such as resistance to high pressure and temperature are seldomly studied.[125] The structural flexibility and versatility of CPs make them ideal candidates to study the effects of external forces such as pressure.[126, 127] These materials exhibit a variety of behaviors under applied high pressure. The most commonly observed response in MOFs (e.g., zeolitic imidazolate frameworks, ZIFs) is pressure-induced amorphization.[128] For example, Kitagawa et al. have studied the effect of pressure on proton conductivity and discovered that conductivity decreases 1000-fold upon 3-7 GPa.[129] Haines, J. et al., studied the phase transition of siliceous zeolite TON from the $Cmc2_1$ to a $Pbn2_1$ structure near

0.6 GPA. Some CPs demonstrated unique mechanical effect known as negative linear compressibility (NLC), which has potential applications, such as sensor systems in high pressure environments. Cheeetham et al. have reported a 3D hybrid zinc formate framework with a high degree of mechanical anisotropy and NLC along its c-axis.[130] Suslick et al. have reported the mechanochemical bond breaking accompanied amorphization under high pressure using EXAFS and IR spectroscopy.[131]

In the present study, the flexibility of a 1D chain Cu-pyrazolate have been investigated under high pressure. The material is elastic up to 3.0 GPa and is amorphized irreversibly at 4.2 GPa, as indicated by variable pressure PXRD (Figure 64).

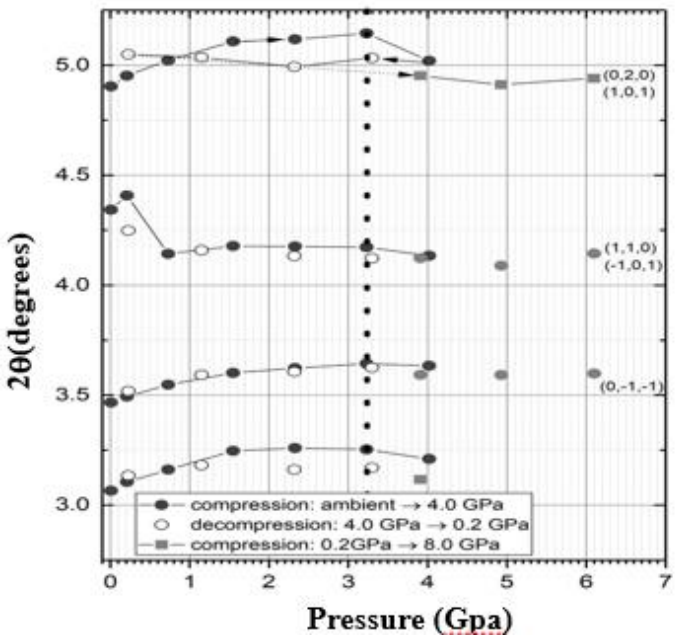

Figure 64. 2θ vs pressure for $\{[Cu_3(\mu_3\text{-}OH)(\mu\text{-}Cl)(\mu\text{-}pz)_3Cl(tmpy)(CH_3CN)]\}_n$ **[22]**.

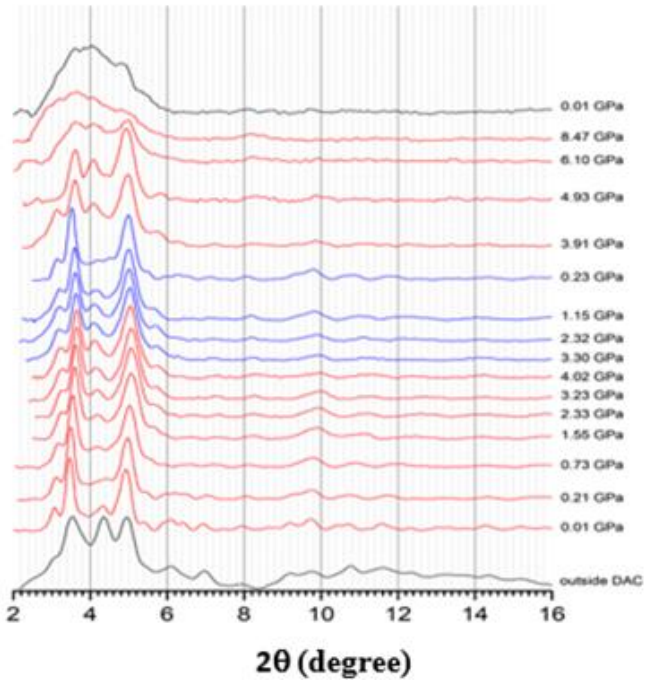

Figure 65. High pressure powder X-ray diffraction for $\{[Cu_3(\mu_3\text{-}OH)(\mu\text{-}Cl)(\mu\text{-}pz)_3Cl\ (tmpy)(CH_3CN)]\}_n$ **[22]**.

3.5. Synthesis of 2D coordination polymers based on trinuclear copper pyrazolate complexes

3.5.1. Experiment

3.5.1.1. Synthesis of $\{[Cu_3(\mu_3\text{-}OH)(\mu\text{-}4\text{-}Ph\text{-}pz)_3\ (abp)_{1.5}][(CF_3SO_3)_2]\}_n$ [25]

A 5 mL solution of 4,4-azobis(pyridine) (0.1 mmol, 18.4 mg) dissolved in CH_2Cl_2 was put on the test tube, then 4 mL CH_2Cl_2/CH_3CN (1:1, V/V) as blank solvent were layered on the top. The reaction of $Cu(CF_3SO_3)_2$ (0.1 mmol, 36.2 mg), 4-Ph-pzH (0.1 mmol, 14.4 mg) with NaOH (0.4 mmol, 16 mg) in 8 mL CH_3CN solvent lead to a green mixture after stirring 12h and filtration, the final mixture were successively layered on the top of blank solvent carefully. Crystals were obtained after several days at room temperature. These crystals of **[25]** in a 57% after filtration, washed with CH_2Cl_2 and CH_3CN, ether and dried in air. Anal. Calcd/Foud for $C_{44}H_{33}Cu_3F_6N_{12}O_7S_2$ (%): C, 42.98/42.87; H, 2.95/3.06; N, 13.67/13.66.

3.5.1.2. Synthesis of $\{[Cu_3(\mu_3\text{-}OH)(\mu\text{-}4\text{-}Ph\text{-}pz)_3(CH_3CN)(abp)_{1.5}][(\mu\text{-}4\text{-}Ph\text{-}pz)(\mu\text{-}Cl)Cu(py)(abp)_{0.5}](CF_3SO_3)_2\}_n$ [26]

A 4mL of abp (0.01 mmol, 1.8 g) in the CH_2Cl_2 was placed in the test tube. 1:1 mixture of CH_2Cl_2: CH_3CN was layered over the CH_2Cl_2 layer. $Cu(CF_3SO_3)_2$ (0.06 mmol, 21.7 mg), 4-Ph-pzH (0.06 mmol, 8.7 mg), NaOH (0.18 mmol, 7.2 mg) and pyridine (0.04 mmol, 3.2 µL) were stirred in 4 mL CH_3CN at room temperature for an hour and then after filtration, the solution was layered on top.

3.5.1.3. Synthesis of $\{Cu_6(\mu_3\text{-}OH)(\mu\text{-}pz)_7(\mu\text{-}Cl)Cl_2(bpe)_2\}_n$ [27]

$CuCl_2 \cdot 2H_2O$ (0.12 mmol, 20.4 mg), PzH (0.12 mmol, 8.4 mg), NaOH (0.24 mmol, 9.6 mg) and PPNCl (0.08 mmol, 47.4 mg) were stirred in 10 mL CH_2Cl_2 for 6h at ambient temperature. The green solution was transferred to a test tube after filtration. A 4 mL 1:1 mixture of CH_2Cl_2: CH_3CN was layered over the CH_2Cl_2 layer, bpe (0.12 mmol, 22.6 mg) in 4 mL CH_3CN was added as the third layer on top of the lower two. Suitable crystals for X-ray diffraction were obtained one month later. Yield: 29%.

3.5.2. Result and discussion

3.5.2.1 Two dimensional (2D) sheet based on trinuclear Copper pyrazolate clusters $\{[Cu_3(\mu_3\text{-}OH)(\mu\text{-}4\text{-}Ph\text{-}pz)_3(abp)_{1.5}][(CF_3SO_3)_2]\}_n$ [25]

Complex **[25]** crystallize in the triclinic space group $P\bar{1}$, and contains a trinuclear Cu_3 cluster as an SBU, as shown in Figure 66. The asymmetric unit consists of $[Cu_3(\mu_3\text{-}OH)(\mu\text{-}4\text{-}Ph\text{-}pz)_3(4,4\text{-}abp)_{1.5}]^{2+}$ and two triflate anions providing charge balance. The central μ_3-OH capping ligand shows a 0.469 (2) Å out-of-plane displacement above the mean plane of the $[Cu(4\text{-}Ph\text{-}pz)]_3$ core. Two triflate anions per Cu_3 unit are positioned one above and one below the Cu_3 plane. A distinct feature of the SBU in **[25]** is the two coordination environments around the three Cu atoms: Two copper

atoms of $[Cu_3(\mu_3\text{-}OH)(\mu\text{-}4\text{-}Ph\text{-}pz)_3]^{2+}$ unit adopt square-pyramidal geometry with N_3O_2 coordination environments, if the long Cu…O interactions of 2.483(1) - 2.666(1) Å are taken into account. The third one possesses a square-planar geometry with (N_3O) coordination environment. This tricopper cluster $[Cu_3(\mu_3\text{-}OH)(\mu\text{-}4\text{-}Ph\text{-}pz)_3]^{2-}$ SBU acts as a three-connected node (Figure 67), while 4,4-bis(pyridine) ligands provide the bridging among the SBUs to form a two dimensional sheet. Extended structure analyses revealed a novel two-dimensional network supported by intermolecular hydrogen bonds, in addition to the π–π stacking interactions (Figure 68).

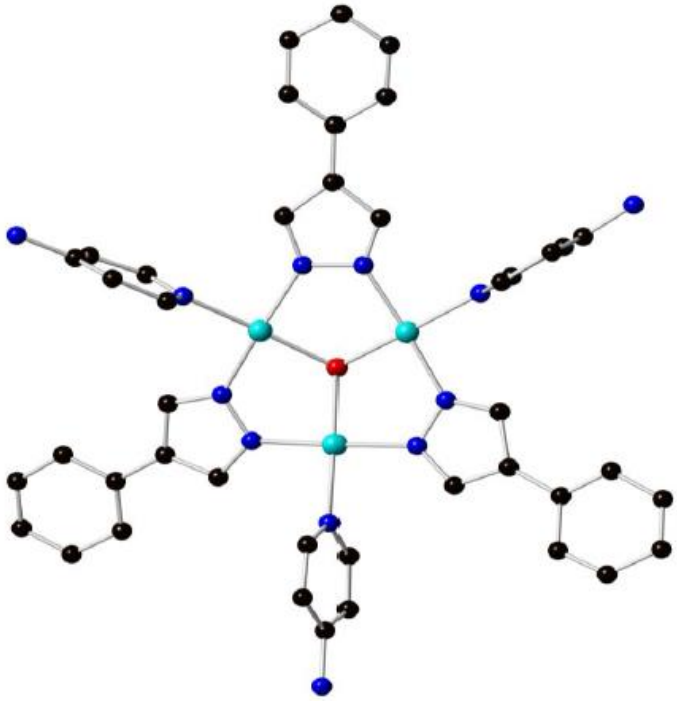

Figure 66. Asymmetric unit of compound **[25]**, hydrogen atoms and triflate anions are omitted for clarity. Color code: black, C; blue, N; red, O; cyan, Cu.

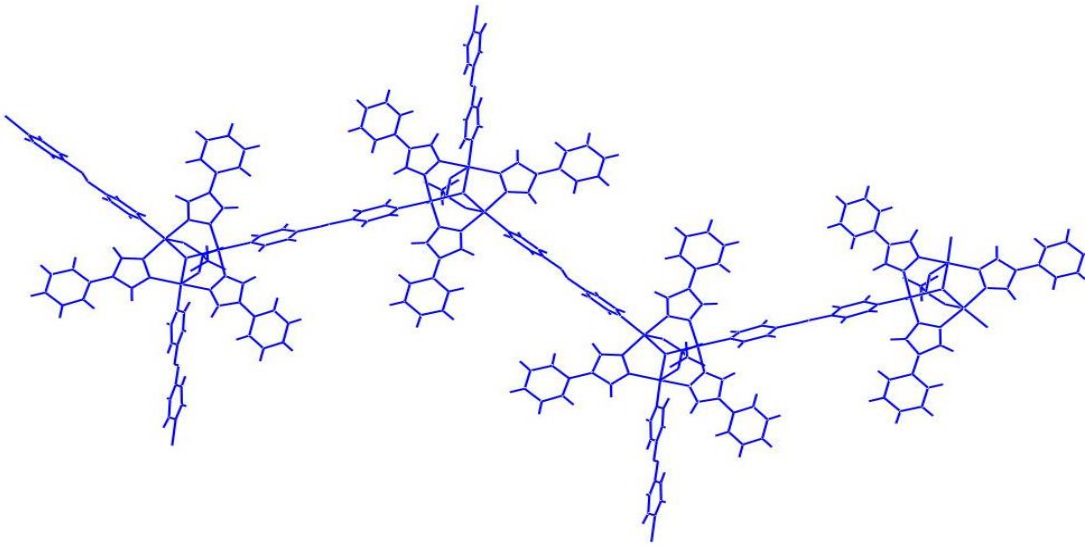

Figure 67. One net of **[25]** showing the SBU acting as 3-connecting node.

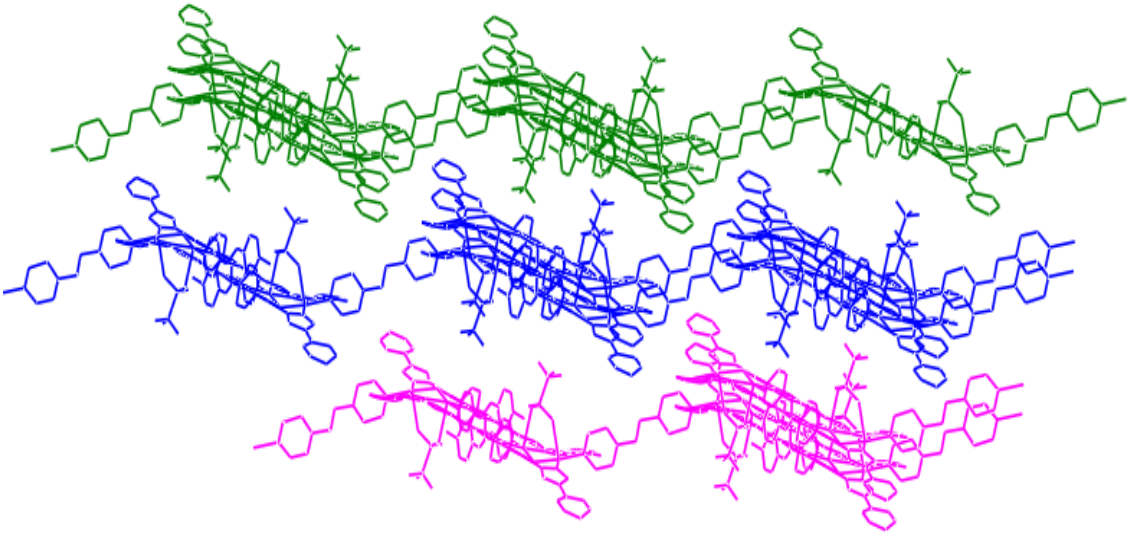

Figure 68. Side view of the 2D structure in **[25]**.

3.5.2.1.1. Redox activity of [25]

A 2D material, $\{[Cu_3(\mu_3\text{-}OH)(\mu\text{-}4\text{-}Ph\text{-}pz)_3(4,4\text{-}abp)_{1.5}][(CF_3SO_3)_2]\}_n$ **[25]**, was studied with regard to its redox activity, as follows: A thin film of **[25]** was deposited and used in lieu of a cathode in Li-battery, which was then cycled between -0.1 and +0.9 V, showing full reversibility (Figure 69).

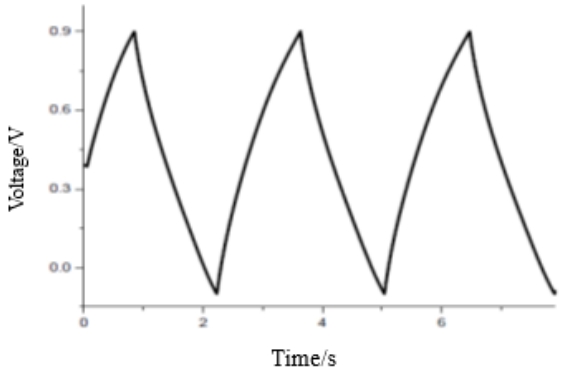

Figure 69. Galvanostatic charge/discharge cycling of **[25]** at current density of 0.1 A g^{-1}.

3.5.2.2. 2D sheet based on tetranuclear Cu_4 clusters {[$Cu_3(\mu_3\text{-}OH)(\mu\text{-}4\text{-}Ph\text{-}pz)_3$ (CH_3CN) $(abp)_{1.5}$][$(\mu\text{-}4\text{-}Ph\text{-}pz)(\mu\text{-}Cl)Cu(py)(abp)_{0.5}$][$(CF_3SO_3)_2$]}$_n$ [26]

Single-crystal X-ray diffraction analysis shows that compound **[26]** is 2D coordination polymer and crystallizes in the triclinic space group $P\bar{1}$. Four crystallographically independent Cu^{2+} ions are bridged by four deprotonated 4-Ph-pz ligands and μ_3-OH to form a tetranuclear Cu_4 cluster. The asymmetric unit contains four Cu(II) ions, the local coordination geometry around Cu(II) ions is depicted in Figure 70, showing that all copper atoms are five-coordinate with square-pyramidal geometries. The Cu1 is coordinated by three nitrogen atoms from three 4-phenyl pyrazoles, the bridging μ_3-OH oxygen and one μ-Cl atom. The weak Cu1-Cl bond (2.771(4) Å) is at axial site, which make the coordination geometry aroud Cu1 close to a distorted square-pyramid. The Cu3 atom is coordinated to two nitrogens from two 4-phenyl-pyrazoles, one nitrogen of the abp linker, and the bridging μ_3-OH oxygen, the axial site is occupied by a triflate oxygen with weak Cu3…O bond (2.780 (4) Å). The average bond lengths of Cu3-O and Cu3-N_{pz}- are 2.011 and 1.967 Å, slightly longer than these of Cu2-O and Cu2-$N_{pz\text{-}}$ (2.009 and 1.951 Å). Compared with Cu3, Cu2

coordinated to acetone, instead of oxygen from triflate anion. The Cu4 is coordinated to one pyridine nitrogen atom, one μ-Cl atom, one abp nitrogen atom, and one pyrazole nitrogen atom. The distances of Cu1…Cu2, Cu1…Cu3, Cu2…Cu3, Cu1…Cu4 are 3.290(6), 3.274(9), 3.375(0) and 3.642(6) Å, respectively. The tetranuclear Cu_4 clusters are connected by four abp linkers to form 2D sheet (Figure 72).

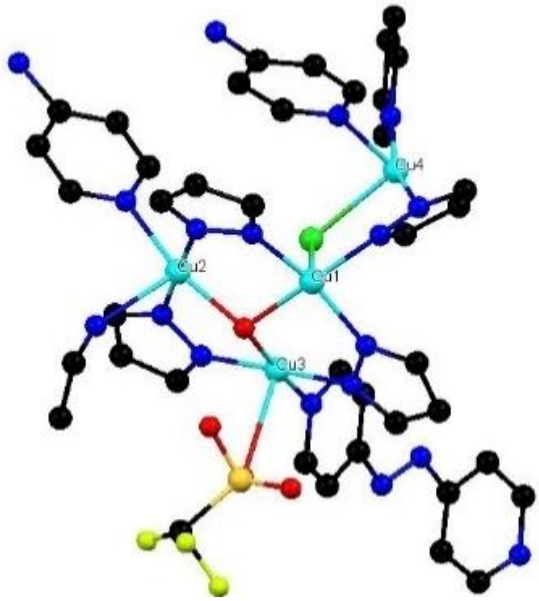

Figure 70. The coordination environment of tetranuclear Cu_4 cluster in **[26]** with partial atom labeling scheme. Uncoordinated triflate anions and hydrogen atoms are omitted for clarity. Color code: black, C; blue, N; red, O; yellow, F; green, Cl; orange, S; cyan, Cu.

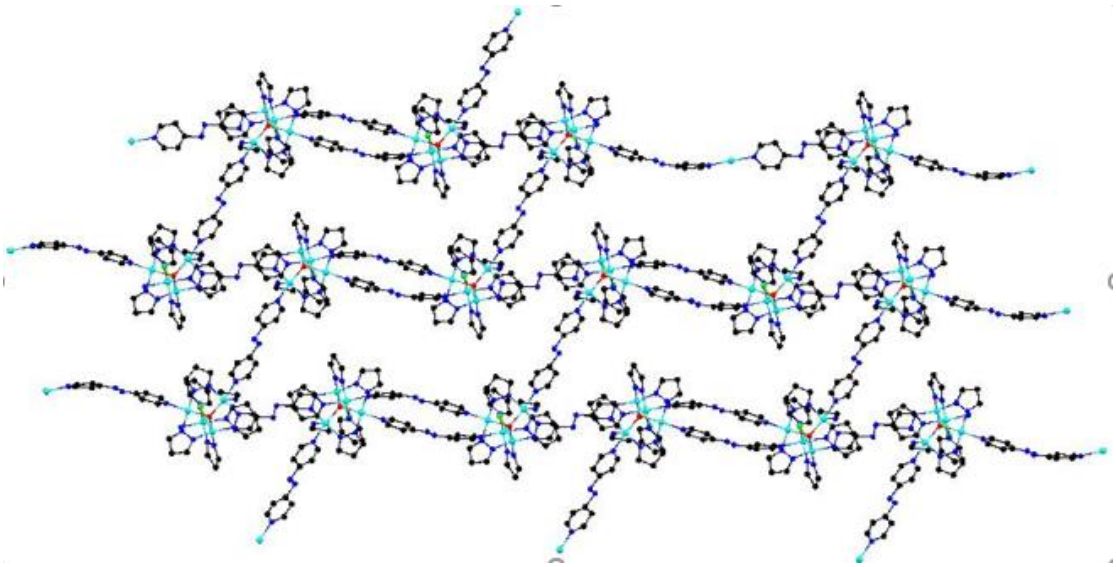

Figure 71. The SBU of compound **[26]** acts as 4-connected node.

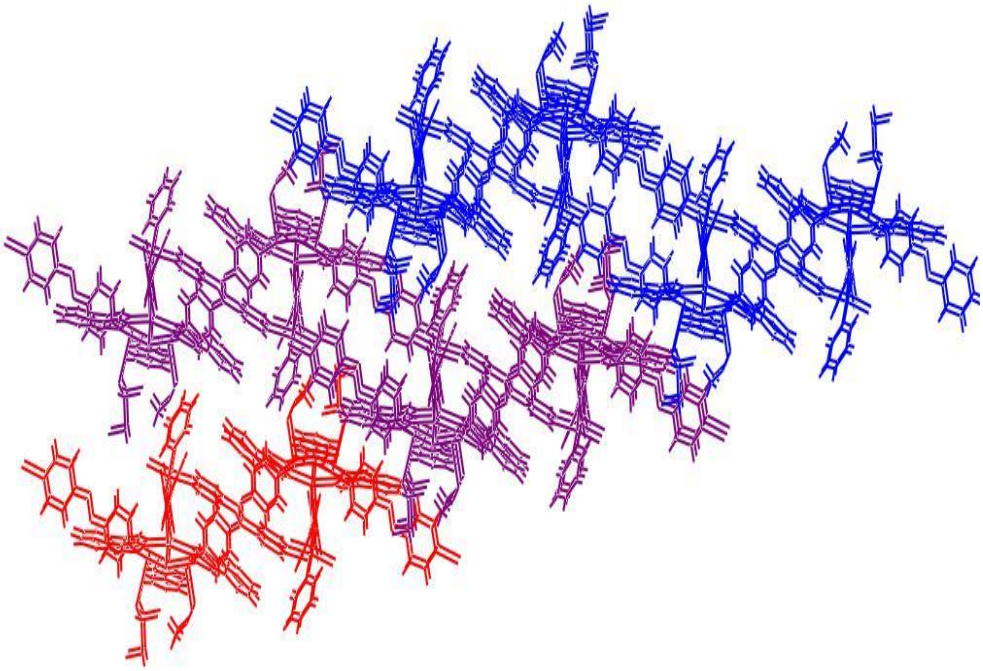

Figure 72. Packing diagram of compound **[26]** exhibits a two-dimensional sheet.

3.5.2.3. 2D structure based on hexanuclear Cu_6 clusters $\{Cu_6(\mu_3\text{-}OH)(\mu\text{-}pz)_7(\mu\text{-}Cl)Cl_2(bpe)_2\}_n$ [27]

Compound **[27]** crystallizes in the orthorhombic *Cmca* space group with $[Cu_3(\mu_3\text{-}OH)(\mu\text{-}pz)_{3.5}Cl_2(bpe)]$ in the asymmetric unit, as shown in Figure 73. Two Cu(II) atoms are five-coordinated by three nitrogens of three pz, one Cl atom and hydroxyl oxygen. The third copper atom of the trinuclear unit adopts a square planar geometry. The Cu-O bonds have distances in the range of 1.987(3)-2.024(4) Å, the Cu-O-Cu bond angles are in the range of 107.30(9)-114.21(1)º. The SBU (Figure 74) of the molecular structure can be better described as a hexanuclear unit formed by two trinuclear triangular $Cu_3(\mu_3\text{-}OH)(\mu\text{-}pz)_3$ moieties bridged by Cl atom. The Cu-Cl bond lengths are 2.694(2) Å (Cu_3-Cl_1) and 2.569(1) Å (Cu_1-Cl_2). The SBU acts as 6-connected node bridged by four linkers and two Cl atoms to construct the MOF (Figure 76). Two linkers between two Cu_6 SBU are perpendicular each other instead of parallel to each other (Figure 75).

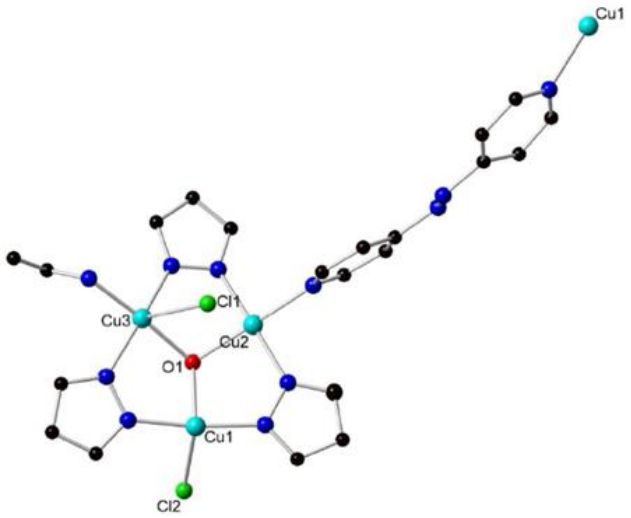

Figure 73. The asymmetric unit of **[27]**.

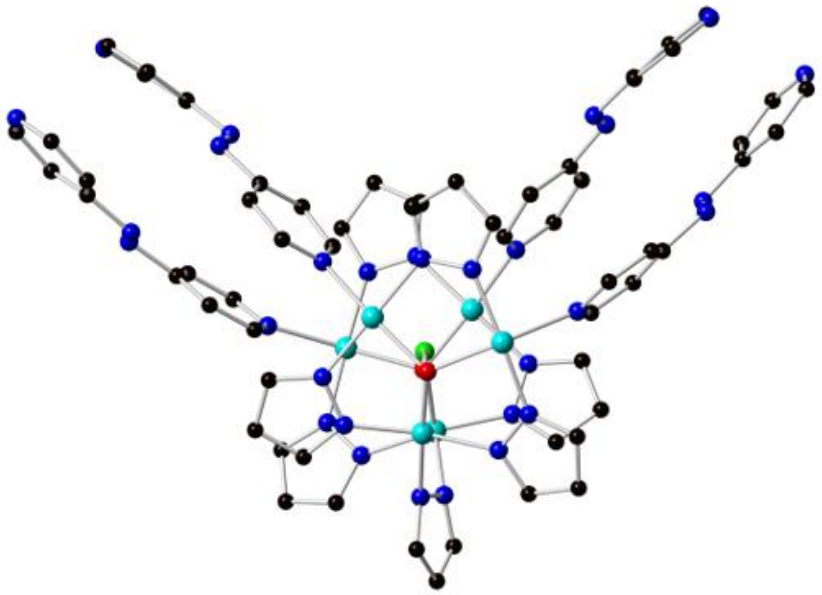

Figure 74. The hexanuclear copper second building unit (SBU) in **[27]**. Color code: black, C; blue, N; red, O; green, Cl; cyan, Cu.

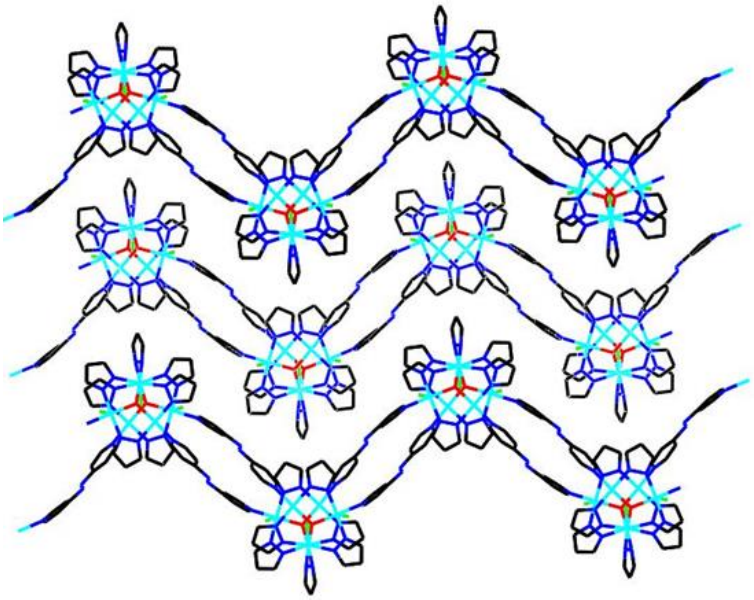

Figure 75. The 2D constructed by hexanuclear secondary building blocks of **[27]** along a axis.

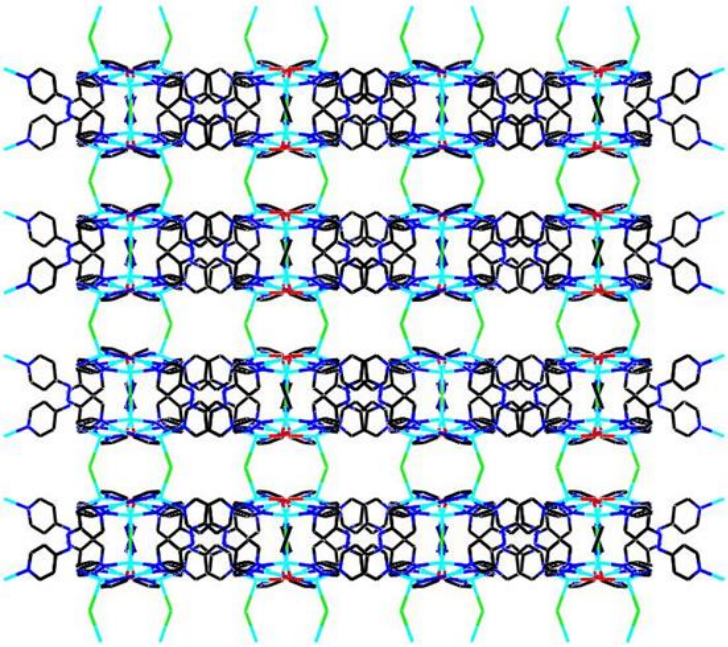

Figure 76. View of 2D framework constructed by two weak Cu…Cl bonds in **[27]** along b axis.

3.6. Synthesis of 3D MOFs based on Cu_3 SBU

We have succeeded in the synthesis of a series of 1D, 2D, 3D-MOFs based on [Cu_3]-SBU by replacing terminal monodentate ligands, such as py with bridging bidentate ones such as 4,4-bipy, 4,4-azo- bispyridine (abp) and 1,2-di(4-pyridyl)ethylene (bpe).[16,17] Herein as a part of our ongoing investigation synthesizing MOFs with nitrogen donor ligands, 4-Cl-pzH, 4,4-azobispyridine and 1,2-di(4-pyridyl) ethylene were used to synthesize coordination polymer with a triangular Cu_3(μ_3-OH)-SBU. Three copper(II) complexes, namely, {[Cu_3(μ_3-OH)(μ-4-Cl-pz)$_3$(bpe)$_3$] [CF_3SO_3]$_2$}$_n$ **[FIU-1]**, {[Cu_3(μ_3-OH) (μ-4-Cl-pz)$_3$ (abp)$_2$][CF_3SO_3]$_2$}$_n$ **[FIU-2]** and {[Cu_3(μ_3-OH)(μ-4-Cl-pz)$_3$(abp)$_{2.5}$][CF_3SO_3]$_2$}$_n$ **[FIU-3]** were synthesized and characterized by X-ray single crystal diffraction analysis. The structure was further identified by elemental analysis and IR, the phase purity was confirmed by Powder X-ray Diffraction (PXRD), and thermal stability was analyzed by thermogravimetric analyses (TGA). The permanent porosity and CH_4, CO_2, N_2 uptake properties of **FIU-1**, **FIU-2**, **FIU-3** were analyzed by gas adsorption studies.

3.6.1. Experimental section

3.6.1.1. Synthesis of {[$Cu_3(\mu_3\text{-}OH)(\mu\text{-}4\text{-}Cl\text{-}pz)_3(bpe)_3$] $[CF_3SO_3]_2$}$_n$ [FIU-1]

A 5 mL solution of 1,2-di(4-pyridyl)ethylene (bpe) in CH_2Cl_2 was placed in test tube. A 4 mL 1:1 mixture of CH_2Cl_2: CH_3CN was layered over the CH_2Cl_2 layer, $Cu(CF_3SO_3)_2$ (0.1 mmol, 36.2 mg), 4-Cl-pzH (0.1 mmol, 10.3 mg) and NaOH (0.2 mmol, 8 mg) in 5 mL of CH_3CN was stirred at ambient temperature until the solution turned the teal, then transferred to the test tube after filtration and layered on top. The cyan-tetragonal prism crystals were formed on the walls of the test tube at the interface of the layers two days later. Yield ~ 51%. Phase purity was confirmed by comparing the PXRD patterns of as-synthesized sample and a simulated one from the single crystal X-ray data. Elem. Anal. Calcd/Foud for $C_{47}H_{43}Cu_3F_6S_2Cl_3N_{12}O_9$ (%): C, 40.52/40.54; H, 2.97/3.06; N, 12.07/12.04. IR: 3048w, 1610s, 1557w, 1506w, 1431m, 1277w, 1222s,1161s, 998s, 1023s, 970s, 828s,636s, 636s.

3.6.1.2. Synthesis of {[$Cu_3(\mu_3\text{-}OH)(\mu\text{-}4\text{-}Cl\text{-}pz)_3(abp)_2$][$CF_3SO_3]_2$}$_n$ [FIU-2]

Compound MOF-2 was synthesized following the same procedure as that of MOF-1 using 4,4'-azopyridine (0.1 mmol, 18.8 mg) in the place of 1,2-di(4-pyridyl)ethylene. Brown crystal of **FIU-2** were isolated in 45% yield. Elem. Anal. calcd, found for **FIU-2** (%） C, 30.50/ 29.26; H, 2.00/ 2.00; N,15.57/15.70.

3.6.1.3. Synthesis of {[$Cu_3(\mu_3\text{-}OH)(\mu\text{-}4\text{-}Cl\text{-}pz)_3(abp)_{2.5}$][$CF_3SO_3]_2$}$_n$ [FIU-3]

The complex was synthesized by the same method used for preparation of **FIU-2**. The molar ratio is 6:6:24:6 instead of 6:6:12:6 of MOF-2.

3.6.2. Results and Discussion

3.6.2.1. Crystal structure description of {[$Cu_3(\mu_3\text{-}OH)(\mu\text{-}4\text{-}Cl\text{-}pz)_3(bpe)_3][CF_3SO_3]_2\}_n$ [FIU-1]

Compound **FIU-1** crystallizes in the monoclinic space group, C2/c The asymmetric unit consists of $[Cu_3(\mu_3\text{-}OH)(\mu\text{-}4\text{-}Cl\text{-}pz)_3(bpe)_3][CF_3SO_3]_2$, the characteristic triangular trinuclear core was formed when the μ_3-OH group unsymmetrically bridged three copper atoms with Cu−OH distances of 1.996(4), 1.994(4), and 1.980(4)Å. The hydroxyl O-atom shows a 0.410(4) Å out-of-plane displacement above the mean plane of the $[Cu(pz)]_3$ core, while the Cu-N_{pz} bond distances are in the range of 1.953(6)-1.977(7) Å. All those values are in the ranges normally found in analogous compounds.[30-43] The Cu-Cu intramolecular distances are 3.350(4), 3.384(3), 3.346(3) Å. All copper atoms are in square-pyramidal N_3O_2/N_4O-coordination environment. There are two triflate counterions per Cu_3 unit, one of them weakly coordinated with Cu atom through O atom (Figure 77). The Cu···O distances are 2.601(2), 2.735(3) Å. The second triflate anion is crystallographically disordered; this anion are removed from structure refinement using the SQUEEZE routine.

The compound self-assembles forming a hexanuclear cluster (Cu_6 core) as SBU generated by two trinuclear $[Cu_3(\mu_3\text{-}OH)(\mu\text{-}4\text{-}Cl\text{-}pz)_3]^{2-}$ moieties, triply bridged by three bpe organic linkers through N atoms (Figure 78). These hexanuclear clusters act as 6-connecting nodes to construct the 3D framework, as shown in Figure 79. This structure consists of 3-fold interpenetrated nets (Figure 81). Pettinari, *et al*. have demonstrated the usefulness of a hexanuclear Cu(II) -pyrazolate moiety as an SBU for generating 3D polymeric network in a recent study.[44] The structure of **FIU-1** is porous with 7237.24 $Å^3$ of solvent accessible void per unit cell (unit cell volume: 16015.33 $Å^3$) representing 45.2% of the unit cell volume. This MOF has interstitial solvent molecules that were removed using the SQUEEZE protocol available with PLATON. The solvent content of **FIU-1** was determined from a combination TGA and elemental analysis.

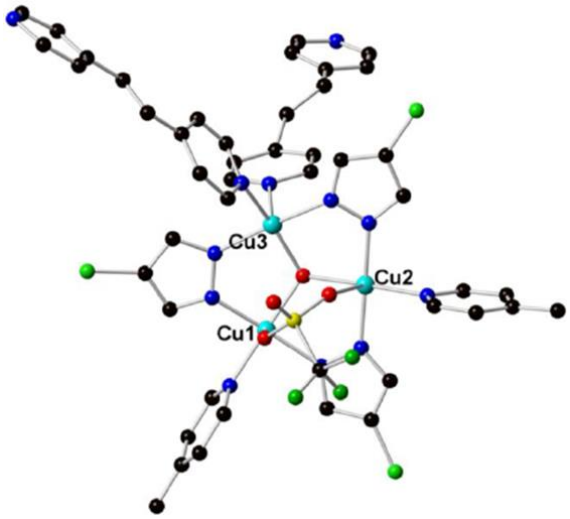

Figure 77. Asymmetric unit of **FIU-1**, and coordination environment of the Cu(II) ions in **FIU-1**. Color code: black, C; blue, N; red, O; yellow, F; green, Cl; orange, S; cyan, Cu.

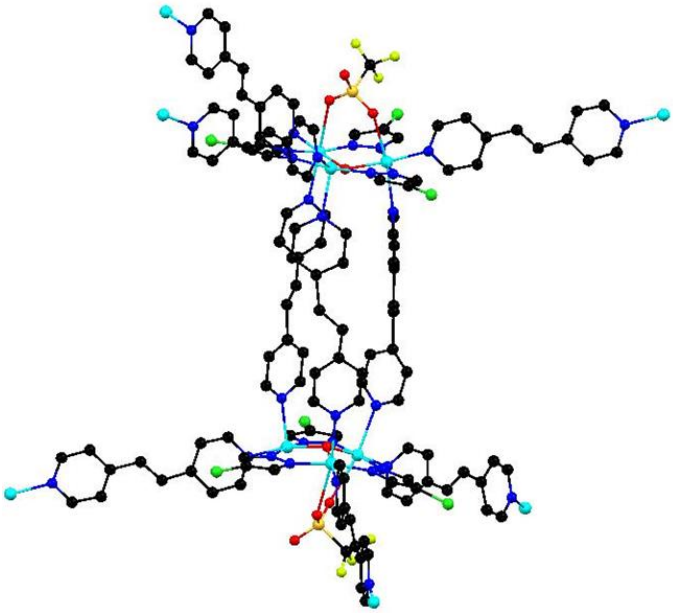

Figure 78. Hexanuclear cluster (SBU) of **FIU-1**. Color code: black, C; blue, N; red, O; yellow, F; green, Cl; orange, S; cyan, Cu.

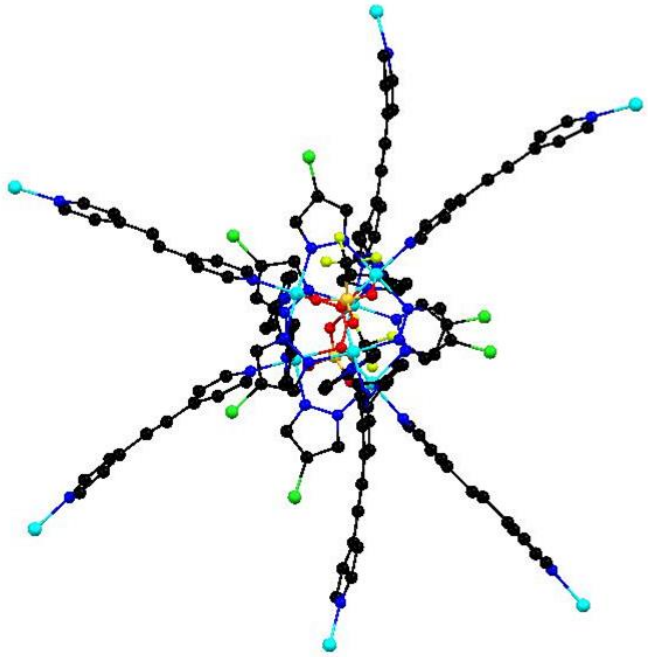

Figure 79. SBU acts a 6-connecting code in **FIU-1**. Color code: black, C; blue, N; red, O; yellow, F; green, Cl; orange, S; cyan, Cu.

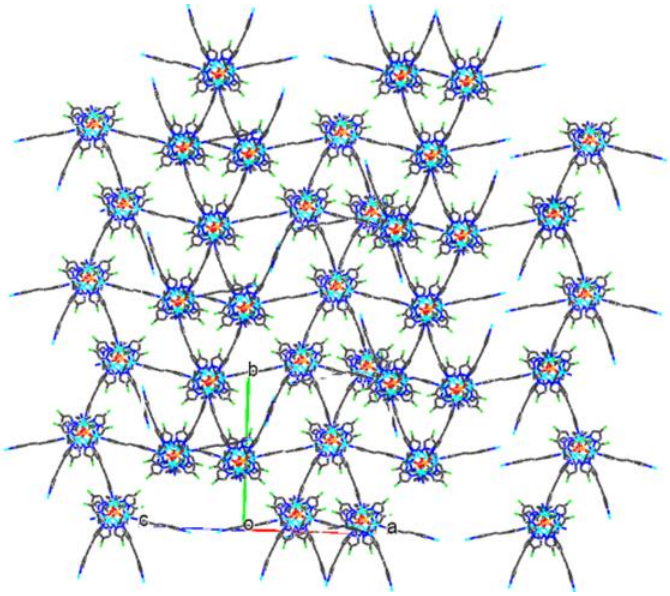

Figure 80. One of the three nets of **FIU-1**.

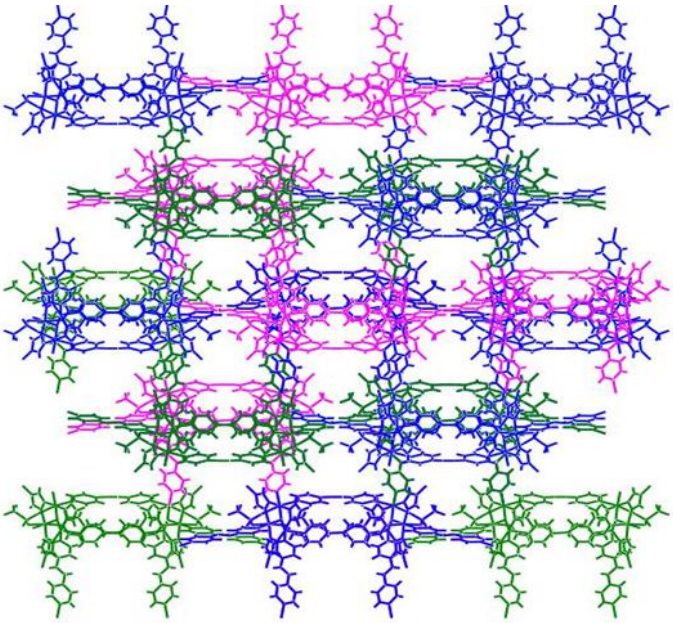

Figure 81. 3-fold interpenetrating 3D architecture of **FIU-1**, viewed along the crystallographic c-axis. Each color represent one net.

3.6.2.2. Crystal structure description of {[$Cu_3(\mu_3\text{-}OH)(\mu\text{-}4\text{-}Cl\text{-}pz)_3(abp)_2$][$CF_3SO_3$]$_2$}$_n$ [FIU-2]

Compound **FIU-2** crystallizes in the monoclinic crystal system with the *P2₁/c* space group. The asymmetric unit $[Cu_3(\mu_3\text{-}OH)(\mu\text{-}4\text{-}Cl\text{-}pz)_3(abp)_2]^{2+}$ can be viewed as an SBU generating the polymeric network of **FIU-2** (Figure 82). Actually, the double positive charge of each trinuclear cluster is neutralized by two triflate anions. In each trinuclear fragment, the Cu_3N_6 ring is almost planar, the non-bonding Cu…Cu distances , the μ_3-OH-Cu bond distances as well as the distances between the capping oxygen and plane defined by Cu_3 ions (ca. 0.534(4)Å, 0.527(4), 0.530(4), respectively) are in the ranges normally found in this kind of compounds.[30-43] Two Cu(II) ions adopt distorted square pyramidal N_4O/N_3O_2 coordination environments with μ_3-OH, two nitrogen atoms from two pyrazole ligands, and two N atoms from linkers (or one N atom from linker, one O atom from triflate anion). The third Cu(II) ion is in an elongated octahedral geometry (Figure 83). The triangular $[Cu_3(\mu_3\text{-}OH)]$ hydroxo-clusters can serve as self-associating building units. Each triangular subunit is connected to four surrounding linkers through N from 4,4-azobis(pyridine), all

the $[Cu_3(\mu_3\text{-}OH)(\mu\text{-}4\text{-}Cl\text{-}pz)_3]^{2-}$ clusters act as 4-fold-connected node (Figure 85). As shown in Figure 84, 3-fold interpenetrating MOF-1 (86) also show the hexagonal channel.

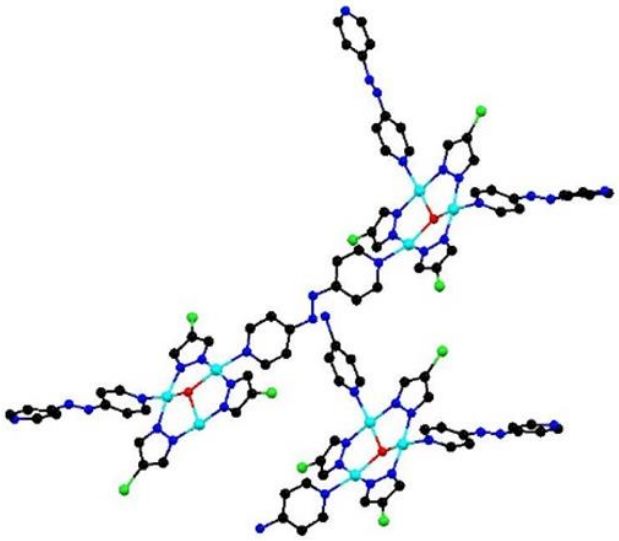

Figure 82. The asymmetric unit of compound **FIU-2**, H atoms and trifilates anions are omitted for clarity. Color code: black, C; blue, N; red, O; green, Cl; cyan, Cu.

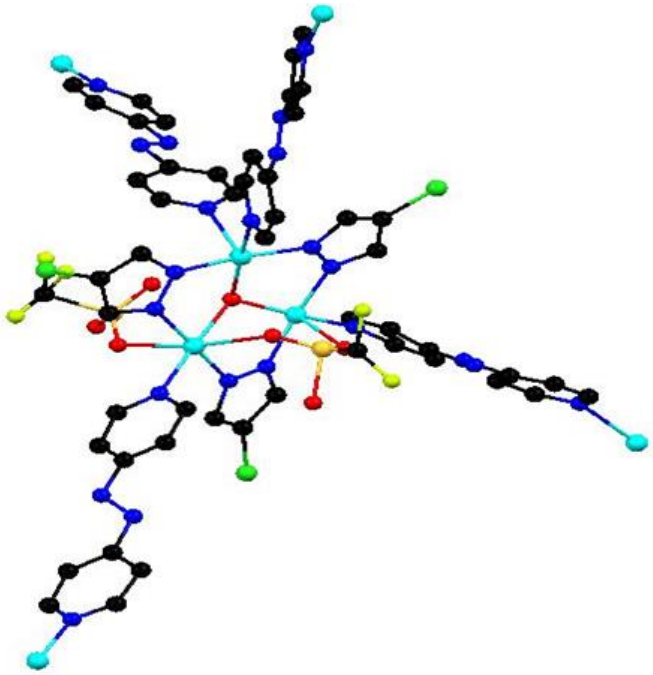

Figure 83. Coordination environment around the Cu(II) ions in the compound **FIU-2**. Color code: black, C; blue, N; red, O; yellow, F; green, Cl; orange, S; cyan, Cu.

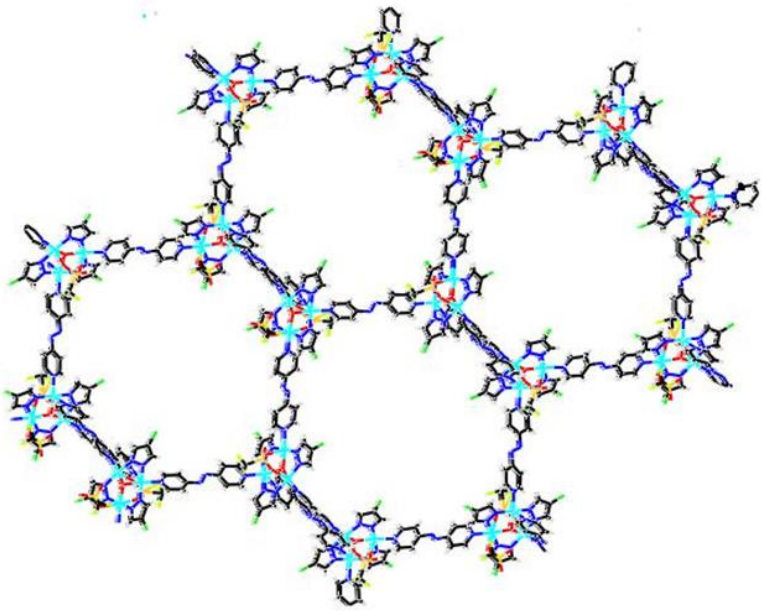

Figure 84. One of the nets showing hexagonal channels in compound **FIU-2**.

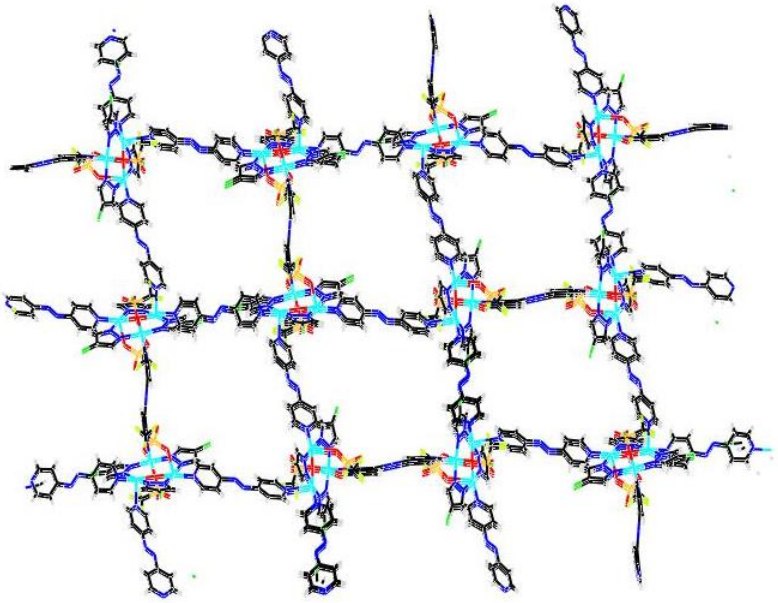

Figure 85. Four-fold connecting node of compound **FIU-2**.

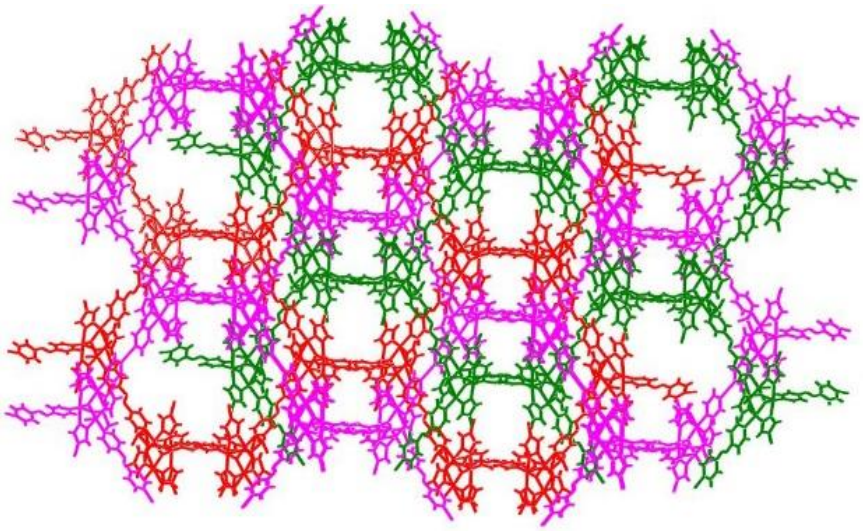

Figure 86. Schematic view of the threefold-interpenetrating net of compound **FIU-2**.

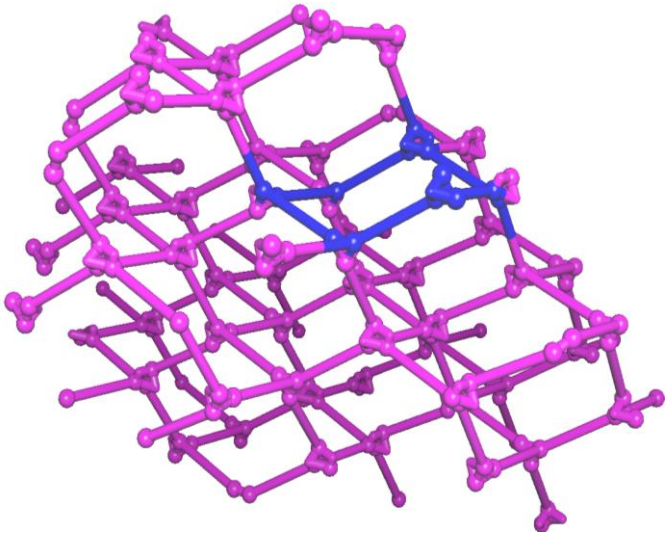

Figure 87. One of nets highlighting (in blue) the chair configuration of compound **FIU-2**.

3.6.2.3. Crystal structure description of {[$Cu_3(\mu_3\text{-}OH)(\mu\text{-}4\text{-}Cl\text{-}pz)_3(abp)_{2.5}][CF_3SO_3]_2\}_n$ [FIU-3]

Compound **FIU-3** crystallizes in triclinic space group $P\bar{1}$ with three $Cu_3(\mu_3\text{-}OH)(\mu\text{-}4\text{-}Cl\text{-}pz)_3(abp)_{2.5}$ repeating units, The capping μ_3-OH group are located 0.465(0) Å, 0.423(2) Å, 0.512(1) Å above the Cu_3 plane. Copper atoms exhibit five and four coordination with N_4O (N_3O_2) and N_3O donor set, and adopt square pyramidal and distorted square planar geometries, respectively. The Cu···Cu distances within the trinuclear units vary between 3.293(4) Å and 3.422(3) Å, similar to those of **FIU-2**, 3.330(4)-3.348(2) Å. The crystal structure is characterized by a polymeric 3D architecture with 42.5% solvent–accessible void (4743.79 $Å^3$).

In compound **FIU-3**, each trinuclear SBU further links five neighboring SBUs through abp spacers in three dimensions to generate 3-fold interpenetration framework with large hexagonal channels (Figure 89 and 90). In compound **FIU-2**, each SBU links four neighboring SBUs through the same linkers (Figure 85).

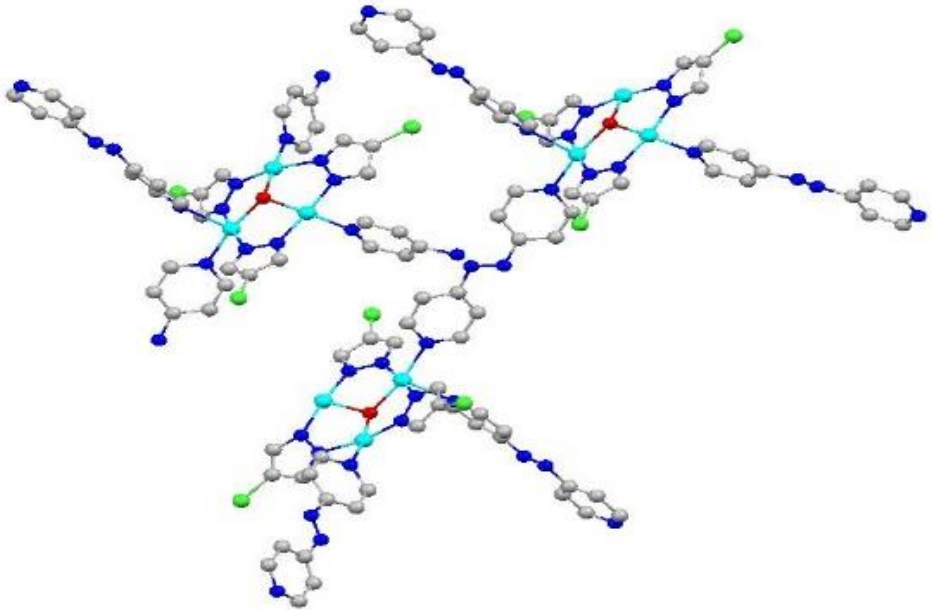

Figure 88. Asymmetric unit of compound **FIU-3**. Triflates and hydrogen atoms are omitted for clarity.

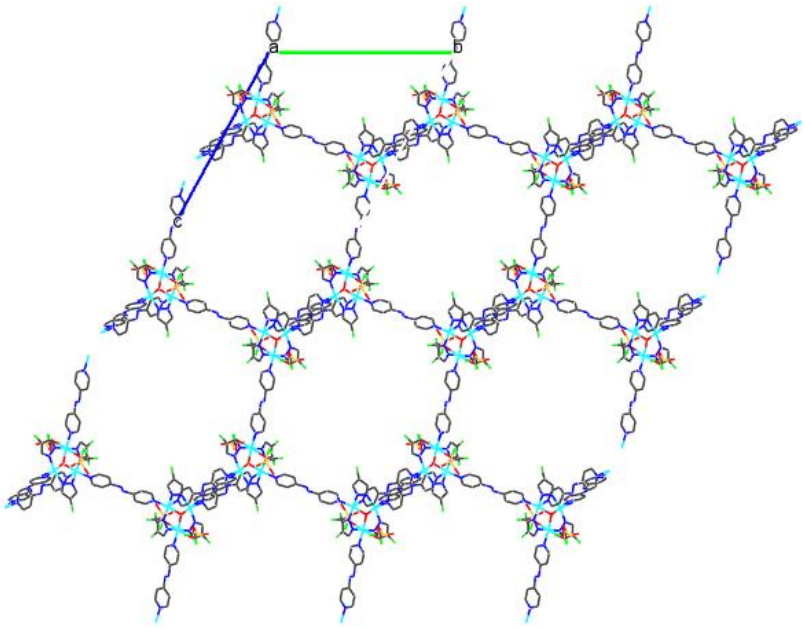

Figure 89. One of the net in three-fold interpenetrated of **FIU-3**, showing the hexagonal channels.

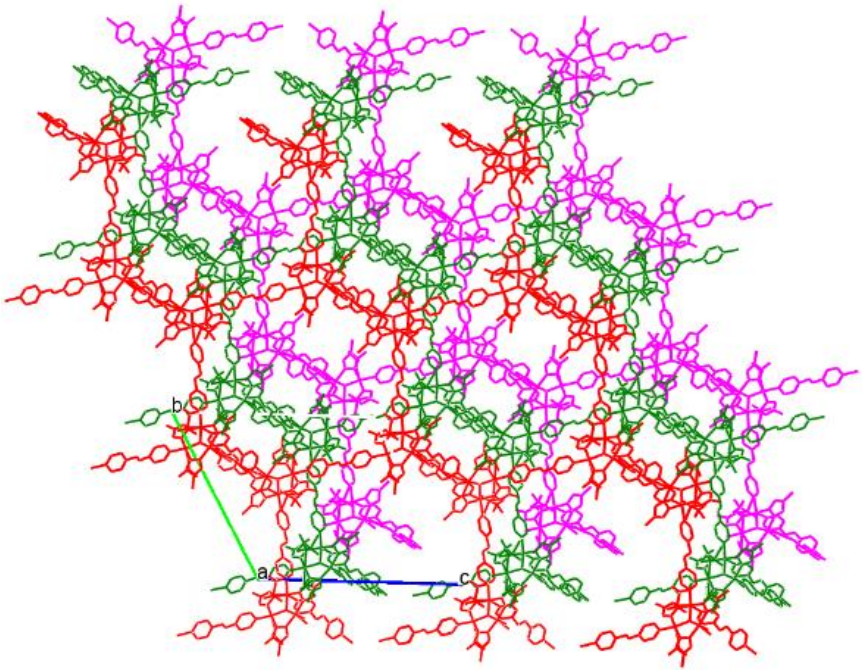

Figure 90. Three interpenetrated nets in compound **FIU-3**, each color depicting an individual net.

3.6.3. Preliminary results of photo-chemical reaction of FIU-1 solution precursor.

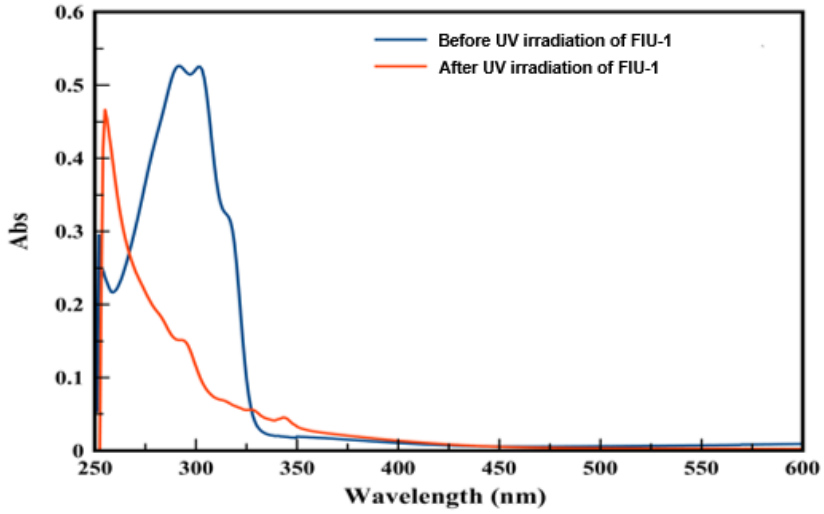

Figure 91. UV irradiation of FIU-1 at 365 nm in DMSO.

Compound FIU-1 was irradiated at 365 nm for 1 h in DMSO solution, the absorption spectra recorded before and after irradiation indicate a structural change (Figure 91). The structural characterization of the irradiation product(s) is currently in progress.

3.6.4. Thermal Stability of FIU-1

To examine the thermal stabilities of the complex **FIU-1**, thermogravimetric (TG) analyses were carried out (Figure 92). TGA data revealed a weight loss of 3% from the room temperature to 100 °C for **FIU-1**, corresponding to the loss of two interstitial water molecules, in agreement with elemental analysis.

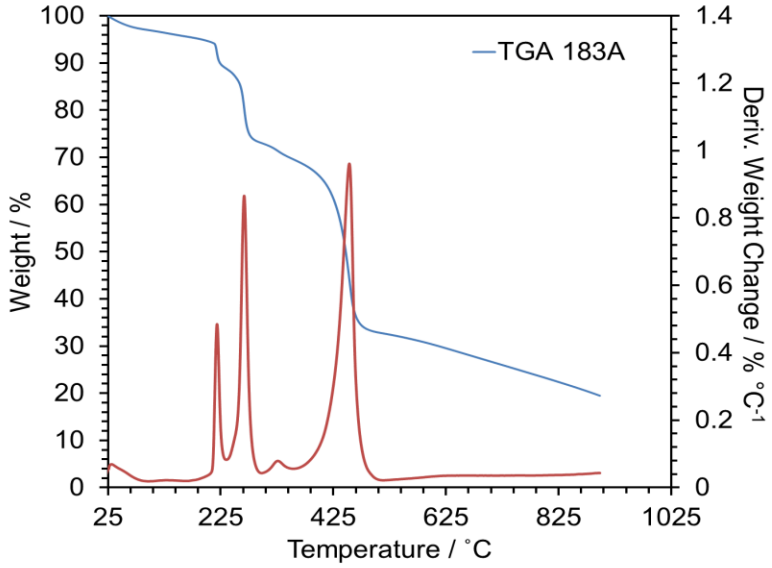

Figure 92. TGA diagram of **FIU-1** (blue trace) and its first derivative (red trace).

3.6.5. Gas Adsorption Studies of complexes FIU-1, FIU-2 and FIU-3

On the basis of TGA analysis, activation at 423 K was performed to evacuate guest molecules from the material prior to adsorption measurement; the framework of compound **FIU-1** remains intact under this treatment. Gas adsorption experiments were conducted at 298 K to evaluate its

permanent porosity. Gas sorption studies performed on the material revealed a small uptake of N_2, CH_4, and a comparatively larger uptake of CO_2 at 298 K, which is likely due to the different kinetic diameter for the three gases (CO_2, 3.3 Å; N_2, 3.64 Å; CH_4, 3.8 Å).

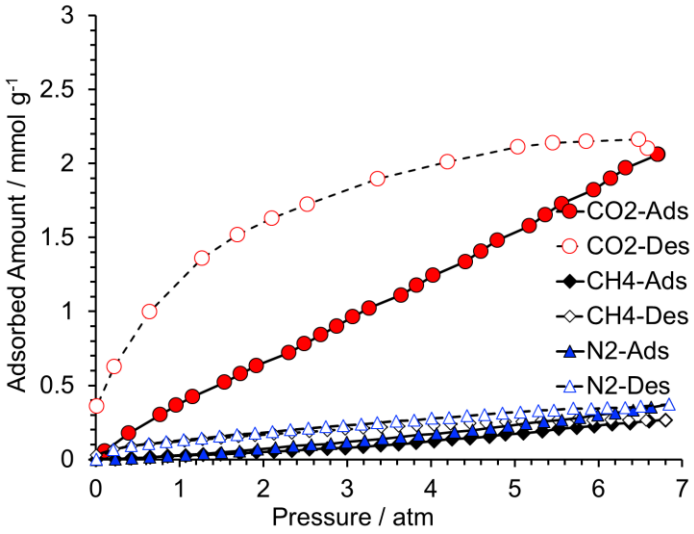

Figure 93. Pure component equilibrium adsorption/desorption isotherm of **FIU-1** at 298K.

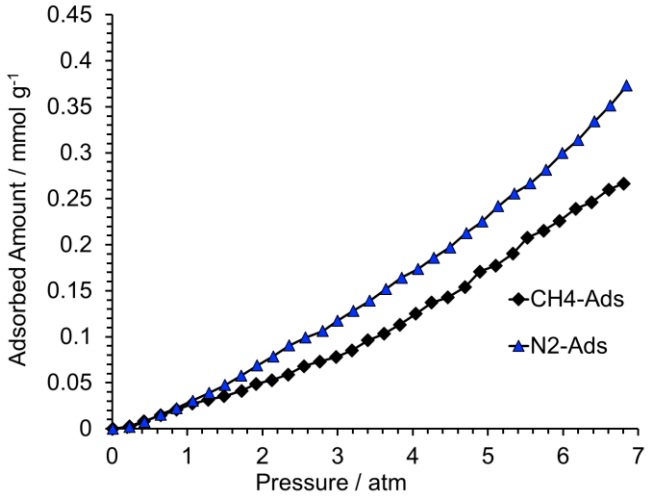

Figure 94. CH_4/N_2 sorption isotherms for **FIU-1**.

The gas adsorption isotherms of compound **FIU-1** in the 0-7 atm range are depicted in Figure 93. Prior to adsorption, the materials were degassed at temperature as high as 423K. Figure 93 shows the result for the CO_2, CH_4 and N_2 equilibrium adsorption-desorption at 298 K. This MOF is selective for CO_2 over CH_4 or N_2; there is little adsorption of CH_4 or N_2 up to 7 atm. The adsorption capacity of CO_2 increased at increasing pressure up to 6.5 atm. The gas adsorption profile exhibit type III adsorption isotherms, indicating weak interaction between adsorbate and adsorbent. The desorption trace is different from adsorption, leading to hysteretic adsorption /desorption profile of the isotherm. 0.361 mmol/g of CO_2 (16.7% of total CO_2 adsorbed) remain sorbed, even after the pressure returns to 0.01 atm.

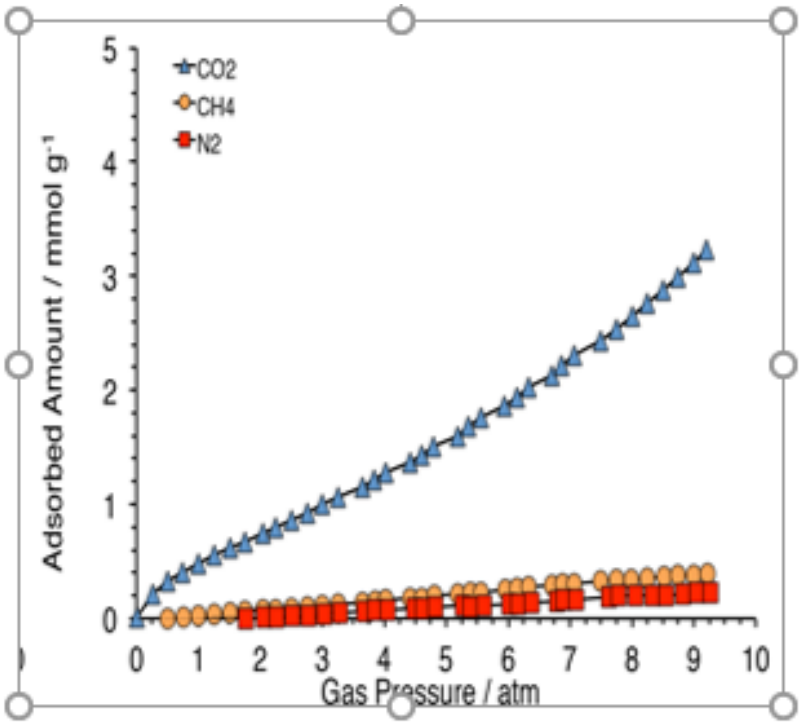

Figure 95 . $CH_4/CO_2/N_2$ sorption isotherms for **FIU-2**.

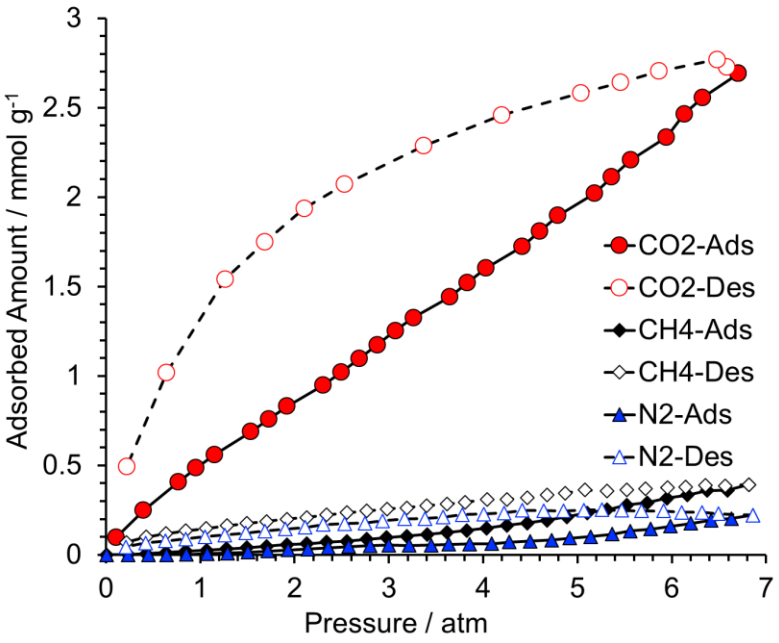

Figure 96. Pure component equilibrium adsorption/desorption isotherms of compound **FIU-3** at 298K.

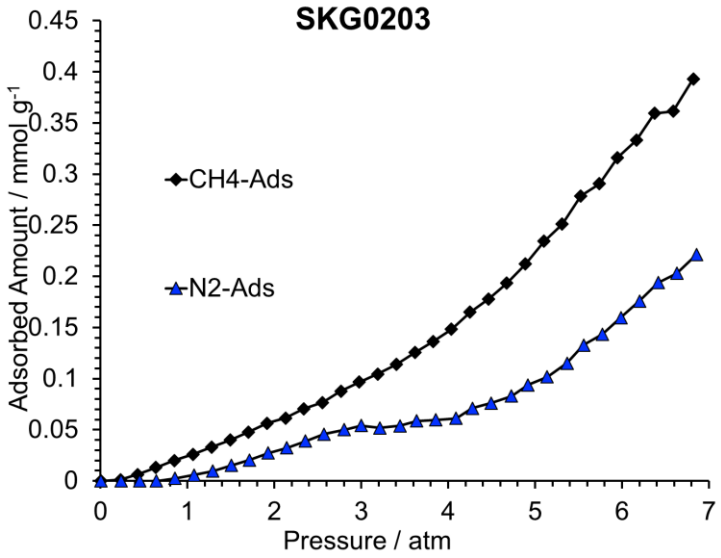

Figure 97. CH_4/N_2 sorption isotherms of compound **FIU-3**.

Compared with isotherms for the same sorbates on compound **FIU-1**, complex **FIU-3** has the larger CO_2 adsorption capacity, due to surface area and pore volume differences (Figure 96). Adsorption isotherms for CO_2 display approximately type III isotherms with hysteresis. CO_2 sorption capacity

reaches a maximum of 2.77 mmol/g at 6.4 atm, comparatively, the CH_4 uptake is only 0.36 mmol/g, and the N_2 uptake is 0.19 mmol/g at same pressure (CO_2 uptake values as high as 2.77 mmol/g at 6.4 atm). Interesting, the isotherms for CO_2, H_4, N_2 exhibit significant desorption hysteresis. Upon desorption, complex **FIU-3** retained approximately 17.7%, 18.9% and 16% respectively of its sorbed CO_2, CH_4 and N_2 at the same desorption pressure (approximate 0.22 atm), while MOF-3 is also selective for CO_2 over CH_4 or N_2, as expected, there was little adsorption of CH_4 and N_2, even at pressure as high as 7 atm. Compared with N_2, complex **FIU-3** has higher selectivity for CH_4, the maximum CH_4 uptake is 0.39 mmol/g at 6.8 atm, while the maximum N_2 uptake is only 0.25 mmol/g at 5 atm. It also exhibits higher selectivities for CH_4 over N_2.

Table 13. Summary of 3-fold interpenetrated 3D Cu^{II}-MOFs.

Name	Stoichiometry	Crystal system /Space group	Node structure	Pore volume	CO_2 adsorption capacity/pressure	Remarks
FIU-1	1:1:2:1	Monoclinic, *C2/c*	6- connecting	45.2%	2.16 mmol/g 6.5atm	3D, 3-fold interpene-trated
FIU-2	1:1:2:1	Monoclinic, *P2/c*	4- connecting	46.7%	2.1 mmol/g 6.5 atm	
FIU-3	1:1:4:1	Triclinic, $P\bar{1}$	5- connecting	42.5%	2.77 mmol/g 6.5atm	

3.7. Conclusions

To prepare MOFs, the best method is to use a copper salt with a non-coordinating anion, pyrazole and and base in order to first synthesize the SBUs. The linker must be layered over the solution containing the SBU afterwards, to facilitate slow reaction and crystallization. Metathesis reactions with linker and Cl-terminal trinuclear Cu-pyrazolate complex were not successful, as they tended to form precipitates or 1D chains (tmpy linker).

Before embarking on the study of photo-active MOFs, we intended to study the chemistry and optimize the conditions using a simpler fragment, a dimer of trimers connected by photo-active linkers. $[\{Cu_3(\mu_3\text{-}OH)(\mu\text{-}4\text{-}Cl\text{-}pz)_3(py)_2\}_2(\mu\text{-}abp)](ClO_4)_4$ **[10]** , where abp = 4,4'-azopyridine, was synthesized as a model of the photochemical reaction with UV irradiation. The bidentate abp ligand is used as photo-responsive linker that can undergo a conformational change upon UV irradiation. Indeed, the absorption spectra recorded before and after irradiation indicated a structural change. We are in the process of isolating and identifying the structure of the product. 2D and 3D materials with $\{[Cu_3(\mu_3\text{-}OH)(\mu\text{-}4\text{-}R\text{-}pz)_3]^{2+}\}_n$ SBUs where R = Ph or Cl , which can potentially undergo cis/trans-isomerization, have been prepared during this project.

Polymorphic 1D chains were obtained from a one-pot reaction using $[PPN]_2[Cu_3(\mu_3\text{-}O)(\mu\text{-}pz)_3Cl_3]$ and tmpy linker andthe flexibility of Cu-pyrazolate based on 1D chains have been investigated under high pressure. The material is elastic up to 3.0 GPa and is amorphized irreversibly at 4.2 GPa, as indicated by variable pressure PXRD.

Analogous reactions by employing 4-Ph-pz ligands, instead of pz, or 4-Cl-pz, have resulted in two 2D-structures, $\{[Cu_3(\mu_3\text{-}OH)(\mu\text{-}4\text{-}Ph\text{-}pz)_3(abp)_{1.5}][(CF_3SO_3)_2]\}_n$ **[12]**, $\{[Cu_3(\mu_3\text{-}OH)(\mu\text{-}4\text{-}Ph\text{-}pz)_3(CH_3CN)(abp)_{1.5}][(\mu\text{-}4\text{-}Ph\text{-}pz)(\mu\text{-}Cl)Cu(py)(abp)_{0.5}](CF_3SO_3)_2\}_n$ **[13]**. The 2D network propagates

in a similar way through Cu-termini, but the bulky phenyl rings on the pyrazolate ligands prevent the formation of 3D networks, but π-π interactions have been observed between the 2D sheets.

To prepare porous compounds **FIU-1**, **FIU-2** and **FIU-3**, a two-stage synthetic procedure was followed; $Cu(CF_3SO_3)_2$, 4-Cl-pzH and NaOH were mixed to prepare the SBU, dilute solutions of the photo-active linkers (abp or bpe) were layered over the solution of SBU. Crystals of the MOFs were obtained in a few days to weeks.

We have previously shown that the porous-MOF materials with $\{[Cu_3(\mu_3\text{-}OH)(\mu\text{-}4\text{-}R\text{-}pz)_3]^{2+}\}_n$ SBUs, where R = H, Cl, or CHO, have interpenetrated-lattice structures and are capable of adsorbing CO_2 selectively.[17] In this project, we have been prepared three new MOFs with photo-responsive linkers and 4-Cl-pzH. Stoichiometry has been varied and a different synthetic/crystallization method has been used to prepare new materials. Three new metal-organic-frameworks (MOFs) of Cu(II) ion, $\{[Cu_3(\mu_3\text{-}OH)(\mu\text{-}4\text{-}Cl\text{-}pz)_3\ (bpe)_3][CF_3SO_3]_2\}_n$ [**FIU-1**], $\{[Cu_3(\mu_3\text{-}OH)(\mu\text{-}4\text{-}Cl\text{-}pz)_3(abp)_2][CF_3SO_3]_2\}_n$ [**FIU-2**], $\{[Cu_3(\mu_3\text{-}OH)(\mu\text{-}4\text{-}Cl\text{-}pz)_3(abp)_{2.5}][CF_3\text{-}SO_3]_2\}_n$ [**FIU-3**] have been successfully synthesized using mixed ligand systems and characterized by single X-ray analysis. Compound **FIU-1** demonstrated the usefulness of a hexanuclear Cu^{II} -pyrazolate moiety as an SBU for generating 3-fold interpenetrated 3D polymeric network. Structural analyses revealed that both **FIU-2 and FIU-3** have novel 3-fold interpenetrating 3D hexagonal framework structures. Compound **FIU-2** crystallizes in the monoclinic crystal system with the $P2_1/c$ space group, whereas **FIU-3** crystallizes in triclinic space group $P\bar{1}$. Both structures contain Cu_3-SBUs connected by the linkers through the Cu-termini. Complexes **FIU-2** and **FIU-3** illustrate the influence of pH; the only difference between the syntheses is the amount of NaOH added 3 eq. in **FIU-2** and 2 eq. in **FIU-3** on MOF formation.

The gas adsorption properties of the three MOFs have been determined experimentally in the 0-7 atm pressure range. All MOFs sorb CO_2 selectively over N_2, CH_4. Like the previous MOFs studied in our lab, complexes **FIU-1** and **FIU-3** also exhibit hysteretic sorption-desorption profiles indicating the flexibility of the MOFs upon adsorption. Complex **FIU-1** shows slight selectivity toward N_2 over CH_4. Compound **FIU-2** has the largest CO_2 adsorption capacity (Table 13) among the MOFs studied in our group.

In summary, we have made substantial strides in the project: (i) Identified that nitrite coordination lowers the oxidation potential of the SBU significantly; (ii) Prepared key SBUs with varying terminal and pyrazole substitutions that modify structural and electronic properties; (iii) Photochemical modification on a dimer-of-trimers to establish working conditions for the MOFs; (iv) Prepared, characterized and analyzed sorption properties of three new MOFs that show selectivity towards CO_2 over N_2 or CH_4; (v) 4-Ph-pz substitution leads to the formation of new class of 2D sheets based on Cu-pyrazolato SBUs.

3.8. Future work

In this dissertation, MOFs have been prepared by connecting triangular $Cu_3(\mu_3\text{-OH})$-SBUs through nitrogen donor photo-active organic linkers, 1,2-di(4-pyridyl)ethylene (bpe) and 4,4'-azo-bis(4-pyridine) (abp). The future work is photochemical modification of MOFs (FIU-1, FIU-2 and FIU-3) in the solid phase, then determine the gas adsorption after UV-irradiation. But there is no redox activity in these MOFs owing to the redox-inert $Cu_3(\mu_3\text{-OH})$ units, while the planar $[Cu_3(\mu_3\text{-O})]^{4+}$ species can be reversibly oxidized to their mixed-valence counterparts, formally $Cu^{II}_2Cu^{III}$. MOFs using Cu_3 - and Cu_6 -SBUs are expected to maintain their 3D structure upon their redox-modification. We have been approved NO_2 coordination lower the oxidation potential of copper pyrazolate complexes (SBUs). It is necessary to choose Cu-NO_2 complex as SBU to build redox-

active MOF. SBUs with suitable pyrazoles (4-CHO-pzH) will be prepared and then condensation with stoichiometric amount of diamine linkers led to MOFs (Scheme 15). The final goals of redox-active MOFs include: (i) redox modification of MOF; (ii) the redox functionality of the new MOFs will be studied in solution and/or in the sold phase; (iii)determination of the gas-sorption properties of MOFs before and after modification.

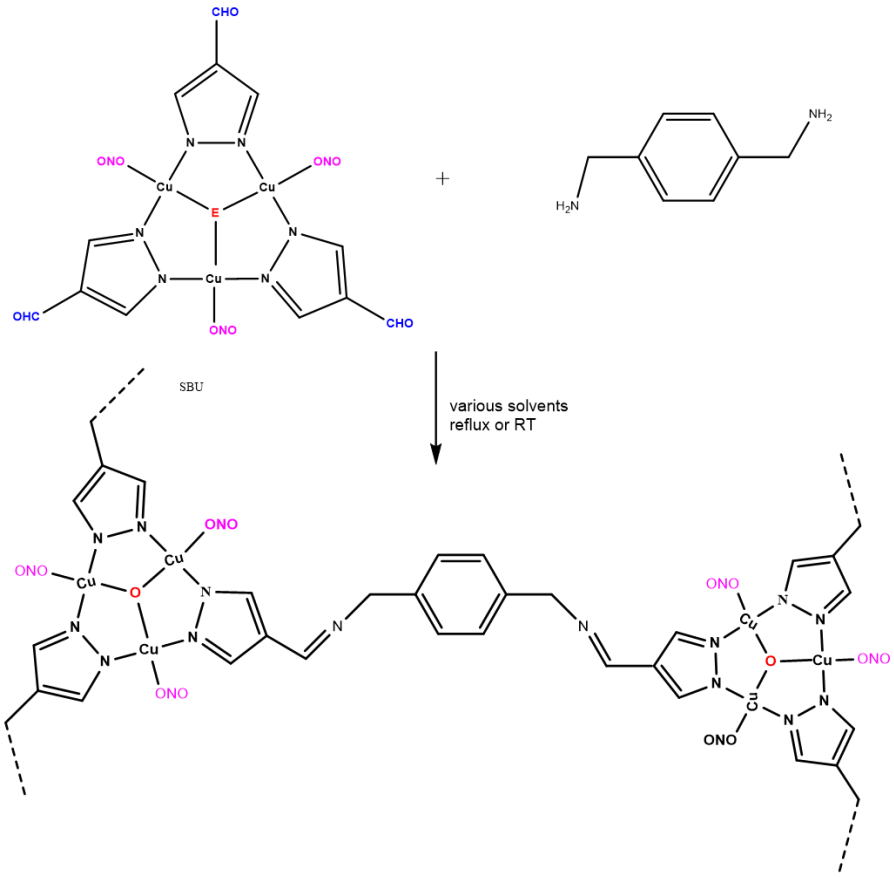

Scheme 15. General scheme for the reaction between SBU and aralkyl amine to form Cu_3-pyrazolate MOFs.

References

(1) Renard, S. L.; Sylvestre, I.; Barrett, S. A.; Kilner, C. A.; Halcrow, M. A. Homoleptic Zinc(II) Complexes with First and Second Coordination Shells of 5-Tert-Butylpyrazole. *Inorg. Chem.* **2006**, *45*, 8711–8718.

(2) A. Halcrow, M. Pyrazoles and Pyrazolides —flexible Synthons in Self-Assembly. *Dalton Trans.* **2009**, 2059–2073.

(3) Ahmed, B. M.; Mezei, G. From Ordinary to Extraordinary: Insights into the Formation Mechanism and pH-Dependent Assembly/Disassembly of Nanojars. *Inorg. Chem.* **2016**, *55*, 7717–7728.

(4) Kirillov, A. M.; Kopylovich, M. N.; Kirillova, M. V.; Haukka, M.; da Silva, M. F. C. G.; Pombeiro, A. J. L. Multinuclear Copper Triethanolamine Complexes as Selective Catalysts for the Peroxidative Oxidation of Alkanes under Mild Conditions. *Angew. Chem. Int. Ed.* **2005**, *44*, 4345–4349.

(5) Ardizzoia, G. A.; Cenini, S.; La Monica, G.; Masciocchi, N.; Moret, M. Synthesis, X-Ray Structure, and Catalytic Properties of the Unprecedented Tetranuclear Copper(I) Species $[Cu(Dppz)]_4$(Hdppz = 3,4-Diphenylpyrazole). *Inorg. Chem.* **1994**, *33*, 1458–1463.

(6) Wang, X.-L.; Zheng, J.; Li, M.; Weng Ng, S.; Chan, S. L.-F.; Li, D. Curved Cyclic Trimers: Orthogonal Cu–Cu Interaction versus Tetrameric Halogen Bonding. *Cryst. Growth Des.* **2016**, *16*, 4991–4998.

(7) Santini, C.; Pellei, M.; Gandin, V.; Porchia, M.; Tisato, F.; Marzano, C. Advances in Copper Complexes as Anticancer Agents. *Chem. Rev.* **2014**, *114*, 815–862.

(8) Meundaeng, N.; Rujiwatra, A.; Prior, T. J. Copper coordination polymers constructed from thiazole-5-carboxylic acid: Synthesis, crystal structures, and structural transformation. *J. Solid State Chem*. **2017**, 245, 138-145.

(9) Hasegawa, S.; Horike, S.; Matsuda, R.; Furukawa, S.; Mochizuki, K.; Kinoshita, Y.; Kitagawa, S. Three-Dimensional Porous Coordination Polymer Functionalized with Amide Groups Based on Tridentate Ligand: Selective Sorption and Catalysis. *J. Am. Chem. Soc.* **2007**, *129*, 2607–2614.

(10) Ferrer, S.; Haasnoot, J. G.; Reedijk, J.; Müller, E.; Biagini Cingi, M.; Lanfranchi, M.; Manotti Lanfredi, A. M.; Ribas, J. Trinuclear N,N-Bridged Copper(II) Complexes Involving a Cu_3OH Core: $[Cu_3(\mu_3\text{-}OH)L_3A(H_2O)_2]A\cdot(H_2O)x$ {L = 3-Acetylamino-1,2,4-Triazolate; A

= CF_3SO_3, NO_3, ClO_4; x = 0, 2} Synthesis, X-Ray Structures, Spectroscopy, and Magnetic Properties. *Inorg. Chem.* **2000**, *39*, 1859–1867.

(11) Huang, S.-F.; Chou, Y.-C.; Misra, P.; Lee, C.-J.; Mohanta, S.; Wei, H.-H. Syntheses, Structures, and Magnetic Properties of Two New μ-Alkoxo-μ-Pyrazolato Bridged Dicopper(II) Complexes. *Inorganica Chim. Acta.* **2004**, *357*, 1627–1631.

(12) Carlucci, L.; Ciani, G.; Maggini, S.; Proserpio, D. M. A New Polycatenated 3D Array of Interlaced 2D Brickwall Layers and 1D Molecular Ladders in $[Mn_2(Bix)_3(NO_3)_4]\cdot 2CHCl_3$ [Bix=1,4-Bis(Imidazol-1-Ylmethyl)Benzene] That Undergoes Supramolecular Isomerization upon Guest Removal. *Cryst. Growth Des.* **2008**, *8*, 162–165.

(13) Kirillov, A. M.; Kopylovich, M. N.; Kirillova, M. V.; Karabach, E. Y.; Haukka, M.; da Silva, M. F. C. G.; Pombeiro, A. J. L. Mild Peroxidative Oxidation of Cyclohexane Catalyzed by Mono-, Di-, Tri-, Tetra- and Polynuclear Copper Triethanolamine Complexes. *Adv. Synth. Catal.* **2006**, *348*, 159–174.

(14) Casarin, M.; Cingolani, A.; Di Nicola, C.; Falcomer, D.; Monari, M.; Pandolfo, L.; Pettinari, C. The Different Supramolecular Arrangements of the Triangular $[Cu_3(\mu_3\text{-}OH)(\mu\text{-}pz)_3]^{2+}$ (pz = pyrazolate) Secondary Building Units. Synthesis of a Coordination Polymer with Permanent Hexagonal Channels. *Cryst. Growth Des.* **2007**, *7*, 676–685.

(15) Mezei, G.; Baran, P.; Raptis, R. G. Anion Encapsulation by Neutral Supramolecular Assemblies of Cyclic Cu^{II} Complexes: A Series of Five Polymerization Isomers, $[\{cis\text{-}Cu^{II}(\mu\text{-}OH)(\mu\text{-}Pz)\}_n]$, N=6, 8, 9, 12, and 14. *Angew. Chem. Int. Ed.* **2004**, *43*, 574–577.

(16) Cingolani, A., Galli, S.; Masciocchi, N.; Pandolfo, L.; Pettinari, C.; Sironi, A. Sorption−Desorption Behavior of Bispyrazolato−Copper(II) 1D Coordination Polymers. *J. Am. Chem. Soc.*, **2005**, *127*, 6144–6145.

(17) Condello, F.; Garau, F.; Lanza, A.; Monari, M.; Nestola, F.; Pandolfo, L.; Pettinari, C. Synthesis and Structural Characterizations of New Coordination Polymers Generated by the Interaction Between the Trinuclear Triangular SBU $[Cu_3(\mu_3\text{-}OH)(\mu\text{-}Pz)_3]^{2+}$ and 4,4′-Bipyridine. 3°. *Cryst. Growth Des.* **2015**, *15*, 4854–4862.

(18) Angaridis, P. A.; Baran, P.; Boča, R.; Cervantes-Lee, F.; Haase, W.; Mezei, G.; Raptis, R. G.; Werner, R. Synthesis and Structural Characterization of Trinuclear Cu^{II}−Pyrazolato Complexes Containing μ_3-OH, μ_3-O, and μ_3-Cl Ligands. Magnetic Susceptibility Study of $[PPN]_2[(\mu_3\text{-}O)Cu_3(\mu\text{-}Pz)_3Cl_3]$. *Inorg. Chem.* **2002**, *41*, 2219–2228.

(19) Sheikh, J. A.; Jena, H. S.; Adhikary, A.; Khatua, S.; Konar, S. An Unprecedented Octadecanuclear Copper(II) Pyrazolate–Phosphonate Nanocage: Synthetic, Structural, Magnetic, and Mechanistic Study. *Inorg. Chem.* **2013**, *52*, 9717–9719.

(20) Mezei, G. Incarceration of One or Two Phosphate or Arsenate Species within Nanojars, Capped Nanojars and Nanohelicages: Helical Chirality from Two Closely-Spaced, Head-to-Head PO_4^{3-} or AsO_4^{3-} Ions. *Chem. Commun.* **2015**, *51*, 10341–10344.

(21) Di Nicola, C.; Forlin, E.; Garau, F.; Gazzano, M.; Lanza, A.; Monari, M.; Nestola, F.; Pandolfo, L.; Pettinari, C.; Zorzi, A.; et al. Coordination Polymers Based on the Trinuclear Triangular Secondary Building Unit $[Cu_3(\mu_3\text{-}OH)(\mu\text{-}pz)_3]^{2+}$ (pz = pyrazolate) and Succinate Anion. *Cryst. Growth Des.* **2013**, *13*, 126–135.

(22) Boča, R.; Dlháň, L.; Mezei, G.; Ortiz-Pérez, T.; Raptis, R. G.; Telser, J. Triangular, Ferromagnetically-Coupled Cu^{II}_3–Pyrazolato Complexes as Possible Models of Particulate Methane Monooxygenase (PMMO). *Inorg. Chem.* **2003**, *42*, 5801–5803.

(23) Liu, X.; Miranda, M. P. de; McInnes, E. J. L.; Kilner, C. A.; Halcrow, M. A. Antisymmetric Exchange in Two Tricopper(II) Complexes Containing a $[Cu_3(\mu_3\text{-}OMe)]^{5+}$ Core. *Dalton Trans.* **2004**, 59–64.

(24) Allen, G. C.; Hush, N. S. Intervalence-Transfer Absorption. Part 1. Qualitative Evidence for Intervalence-Transfer Absorption in Inorganic Systems in Solution and in the Solid State. In *Progress in Inorganic Chemistry*; Cotton, F. A., Ed.; John Wiley & Sons, Inc., **1967**, 357–389.

(25) Creutz, C.; Taube, H. Binuclear Complexes of Ruthenium Ammines. *J. Am. Chem. Soc.* **1973**, *95*, 1086–1094.

(26) Creutz, C.; Taube, H. Direct Approach to Measuring the Franck-Condon Barrier to Electron Transfer between Metal Ions. *J. Am. Chem. Soc.* **1969**, *91*, 3988–3989.

(27) Mezei, G.; McGrady, J. E.; Raptis, R. G. First Structural Characterization of a Delocalized, Mixed-Valent, Triangular Cu_3^{7+} Species: Chemical and Electrochemical Oxidation of a $Cu^{II}_3(\mu_3\text{-}O)$ Pyrazolate and Electronic Structure of the Oxidation Product. *Inorg. Chem.* **2005**, *44*, 7271–7273.

(28) Solomon, E. I.; Heppner, D. E.; Johnston, E. M.; Ginsbach, J. W.; Cirera, J.; Qayyum, M.; Kieber-Emmons, M. T.; Kjaergaard, C. H.; Hadt, R. G.; Tian, L. Copper Active Sites in Biology. *Chem. Rev.* **2014**, *114*, 3659–3853.

(29) Solomon, E. I.; Sundaram, U. M.; Machonkin, T. E. Multicopper Oxidases and Oxygenases. *Chem. Rev.* **1996**, *96*, 2563–2606.

(30) Casarin, M.; Corvaja, C.; Di Nicola, C.; Falcomer, D.; Franco, L.; Monari, M.; Pandolfo, L.; Pettinari, C.; Piccinelli, F. One-Dimensional and Two-Dimensional Coordination Polymers from Self-Assembling of Trinuclear Triangular Cu(II) Secondary Building Units. *Inorg. Chem.* **2005**, *44*, 6265–6276.

(31) Cage, B.; Cotton, F. A.; Dalal, N. S.; Hillard, E. A.; Rakvin, B.; Ramsey, C. M. Observation of Symmetry Lowering and Electron Localization in the Doublet-States of a Spin-Frustrated Equilateral Triangular Lattice: $Cu_3(O_2C_{16}H_{23})\cdot 1.2C_6H_{12}$. *J. Am. Chem. Soc.* **2003**, *125*, 5270–5271.

(32) Belinsky, M. I. Hyperfine Splittings in Spin-Frustrated Trinuclear Cu_3 Clusters. *Inorg. Chem.* **2004**, *43*, 739–746.

(33) Boča, R.; Dlháň, L.; Mezei, G.; Ortiz-Pérez, T.; Raptis, R. G.; Telser, J. Triangular, Ferromagnetically-Coupled Cu^{II}_3−Pyrazolato Complexes as Possible Models of Particulate Methane Monooxygenase (PMMO). *Inorg. Chem.* **2003**, *42*, 5801–5803.

(34) Nguyen, H. H.; Shiemke, A. K.; Jacobs, S. J.; Hales, B. J.; Lidstrom, M. E.; Chan, S. I. The Nature of the Copper Ions in the Membranes Containing the Particulate Methane Monooxygenase from Methylococcus Capsulatus (Bath). *J. Biol. Chem.* **1994**, *269*, 14995–15005.

(35) Casarin, M.; Corvaja, C.; di Nicola, C.; Falcomer, D.; Franco, L.; Monari, M.; Pandolfo, L.; Pettinari, C.; Piccinelli, F.; Tagliatesta, P. Spontaneous Self-Assembly of an Unsymmetric Trinuclear Triangular Copper(II) Pyrazolate Complex, $[Cu_3(\mu_3\text{-}OH)(\mu\text{-}pz)_3(MeCOO)_2(Hpz)]$ (Hpz = Pyrazole). Synthesis, Experimental and Theoretical Characterization, Reactivity, and Catalytic Activity. *Inorg. Chem.* **2004**, *43*, 5865–5876.

(36) Casarin, M.; Corvaja, C.; Di Nicola, C.; Falcomer, D.; Franco, L.; Monari, M.; Pandolfo, L.; Pettinari, C.; Piccinelli, F. One-Dimensional and Two-Dimensional Coordination Polymers from Self-Assembling of Trinuclear Triangular Cu(II) Secondary Building Units. *Inorg. Chem.* **2005**, *44*, 6265–6276.

(37) Di Nicola, C.; Karabach, Y. Y.; Kirillov, A. M.; Monari, M.; Pandolfo, L.; Pettinari, C.; Pombeiro, A. J. L. Supramolecular Assemblies of Trinuclear Triangular Copper(II) Secondary Building Units through Hydrogen Bonds. Generation of Different Metal−Organic Frameworks, Valuable Catalysts for Peroxidative Oxidation of Alkanes. *Inorg. Chem.* **2007**, *46*, 221–230.

(38) Mezei, G.; Rivera-Carrillo, M.; Raptis, R. G. Effect of Copper-Substitution on the Structure and Nuclearity of Cu(II)-Pyrazolates: From Trinuclear to Tetra-, Hexa- and Polynuclear Complexes. *Inorganica Chim. Acta.* **2004**, *357*, 3721–3732.

(39) Mezei, G.; Rivera-Carrillo, M.; Raptis, R. G. Trigonal-Prismatic Cu^{II}_6-Pyrazolato Cages: Structural and Electrochemical Study, Evidence of Charge Delocalisation. *Dalton Trans.* **2006**, 37–40.

(40) Rivera-Carrillo, M.; Chakraborty, I.; Mezei, G.; Webster, R. D.; Raptis, R. G. Tuning of the $[Cu_3(\mu\text{-}O)]^{4+/5+}$ Redox Couple: Spectroscopic Evidence of Charge Delocalization in the Mixed-Valent $[Cu_3(\mu\text{-}O)]^{5+}$ Species. *Inorg. Chem.* **2008**, *47*, 7644–7650.

(41) Mathivathanan, L.; Cruz, R.; Raptis, R. G. A $[Cu_3(\mu_3\text{-}O)]$–pyrazolate Metallacycle with Terminal Nitrate Ligands Exhibiting Point Group Symmetry 3. *Acta Crystallogr. Sect. E Crystallogr. Commun.* **2016**, *72*, 492–494.

(42) Rivera-Carrillo, M.; Chakraborty, I.; Raptis, R. G. Systematic Synthesis of a Metal Organic Framework Based on Triangular $Cu_3(\mu_3\text{-}OH)$ Secondary Building Units: From a 0-D Complex to a 1-D Chain and a 3-D Lattice. *Cryst. Growth Des.* **2010**, *10*, 2606–2612.

(43) Mathivathanan, L.; Torres-King, J.; Primera-Pedrozo, J. N.; García-Ricard, O. J.; Hernández-Maldonado, A. J.; Santana, J. A.; Raptis, R. G. Selective CO_2 Adsorption on Metal-Organic Frameworks Based on Trinuclear Cu_3-Pyrazolato Complexes: An Experimental and Computational Study. *Cryst. Growth Des*. **2013**, *13*, 2628-2635.

(44) Ehlert, M. K.; Rettig, S. J.; Storr, A.; Thompson, R. C.; Trotter, J. Metal Pyrazolate Polymers. Part 2. Synthesis, Structure, and Magnetic Properties of $[Cu(4\text{-}Xpz)_2]x$ Polymers (Where X = Cl, Br, Me, H; pz = Pyrazolate). *Can. J. Chem.* **1991**, *69*, 432–439.

(45) Olguín, J.; Brooker, S. Synthesis of 3- and 5-Formyl-4-Phenyl-1H-Pyrazoles: Promising Head Units for the Generation of Asymmetric Imine Ligands and Mixed Metal Polynuclear Complexes. *New J. Chem.* **2011**, *35*, 1242–1253.

(46) Purification of Laboratory Chemicals - 6th Edition https://www.elsevier. com/ books/ purification-of-laboratory-chemicals/armarego/978-1-85617-567-8 (accessed Jan 24, **2018**).

(47) Spek, A. L. Single-Crystal Structure Validation with the Program PLATON. *J. Appl. Crystallogr.* **2003**, *36*, 7–13.

(48) Carlotto, S.; Casarin, M.; Lanza, A.; Nestola, F.; Pandolfo, L.; Pettinari, C.; Scatena, R. Reaction of Copper(II) Chloroacetate with Pyrazole. Synthesis of a One-Dimensional Coordination Polymer and Unexpected Dehydrochlorination Reaction. *Cryst. Growth Des.* **2015**, *15*, 5910–5918.

(49) Zangrando, E.; Casanova, M.; Alessio, E. Trinuclear Metallacycles: Metallatriangles and Much More. *Chem. Rev.* **2008**, *108*, 4979–5013.

(50) Stamatatos, T. C.; Papaefstathiou, G. S.; MacGillivray, L. R.; Escuer, A.; Vicente, R.; Ruiz, E.; Perlepes, S. P. Ferromagnetic Coupling in a 1D Coordination Polymer Containing a Symmetric $[Cu(\mu_{1,1}\text{-}N_3)_2Cu(\mu_{1,1}\text{-}N_3)_2Cu]^{2+}$ Core and Based on an Organic Ligand Obtained from the Solid State. *Inorg. Chem.* **2007**, *46*, 8843–8850.

(51) Lazari, G.; Stamatatos, T. C.; Raptopoulou, C. P.; Psycharis, V.; Pissas, M.; Perlepes, S. P.; Boudalis, A. K. A Metamagnetic 2D Copper(II)-Azide Complex with 1D Ferromagnetism and a Hysteretic Spin-Flop Transition. *Dalton Trans.* **2009**, 3215–3221.

(52) Fabrizi de Biani, F.; Ruiz, E.; Cano, J.; Novoa, J. J.; Alvarez, S. Magnetic Coupling in End-to-End Azido-Bridged Copper and Nickel Binuclear Complexes: A Theoretical Study. *Inorg. Chem.* **2000**, *39*, 3221–3229.

(53) Manikandan, P.; Muthukumaran, R.; Thomas, K. R. J.; Varghese, B.; Chandramouli, G. V. R.; Manoharan, P. T. Copper(II) Azide Complexes of Aliphatic and Aromatic Amine Based Tridentate Ligands: Novel Structure, Spectroscopy, and Magnetic Properties. *Inorg. Chem.* **2001**, *40*, 2378–2389.

(54) Adak, P.; Das, C.; Ghosh, B.; Mondal, S.; Pakhira, B.; Sinn, E.; Blake, A. J.; O'Connor, A. E.; Chattopadhyay, S. K. Two Pseudohalide-Bridged Cu(II) Complexes Bearing the Anthracene Moiety: Synthesis, Crystal Structures and Catecholase-like Activity. *Polyhedron.* **2016**, *119*, 39–48.

(55) Woollard-Shore, J. G.; Holland, J. P.; Jones, M. W.; Dilworth, J. R. Nitrite Reduction by Copper Complexes. *Dalton Trans.* **2010**, *39*, 1576–1585.

(56) Lehnert, N.; Cornelissen, U.; Neese, F.; Ono, T.; Noguchi, Y.; Okamoto, K.; Fujisawa, K. Synthesis and Spectroscopic Characterization of Copper(II)−Nitrito Complexes with Hydrotris(Pyrazolyl)Borate and Related Coligands. *Inorg. Chem.* **2007**, *46*, 3916–3933.

(57) Wahman, D. G.; Speitel, G. E. Relative Importance of Nitrite Oxidation by Hypochlorous Acid under Chloramination Conditions. *Environ. Sci. Technol.* **2012**, *46*, 6056–6064.

(58) Zueva, E. M.; Petrova, M. M.; Herchel, R.; Trávnícek, Z.; Raptis, R. G.; Mathivathanan, L.; McGrady, J. E. Electronic Structure and Magnetic Properties of a Trigonal Prismatic $Cu^{(II)}_6$ Cluster. *Dalton Trans.* **2009**, 30, 5924–5932.

(59) Mathivathanan, L.; Al-Ameed, K.; Lazarou, K.; Trávníček, Z.; Sanakis, Y.; Herchel, R.; McGrady, J. E.; Raptis, R. G. A Trigonal Prismatic Cu6-Pyrazolato Complex Containing a μ_6-F Ligand. *Dalton Trans.* **2015**, *44*, 20685–20691.

(60) Kamiyama, A.; Kajiwara, T.; Ito, T. Cage-Type Hexacopper(II) Complex Formed by Chloride Template. *Chem. Lett.* **2002**, *31*, 980–981.

(61) Kamiyama, A.; Kajiwara, T.; Ito, T. Cage-Type Hexacopper(II) Complex Formed by Chloride Template. *Chem. Lett.* **2002**, *31*, 980–981.

(62) Sun, Y.-J.; Cheng, P.; Yan, S.-P.; Liao, D.-Z.; Jiang, Z.-H.; Shen, P.-W. Synthesis, Crystal Structure and Properties of Copper(II) Complexes with Different Axial Ligands and Substituted Pyrazoles. *J. Mol. Struct.* **2001**, *597*, 191–198.

(63) Małecka, M.; Chęcińska, L. Di-chloro-tetrakis(3-Phenyl-pyrazole-KN_2)Copper(II). *Acta Crystallogr. C.* **2003**, *59*, m115–m117.

(64) Direm, A.; Tursun, M.; Parlak, C.; Benali-Cherif, N. Trans-Dichlorotetrakis(1H-Pyrazole-KN_2)Copper(II): Synthesis, Crystal Structure, Hydrogen Bonding Graph-Sets, Vibrational and DFT Studies. *J. Mol. Struct.* **2015**, *1093*, 208–218.

(65) Giles, I. D.; DePriest, J. C.; Deschamps, J. R. Effect of Substitution and the Counterion on the Structural and Spectroscopic Properties of CuII Complexes of Methylated Pyrazoles. *J. Coord. Chem.* **2015**, *68*, 3611–3635.

(66) Yaghi, O. M.; O'Keeffe, M.; Ockwig, N. W.; Chae, H. K.; Eddaoudi, M.; Kim, J. Reticular Synthesis and the Design of New Materials. *Nature.* **2003**, *423*, 705-714.

(67) Kitagawa, S.; Kitaura, R.; Noro, S. Functional Porous Coordination Polymers. *Angew. Chem. Int. Ed.* **2004**, *43*, 2334–2375.

(68) Wang, B.; Côté, A. P.; Furukawa, H.; O'Keeffe, M.; Yaghi, O. M. Colossal Cages in Zeolitic Imidazolate Frameworks as Selective Carbon Dioxide Reservoirs. *Nature.* **2008**, *453*, 207-211.

(69) Bhattacharya, B.; Ghoshal, D. Selective Carbon Dioxide Adsorption by Mixed-Ligand Porous Coordination Polymers. *CrystEngComm.* **2015**, *17*, 8388–8413.

(70) Rosi, N. L.; Eckert, J.; Eddaoudi, M.; Vodak, D. T.; Kim, J.; O'Keeffe, M.; Yaghi, O. M. Hydrogen Storage in Microporous Metal-Organic Frameworks. *Science.* **2003**, *300*, 1127–1129.

(71) Double-Layer Structure, Sorption and Magnetism Properties of Metal–organic Frameworks with Trigonal Planar Ligand. *Inorg. Chem. Commun.* **2015**, *55*, 65–68.

(72) Colinas, I. R.; Inglis, K. K.; Blanc, F.; Oliver, S. R. J. Anion Exchange Dynamics in the Capture of Perchlorate by a Cationic Ag-Based MOF. *Dalton Trans.* **2017**, *46*, 5320–5325.

(73) Horcajada, P.; Gref, R.; Baati, T.; Allan, P. K.; Maurin, G.; Couvreur, P.; Férey, G.; Morris, R. E.; Serre, C. Metal–Organic Frameworks in Biomedicine. *Chem. Rev.* **2012**, *112*, 1232–1268.

(74) Tranchemontagne, D. J.; Mendoza-Cortés, J. L.; O'Keeffe, M.; Yaghi, O. M. Secondary Building Units, Nets and Bonding in the Chemistry of Metal–organic Frameworks. *Chem. Soc. Rev.* **2009**, *38*, 1257–1283.

(75) Luo, L.; Lv, G.-C.; Wang, P.; Liu, Q.; Chen, K.; Sun, W.-Y. PH-Dependent Cobalt(II) Frameworks with Mixed 3,3′,5,5′-Tetra(1H-Imidazol-1-Yl)-1,1′-Biphenyl and 1,3,5-Benzenetricarboxylate Ligands: Synthesis, Structure and Sorption Property. *CrystEngComm.* **2013**, *15*, 9537–9543.

(76) Chen, M.; Chen, S.-S.; Okamura, T.; Su, Z.; Chen, M.-S.; Zhao, Y.; Sun, W.-Y.; Ueyama, N. PH Dependent Structural Diversity of Metal Complexes with 5-(4H-1,2,4-Triazol-4-yl)Benzene-1,3-Dicarboxylic Acid. *Cryst. Growth Des.* **2011**, *11*, 1901–1912.

(77) Gu, J.; Gao, Z.; Tang, Y. PH and Auxiliary Ligand Influence on the Structural Variations of 5(2′-Carboxylphenyl) Nicotate Coordination Polymers. *Cryst. Growth Des.* **2012**, *12*, 3312–3323.

(78) Wu, S.-T.; Long, L.-S.; Huang, R.-B.; Zheng, L.-S. PH-Dependent Assembly of Supramolecular Architectures from 0D to 2D Networks. *Cryst. Growth Des.* **2007**, *7*, 1746–1752.

(79) Chen, J.; Ohba, M.; Zhao, D.; Kaneko, W.; Kitagawa, S. Polynuclear Core-Based Nickel 1,4-Cyclohexanedicarboxylate Coordination Polymers as Temperature-Dependent Hydrothermal Reaction Products. *Cryst. Growth Des.* **2006**, *6*, 664–668.

(80) Mo, H.-J.; Zhong, Y.-R.; Cao, M.-L.; Ou, Y.-C.; Ye, B.-H. Hydrothermal Syntheses and Structural Diversity of Cobalt Complexes with 2,2′-Bibenzimidazole Ligand by Temperature Tuning Strategy. *Cryst. Growth Des.* **2009**, *9*, 488–496.

(81) Akhbari, K.; Morsali, A. Effect of the Guest Solvent Molecules on Preparation of Different Morphologies of ZnO Nanomaterials from the $[Zn_2(1,4\text{-}Bdc)_2(Dabco)]$ Metal-Organic Framework. *J. Coord. Chem.* **2011**, *64*, 3521–3530.

(82) Pachfule, P.; Das, R.; Poddar, P.; Banerjee, R. Solvothermal Synthesis, Structure, and Properties of Metal Organic Framework Isomers Derived from a Partially Fluorinated Link. *Cryst. Growth Des.* **2011**, *11*, 1215–1222.

(83) Eddaoudi, M.; Kim, J.; Rosi, N.; Vodak, D.; Wachter, J.; O'Keeffe, M.; Yaghi, O. M. Systematic Design of Pore Size and Functionality in Isoreticular MOFs and Their Application in Methane Storage. *Science*. **2002**, *295*, 469–472.

(84) Moreau, F.; Kolokolov, D. I.; Stepanov, A. G.; Easun, T. L.; Dailly, A.; Lewis, W.; Blake, A. J.; Nowell, H.; Lennox, M. J.; Besley, E.; et al. Tailoring Porosity and Rotational Dynamics in a Series of Octacarboxylate Metal-Organic Frameworks. *Proc. Natl. Acad. Sci. U. S. A.* **2017**, *114*, 3056–3061.

(85) Trends in atmospheric carbon dioxide. https://www.esrl.noaa.gov/gmd/ccgg/trends/index.html. accessed on 3/23/2017.

(86) Banerjee, R.; Phan, A.; Wang, B.; Knobler, C.; Furukawa, H.; O'Keeffe, M.; Yaghi, O. M. High-Throughput Synthesis of Zeolitic Imidazolate Frameworks and Application to CO_2 Capture. *Science*. **2008**, *319*, 939–943.

(87) Plaza M. G.; Pevida C.; Arias B.; Casal M. D.; Martín C. F.; Fermoso J.; Rubiera F.; Pis J. J. Different Approaches for the Development of Low-Cost CO_2 Adsorbents. *J. Environ. Eng.* **2009**, *135*, 426–432.

(88) Chen, B.; Lv, Z.-P.; Leong, C. F.; Zhao, Y.; D'Alessandro, D. M.; Zuo, J.-L. Crystal Structures, Gas Adsorption, and Electrochemical Properties of Electroactive Coordination Polymers Based on the Tetrathiafulvalene-Tetrabenzoate Ligand. *Cryst. Growth Des.* **2015**, *15*, 1861–1870.

(89) An, J.; Geib, S. J.; Rosi, N. L. High and Selective CO_2 Uptake in a Cobalt Adeninate Metal-Organic Framework Exhibiting Pyrimidine- and Amino-Decorated Pores. *J. Am. Chem. Soc.* **2010**, *132*, 38–39.

(90) Maity, D. K.; Halder, A.; Bhattacharya, B.; Das, A.; Ghoshal, D. Selective CO_2 Adsorption by Nitro Functionalized Metal Organic Frameworks. *Cryst. Growth Des.* **2016**, *16*, 1162–1167.

(91) Xiong, S.; He, Y.; Krishna, R.; Chen, B.; Wang, Z. Metal–Organic Framework with Functional Amide Groups for Highly Selective Gas Separation. *Cryst. Growth Des.* **2013**, *13*, 2670–2674.

(92) Chen, Z.; Xiang, S.; Arman, H. D.; Mondal, J. U.; Li, P.; Zhao, D.; Chen, B. Three-Dimensional Pillar-Layered Copper(II) Metal−Organic Framework with Immobilized Functional OH Groups on Pore Surfaces for Highly Selective CO_2/CH_4 and C_2H_2/CH_4 Gas Sorption at Room Temperature. *Inorg. Chem.* **2011**, *50*, 3442–3446.

(93) Morris, W.; Leung, B.; Furukawa, H.; Yaghi, O. K.; He, N.; Hayashi, H.; Houndonougbo, Y.; Asta, M.; Laird, B. B.; Yaghi, O. M. A Combined Experimental−Computational Investigation of Carbon Dioxide Capture in a Series of Isoreticular Zeolitic Imidazolate Frameworks. *J. Am. Chem. Soc.* **2010**, *132*, 11006–11008.

(94) Foo, M. L.; Horike, S.; Fukushima, T.; Hijikata, Y.; Kubota, Y.; Takata, M.; Kitagawa, S. Ligand-Based Solid Solution Approach to Stabilisation of Sulphonic Acid Groups in Porous Coordination Polymer $Zr_6O_4(OH)_4(BDC)_6$ (UiO-66). *Dalton Trans.* **2012**, *41*, 13791–13794.

(95) Bae, Y.-S.; Liu, J.; Wilmer, C. E.; Sun, H.; Dickey, A. N.; Kim, M. B.; Benin, A. I.; Willis, R. R.; Barpaga, D.; LeVan, M. D.; et al. The Effect of Pyridine Modification of Ni–DOBDC on CO_2 Capture under Humid Conditions. *Chem. Commun.* **2014**, *50*, 3296–3298.

(96) Cavenati, S.; Grande, C. A.; Rodrigues, A. E. Adsorption Equilibrium of Methane, Carbon Dioxide, and Nitrogen on Zeolite 13X at High Pressures. *J. Chem. Eng. Data*. **2004**, *49*, 1095–1101.

(97) Llewellyn, P. L.; Bourrelly, S.; Serre, C.; Vimont, A.; Daturi, M.; Hamon, L.; De Weireld, G.; Chang, J.-S.; Hong, D.-Y.; Kyu Hwang, Y.; et al. High Uptakes of CO_2 and CH_4 in Mesoporous Metal—Organic Frameworks MIL-100 and MIL-101. *Langmuir* **2008**, *24*, 7245–7250.

(98) Dietzel, P. D. C.; Johnsen, R. E.; Fjellvåg, H.; Bordiga, S.; Groppo, E.; Chavan, S.; Blom, R. Adsorption Properties and Structure of CO_2 Adsorbed on Open Coordination Sites of Metal–organic Framework Ni_2(Dhtp) from Gas Adsorption, IR Spectroscopy and X-Ray Diffraction. *Chem. Commun.* **2008**, 5125–5127.

(99) Luo, X.; Kan, L.; Li, X.; Sun, L.; Li, G.; Zhao, J.; Li, D.-S.; Huo, Q.; Liu, Y. Two Functional Porous Metal–Organic Frameworks Constructed from Expanded Tetracarboxylates for Gas Adsorption and Organosulfurs Removal. *Cryst. Growth Des.* **2016**, *16*, 7301–7307.

(100) Wang, Q.; Jiang, J.; Zhang, M.; Bai, J. A (3,6)-Connected Metal–Organic Framework with Pyr Topology and Highly Selective CO_2 Adsorption. *Cryst. Growth Des.* **2017**, *17*, 16–18.

(101) Yang, Q.; Ren, S. S.; Hao, Y.; Zhao, Q.; Chen, Z.; Zheng, H. Cyclopentaneteracarboxylic Metal–Organic Frameworks: Tuning the Distance between Layers and Pore Structures with N-Ligands. *Inorg. Chem.* **2016**, 55, 4951-4957.

(102) Liu, D.; Li, N.-Y.; Lang, J.-P. Single-Crystal to Single-Crystal Transformation of 1D Coordination Polymervia Photochemical [2+2] Cycloaddition Reaction. *Dalton Trans.* **2011**, *40*, 2170–2172.

(103) Nagaraja, C. M.; Haldar, R.; Maji, T. K.; Rao, C. N. R. Chiral Porous Metal–Organic Frameworks of Co(II) and Ni(II): Synthesis, Structure, Magnetic Properties, and CO_2 Uptake. *Cryst. Growth Des.* **2012**, *12*, 975–981.

(104) Bhattacharya, B.; Dey, R.; Pachfule, P.; Banerjee, R.; Ghoshal, D. Four 3D Cd(II)-Based Metal Organic Hybrids with Different N,N′-Donor Spacers: Syntheses, Characterizations, and Selective Gas Adsorption Properties. *Cryst. Growth Des.* **2013**, *13*, 731–739.

(105) Huo, P.; Chen, T.; Hou, J.-L.; Yu, L.; Zhu, Q.-Y.; Dai, J. Ligand-to-Ligand Charge Transfer within Metal–Organic Frameworks Based on Manganese Coordination Polymers with Tetrathiafulvalene-Bicarboxylate and Bipyridine Ligands. *Inorg. Chem.* **2016**, *55*, 6496–6503.

(106) Liu, X.-M.; Xie, L.-H.; Lin, J.-B.; Lin, R.-B.; Zhang, J.-P.; Chen, X.-M. Flexible Porous Coordination Polymers Constructed from 1,2-Bis(4-Pyridyl)Hydrazine via Solvothermal in Situ Reduction of 4,4′-Azopyridine. *Dalton Trans.* **2011**, *40*, 8549–8554.

(107) Liu, X.-M.; Lin, R.-B.; Zhang, J.-P.; Chen, X.-M. Low-Dimensional Porous Coordination Polymers Based on 1,2-Bis(4-Pyridyl)Hydrazine: From Structure Diversity to Ultrahigh CO_2/CH_4 Selectivity. *Inorg. Chem.* **2012**, *51*, 5686–5692.

(108) Modrow, A.; Zargarani, D.; Herges, R.; Stock, N. The first porous MOF with photoswitchable linker molecules. *Dalton Trans.*, **2011**, *40*, 4217-4222.

(109) Park, J.; Yuan, D.; Pham, K. T.; Li, J.-R.; Yakovenko, A.; Zhou, H.-C. Reversible Alteration of CO_2 Adsorption upon Photochemical or Thermal Treatment in a Metal–Organic Framework. *J. Am. Chem. Soc.* **2012**, *134*, 99–102.

(110) Leong, C. F.; Faust, T. B.; Turner, P.; Usov, P. M.; Kepert, C. J.; Babarao, R.; Thornton, A. W.; D'Alessandro, D. M. Enhancing Selective CO_2 Adsorption via Chemical Reduction of a Redox-Active Metal–organic Framework. *Dalton Trans.* **2013**, *42*, 9831–9839.

(111) Lin, Z.-J.; Lü, J.; Hong, M.; Cao, R. Metal–organic Frameworks Based on Flexible Ligands (FL-MOFs): Structures and Applications. *Chem. Soc. Rev.* **2014**, *43*, 5867–5895.

(112) Xu, L.; Zhu, B. Syntheses and Characterization of Two Cd(II) Coordination Polymers Based on Mixed Flexible Ligands. *J. Inorg. Organomet. Polym.* **2016**, 26, 264-269.

(113) Yuan, Y.; Xue, X.-N.; Fan, W.-W.; Qiu, Q.-M.; Cui, Y.-Z.; Liu, M.; Li, Z.-F.; Jin, Q.-H.; Yang, Y.-P.; Zhang, Z.-W.; et al. Effect of Solvent on the Architectures of Six Ag(I)

Coordination Polymers Based on Flexible and Quasi-Flexible Organic Nitrogen Donor Ligands. *Polyhedron.* **2016**, *106*, 178–186.

(114) Huang, W.; Jiang, J.; Xu, J.; Kirillov, A. M.; Wu, D. Tuning Topological and Dimensional Versatility from 1D to 3D of Zn/Cd Luminescent Biphenyl-3,5-Dicarboxylate Coordination Polymers by Ancillary Ligand. *J. Coord. Chem.* **2016**, *69*, 2200–2209.

(115) Zhang, J.; Chew, E.; Chen, S.; Pham, J. T. H.; Bu, X. Three-Dimensional Homochiral Transition-Metal Camphorate Architectures Directed by a Flexible Auxiliary Ligand. *Inorg. Chem.* **2008**, *47*, 3495–3497.

(116) Hu, L.; Fan, J.; Slebodnick, C.; Hanson, B. E. Structural Diversity in 4,4‘-Trimethylenedipyridine−zinc Phosphite Hybrids: Incorporation of Neutral Guest Molecules in Hybrid Materials. *Inorg. Chem.* **2006**, *45*, 7681–7688.

(117) Wang, G.-H.; Li, Z.-G.; Jia, H.-Q.; Hu, N.-H.; Xu, J.-W. Topological Diversity of Coordination Polymers Containing the Rigid Terephthalate and a Flexible N,N′-Type Ligand: Interpenetration, Polyrotaxane, and Polythreading. *Cryst. Growth Des.* **2008**, *8*, 1932–1939.

(118) Han, L.; Valle, H.; Bu, X. Homochiral Coordination Polymer with Infinite Double-Stranded Helices. *Inorg. Chem.* **2007**, *46*, 1511–1513.

(119) Contaldi, S.; Nicola, C. D.; Garau, F.; Karabach, Y. Y.; Martins, L. M. D. R. S.; Monari, M.; Pandolfo, L.; Pettinari, C.; Pombeiro, A. J. L. New Coordination Polymers Based on the Triangular $[Cu_3(\mu_3\text{-}OH)(\mu\text{-}Pz)_3]^{2+}$ Unit and Unsaturated Carboxylates. *Dalton Trans.* **2009**, 4928–4941.

(120) Fu, Z.-Y.; Wu, X.-T.; Dai, J.-C.; Wu, L.-M.; Cui, C.-P.; Hu, S.-M. Interpenetration in $[Cd(Isonicotinate)_2(1,2\text{-}Bis(4\text{-}Pyridyl)Ethane)0.5(H_2O)]_n$, a Novel Octahedral Polymer Containing an Unusual Two-Dimensional Bilayer Motif Generated by Self-Assembly of Rectangle Building Blocks. *Chem. Commun.* **2001**, 1856–1857.

(121) Pan, L.; Woodlock, E. B.; Wang, X.; Lam, K.-C.; Rheingold, A. L. Novel Silver(I)–organic Coordination Polymers: Conversion of Extended Structures in the Solid State as Driven by Argentophilic Interactions. *Chem. Commun.* **2001**, 1762–1763.

(122) Luan, X.-J.; Cai, X.-H.; Wang, Y.-Y.; Li, D.-S.; Wang, C.-J.; Liu, P.; Hu, H.-M.; Shi, Q.-Z.; Peng, S.-M. An Investigation of the Self-Assembly of Neutral, Interlaced, Triple-Stranded Molecular Braids. *Chem. – Eur. J.* **2006**, *12*, 6281–6289.

(123) Casarin, M.; Cingolani, A.; Di Nicola, C.; Falcomer, D.; Monari, M.; Pandolfo, L.; Pettinari, C. The Different Supramolecular Arrangements of the Triangular $[Cu_3(\mu_3\text{-}OH)(\mu\text{-}pz)_3]^{2+}$ (pz =pyrazolate) Secondary Building Units. Synthesis of a Coordination Polymer with Permanent Hexagonal Channels. *Cryst. Growth Des.* **2007**, *7*, 676–685.

(124) Wang, G.-H.; Li, Z.-G.; Jia, H.-Q.; Hu, N.-H.; Xu, J.-W. Topological Diversity of Coordination Polymers Containing the Rigid Terephthalate and a Flexible N,N′-Type Ligand: Interpenetration, Polyrotaxane, and Polythreading. *Cryst. Growth Des.* **2008**, *8*, 1932–1939.

(125) Coundert, F. Responsive Metal–Organic Frameworks and Framework Materials: Under Pressure, Taking the Heat, in the Spotlight, with Friends. *Chem. Matter*. **2015**, *27*, 1905-1916.

(126) Tan, J. C.; Cheetham, A. K. Mechanical Properties of Hybrid Inorganic–organic Framework Materials: Establishing Fundamental Structure–property Relationships. *Chem. Soc. Rev.* **2011**, *40*, 1059–1080.

(127) Ogborn, J. M.; Collings, I. E.; Moggach, S. A.; Thompson, A. L.; Goodwin, A. L. Supramolecular Mechanics in a Metal–organic Framework. *Chem. Sci.* **2012**, *3*, 3011–3017.

(128) Cao, S.; Bennett, T. D.; Keen, D. A.; Goodwin, A. L.; Cheetham, A. K. Amorphization of the Prototypical Zeolitic Imidazolate Framework ZIF-8 by Ball-Milling. *Chem. Commun.* **2012**, *48*, 7805–7807.

(129) Umeyama, D.; Horike, S.; Tassel, C.; Kageyama, H.; Higo, Y.; Ogiwara, N.; Kitagawa, S. Pressure-induced amorphization of a dense coordination polymer and its impact on proton conductivity. *APL Materials*. **2014**, *12*, 124401.

(130) Li, W.; Probert, M. R.; Kosa, M.; Bennett, T. D.; Thirumurugan, A.; Burwood, R. P.; Parinello, M.; Howard, J. A. K.; Cheetham, A. K. Negative Linear Compressibility of a Metal–Organic Framework. *J. Am. Chem. Soc.* **2012**, *134*, 11940–11943.

(131) Su, Z.; Miao, Y.-R.; Zhang, G.; Miller, J. T.; Suslick, K. S. Bond Breakage under Pressure in a Metal Organic Framework. *Chem. Sci.* **2017**, *8*, 8004–8011.

Appendices

Table A.1. Crystallographic data and structure refinement for (PPN)($C_5H_{10}NH_2$)[Cu_3(μ$_3$-OH) (μ-Cl)(μ-4-Ph-Pz)$_3$$Cl_3$] **[1]**, (PPN)[$Cu_3$(μ$_3$-OH)(μ-4-Ph-pz)$_3$$Cl_3$]·$CH_2Cl_2$ **[2]** and (PPN)[Cu_3(μ$_3$-OH) (μ-4-Ph-pz)$_3$ Cl_3]· CH_3CN **[3]**.

Compound	**[1]**	**[2]**	**[3]**
Chemical formula	$C_{68}H_{64}Cl_4Cu_3N_8OP_2$	$C_{31.5}H_{26.5}Cl_{1.5}Cu_{1.5}N_{3.5}O_{1.5}P$	$C_{65}H_{55}Cl_3Cu_3N_8OP_2$
FW	1403.63	657.60	1323.08
Wavelength (Å)	0.71073	0.71073	0.71073
Crystal system	Triclinic	Monoclinic	Triclinic
space group	*P-1*	*P2$_1$/n*	*P-1*
a (Å)	13.5479 (10)	14.581(2)	11.7975 (9)
b (Å)	15.6793 (11)	18.441(3)	16.2486 (12)
c (Å)	17.3297 (12)	24.324(4)	17.3874 (13)
α (º)	74.957 (2)	90	109.8070(10)
β (º)	69.425 (2)	105.250(4)	98.6350 (10)
γ (º)	79.368 (2)	90	95.0280 (10)
V (Å^3)	3310.5 (4)	6310.1(16)	3065.7 (4)
Z	2	8	2
D_c, g cm^{-3}	1.408	1.384	1.433
μ (Mo Kα) mm^{-1}	1.213	1.229	1.263
F (000)	1442.0	2688.0	1354.0
Crystal size, mm	0.39 × 0.23 × 0.15	0.20 × 0.08 × 0.05	0.15 × 0.06 × 0.05
T (K)	298	273	296.15
θ limits, °	3.004-27.239	2.896-26.636	1.766-27.081
Reflections collected	40290	147054	34487
ind. refl.	14698	13050	13306
idn.refl.[[I>2σ]	10392	8909	6299
Data/restraints/parameters.	14698/0/775	13050/0/737	13306/3/744
goodness-of-fit on F^2	1.119	1.120	0.922
R(F); R_w(F) [I>2σ]	0.0755/0.1402	0.1065/0.2086	0.0485/0.0803
R; R_w (all data)	0.1043/0.1591	0.1478/0.2332	0.1410/0.1047
Largest peak/hole (e Å^{-3})	1.37/-1.14	1.03/-0.76	0.35/-0.31

Table A. 2. Crystallographic data and structure refinement for (PPN)[$Cu_3(\mu_3\text{-}OH)(\mu\text{-}pz)_3(\mu_{1,1}\text{-}N_3)_2(N_3)$]**[4]**, [$Cu_3(\mu_3\text{-}OMe)(\mu_2\text{-}Cl)(\mu\text{-}Pz)_3(py)_2$]Cl **[5]** and [$Cu_3(\mu_3\text{-}OH)(\mu_2\text{-}Cl)(\mu\text{-}Pz)_3(py)_2Cl$](py) **[6]**.

Compound	**[4]**	**[5]**	**[6]**
Chemical formula	$C_{45}H_{40}Cu_3N_{16}OP_2$	$C_{20}H_{22}Cl_2Cu_3N_8O$	$C_{24}H_{25}Cl_2Cu_3N_9O$
FW	1073.49	651.97	717.05
Wavelength (Å)	0.71073	0.71073	0.71073
Crystal system	monoclinic	Triclinic	Orthorhombic
space group	*$P2_1/c$*	*P-1*	*Pnma*
a (Å)	8.6459(8)	9.2009(10)	19.8505 (12)
b (Å)	17.1790(16)	11.1495(12)	15.0337 (9)
c (Å)	32.397(3)	12.4400(14)	9.4632 (5)
α (°)	90	77.6670(10)	90
β (°)	96.4270(10)	79.9440(10)	90
γ (°)	90	81.421(1)	90
V ($Å^3$)	4781.6(8)	1219.2(2)	2824.1 (3)
Z	4	2	4
D_c, g cm^{-3}	1.491	1.776	1.686
μ (Mo Kα) mm^{-1}	1.443	2.843	2.464
F (000)	2188.0	654.0	1444.0
Crystal size, mm	0.27 × 0.07 × 0.06	0.499 × 0.164 × 0.152	0.451 × 0.17 × 0.161
T (K)	296.15	293(2)	293(2)
θ limits, °	1.824-28.338	2.263-28.198	2.974-28.252
Reflections collected	54361	13494	16860
ind. refl.	11367	5460	3571
idn.refl.[[I>2σ]	7240	4581	2697
Data/restraints/param.	11367/0/628	5460/0/307	3571/0/193
goodness-of-fit on F^2	1.031	1.039	1.019
R(F); R_w(F) [I>2σ]	0.0580/0.1529	0.0233/0.0559	0.0328/0.0779
R; R_w (all data)	0.0999/0.1753	0.0320/0.0601	0.0522/0.0869
Largest peak/hole (e $Å^{-3}$)	3,38/-0.47	0.27/-0.34	0.5/-0.42

Table A. 3. Crystallographic data and structure refinement for $Cu_3(\mu_3\text{-}OH)(\mu_3\text{-}4\text{-}Cl)_3(py)_3(ClO_4)_2]\cdot(CH_2Cl_2)(CH_3)_2CO$**[7]**, $(PPN)_2[Cu_3(\mu_3\text{-}O)(\mu\text{-}pz)_3(\eta^1\text{-}NO_2)_2(\eta^2\text{-}NO_2)]$**[8]**, $(PPN)_3[Cu_3(\mu_3\text{-}OH)(\mu\text{-}pz)_3(\eta^1\text{-}NO_2)_3](OH)(NO_3)$ **[9]**

Compound	**[7]**	**[8]**	**[9]**
Chemical formula	$C_{28}H_{30}Cl_7Cu_3N_9O_{10}$	$C_{81}H_{69}Cu_3N_{11}O_7P_4$	$C_{117}H_{100}Cu_3N_{13}O_{11.12}P_6$
FW	1091.38	1622.97	2242.48
Wavelength (Å)	0.71073	0.71073	0.71073
Crystal system	monoclinic	monoclinic	trigonal
space group	*$P2_1/n$*	*P2/c*	*R3*
a (Å)	10.6000(6)	12.5887(7)	22.7476(12)
b (Å)	29.3617(17)	13.0204(7)	22.7476(12)
c (Å)	13.6591(8)	23.2687(13)	18.1826(10)
α (°)	90	90	90
β (°)	97.8390(10)	103.6000(10)	90
γ (°)	90	90	120
V ($Å^3$)	4211.4(4)	3707.0(4)	8148.1(10)
Z	4	2	3
D_c, g cm^{-3}	1.721	1.454	1.371
μ (Mo Kα) mm^{-1}	2.007	1.003	0.737
F (000)	2188.0	1670.0	3477.0
Crystal size, mm	0.223 × 0.198 × 0.183	0.49 × 0.294 × 0.254	0.124 × 0.093 × 0.084
T (K)	273.15	150.0	200.42
θ limits, °	2.845-26.483	3.122-27.08	2.956-28.357
Reflections collected	51256	47110	40177
ind. refl.	8679	8091	9023
idn.refl.[[I>2σ]	7009	6804	5492
Data/restraints/param.	8679/0/520	8091/0/480	9023/1/452
goodness-of-fit on F^2	1.041	1.062	1.042
R(F); R_w(F) [I>2σ]	0.0462/0.1004	0.0374/0.0842	0.0695/0.1415
R; R_w (all data)	0.0623/0.1078	0.0480/0.0893	0.1393/0.1679
Largest peak/hole (e $Å^{-3}$)	1.04/-0.85	0.71/-0.62	1.39/-1.19

Table A. 4. Crystallographic data and structure refinement for $(PPN)_2[Cu_3(\mu_3\text{-}O)(\mu\text{-}pz)_3(\eta^1\text{-}NO_2)_2Cl]$ **[10],** $(PPN)[Cu_3(\mu_3\text{-}OH)(\mu\text{-}4\text{-}Ph\text{-}pz)_3(\eta^1\text{-}NO_2)_3](CH_2Cl_2)_{0.5}$ **[11]**, $(PPN)_3[Cu_3(\mu_3\text{-}O)(\mu\text{-}4\text{-}Me\text{-}pz)_3(\eta^1\text{-}NO_2)_3](NO_3)$ **[12]**.

Compound	**[10]**	**[11]**	**[12]**
Chemical formula	$C_{81}H_{69}ClCu_3N_{10}O_5P_4$	$C_{127}H_{107}Cl_2Cu_6N_{20}O_{13}P_4$	$C_{120}H_{106}Cu_3N_{13}O_{12}P_6$
FW	1612.41	2710.32	2450.30
Wavelength (Å)	0.71073	0.71073	0.71073
Crystal system	monoclinic	Monoclinic	Trigonal
space group	*P2/c*	*P-1*	*R3*
a (Å)	12.6164(7)	14.7002(6)	22.8385(10)
b (Å)	12.9846(8)	15.0742(6)	22.8385(10)
c (Å)	23.1900(14)	17.4451(7)	18.3868(8)
α (°)	90	65.3550(10)	90
β (°)	103.855(2)	65.3470(10)	90
γ (°)	90	65.8460(10)	120
V ($Å^3$)	3688.4(4)	3061.1(2)	8305.6(8)
Z	2	1	3
D_c, g cm^{-3}	1.452	1.470	1.470
μ (Mo Kα) mm^{-1}	1.041	1.191	0.706
F (000)	1658.0	1386.0	3792.0
Crystal size, mm	0.446 × 0.365 × 0.107	0.230× 0.312 × 0.135	0.202 × 0.198 × 0.12
T (K)	149.88	273(2)	273.15
θ limits, °	3.135-26.482	2.99-26.41	2.941-28.299
Reflections collected	45974	38310	79088
ind. refl.	7611	12466	9188
idn.refl.[[I>2σ]	6520	8503	6828
Data/restraints/param.	7611/0/481	12466/0/784	9188/2/466
goodness-of-fit on F^2	1.044	1.028	1.0
R(F); R_w(F) [I>2σ]	0.0426/0.1115	0.0551/0.1372	0.0447-0.1043
R; R_w (all data)	0.0515/0.1176	0.0920/0.1499	0.066/0.1132
Largest peak/hole (e $Å^{-3}$)	1.40/-0.63	1.83/-0.77	0.95/-0.66

Table A. 5. Crystallographic data and structure refinement for and $(PPN)_3[Cu_3(\mu_3\text{-}O)(\mu\text{-}4\text{-}Cl\text{-}pz)_3(\eta^1\text{-}NO_2)_3](NO_3)$ **[13]**, $[PPN][Cu_3(\mu_3\text{-}O)(\mu\text{-}pz)_3(N_3)_2(\eta^2\text{-}NO_2)]$ **[14]** and $[\{Cu_3(\mu_3\text{-}OCH_3)(\mu\text{-}C_3H_2N_2Cl)_3\}_2(\mu\text{-}C_3H_2N_2Cl)_3(\mu_6\text{-}Cl)]$ **[15]**.

Compound	**[13]**	**[14]**	**[15]**
Chemical formula	$C_{117}H_{96}Cl_3Cu_3N_{13}O_{11}P_6$	$C_{40.5}H_{34.5}Cu_{1.5}N_{7.5}O_{1.5}P_2$	$C_{29}H_{24}Cl_{10}Cu_6N_{18}O_2$
FW	2342.88	807.50	1392.40
Wavelength (Å)	0.71073	0.71073	0.71073
Crystal system	Trigonal	monoclinic	orthorhombic
space group	*R3*	*P2/n*	*Pbcn*
a (Å)	22.8693(10)	12.5336(9)	16.5655(10)
b (Å)	22.8693(10)	13.3055(9)	18.4743(11)
c (Å)	18.3055(9)	23.6547(18)	14.6065(9)
α (°)	90	90	90
β (°)	90	104.797(2)	90
γ (°)	120	90	90
V ($Å^3$)	8291.2(8)	3814.0(5)	4470.1(5)
Z	3	4	4
D_c, g cm^{-3}	1.408	1.406	2.069
μ (Mo Kα) mm^{-1}	0.798	0.973	3.456
F (000)	3615.0	1662.0	2736.0
Crystal size, mm	0.302 × 0.258 × 0.123	0.189 × 0.14 × 0.089	0.208 × 0.203 × 0.16
T (K)	295.69	298.14	298.88
θ limits, °	2.94-24.748	3.08-26.32	2.884-26.137
Reflections collected	30157	4701	63202
ind. refl.	6294	3062	5726
idn.refl.[[I>2σ]	4857	1929	4647
Data/restraints/param.	6294/1/460	3062/0/480	5726/0/296
goodness-of-fit on F^2	1.019	1.032	1.078
R(F); R_w(F) [I>2σ]	0.0501/0.1098	0.0674/0.1481	0.0410/0.1096
R; R_w (all data)	0.0773/0.1213	0.1151/0.1728	0.0533/0.1191
Largest peak/hole (e $Å^{-3}$)	0.83/-0.67	0.42/-0.31	0.74/-1.61

Table A. 6. Crystallographic data and structure refinement for $[Cu_6(\mu_3\text{-}OMe)_2(\mu_4\text{-}Cl)(\mu\text{-}4\text{-}Ph\text{-}pz)_8Cl]_2$ [bpe] **[19]**, $[Cu_6(\mu_3\text{-}OMe)_2(\mu 4\text{-}Cl)(\mu\text{-}4\text{-}Ph\text{-}pz)_8Cl]_2$[abp] **[20]** and $[\{Cu_3(\mu_3\text{-}OH)(\mu\text{-}4\text{-}Cl\text{-}pz)_3(py)_2\}_2(abp)](ClO_4)_4$ **[21]**

Compound	**[19]**	**[20]**	**[21]**
Chemical formula	$C_{81}H_{69}Cl_4Cu_6N_{17}O_2$	$C_{81}H_{71}Cl_4Cu_6N_{18}O_3$	$C_{192}H_{176}Cl_{40}Cu_{24}N_{80}O_{72}$
FW	1835.57	1867.59	7699.08
Wavelength (Å)	0.71073	0.71073	0.71073
Crystal system	triclinic	triclinic	orthorhombic
space group	*P-1*	*P-1*	*Fddd*
a (Å)	14.7574(9)	14.588(2)	25.436(3)
b (Å)	17.5451(11)	17.055(3)	34.820(4)
c (Å)	20.6238(12)	20.222(3)	37.667(4)
α (°)	92.9100(17)	93.106(3)	90
β (°)	107.6930(15)	106.082(3)	90
γ (°)	108.9740(16)	109.141(3)	90
V ($Å^3$)	4744.1(5)	4508.4(12)	33362(7)
Z	2	2	4
D_c, g cm^{-3}	1.285	1.376	1.533
μ (Mo Kα) mm^{-1}	1.482	1.562	1.890
F (000)	1864.0	1898.0	15360.0
Crystal size, mm	0.4 × 0.4 × 0.17	0.47 × 0.332 × 0.142	0.161 × 0.156 × 0.151
T (K)	298.84	100.0	273.15
θ limits, °	2.901-24.808	2.911-26.347	2.88-24.957
Reflections collected	16252	45915	7233
ind. refl.	16252	18050	7233
idn.refl.[[I>2σ]	11169	12072	3487
Data/restraints/param.	16252/0/991	18050/3/1015	7233/0/460
goodness-of-fit on F^2	1.070	1.168	0.969
R(F); R_w(F) [I>2σ]	0.0568/0.1635	0.0978/0.2347	0.08003/0.1081
R; R_w (all data)	0.0821/0.1787	0.1275/0.2566	0.1656/0.2212
Largest peak/hole ($eÅ^{-3}$)	1.02/-0.67	2.05/-1.26	0.80/-0.73

Table A.7. Crystallographic data and structure refinement for $\{[Cu_3(\mu_3\text{-}OH)(\mu\text{-}Cl)(\mu\text{-}pz)_3Cl(tmpy)(CH_3CN)]\}_n$ **[22]**, $\{[Cu_3(\mu_3\text{-}OH)(\mu\text{-}Cl)(\mu\text{-}pz)_3Cl]_2(tmpy)_2](CH_3CN)_2\}_n$ **[23]** and $\{[Cu_3(\mu_3\text{-}OH)(\mu\text{-}Cl)(\mu\text{-}pz)_3Cl(tmpy)](CH_3CN)\}_n$ **[24]**

Compound	**[22]**	**[23]**	**[24]**
Chemical formula	$C_{96}H_{108}Cl_8Cu_{12}N_{36}O_4$	$C_{26}H_{30}Cl_2Cu_3N_{10}O$	$C_{46}H_{51}Cl_4Cu_6N_{17}O_2$
FW	2876.26	760.12	1397.08
Wavelength (Å)	0.71073	0.71073	0.71073
Crystal system	Orthorhombic	Monoclinic	monoclinic
space group	*Pnma*	*$P2_1/n$*	*C2/c*
a (Å)	10.8947(6)	11.4342 (8)	26.609(1)
b (Å)	15.7770(9)	17.801 (1)	9.2327(3)
c (Å)	17.785(1)	15.733 (1)	23.543(1)
α (°)	90	90	90
β (°)	90	95.709(2)	96.902(1)
γ (°)	90	90	90
V ($Å^3$)	3057.0(3)	3186.5 (4)	5742.0(4)
Z	1	4	4
D_c, g cm^{-3}	1.562	1.584	1.616
μ(Mo Kα) mm^{-1}	2.276	2.190	2.421
F(000)	1452.0	1540	2816
Crystal size, mm	0.17 × 0.15 × 0.14	0.14 × 0.10 × 0.08	0.20 × 0.13 × 0.10
T (K)	273(2)	200(0)	200(0)
θ limits, °	2.957-26.49	2.91-26.37	2.97-26.42
Reflections collected	46032	38031	48851
ind. refl.	3259	6516	5894
idn.refl.[[I>2σ]	3393	4196	4541
Data/restraints/param.	3259/0/194	4916/0/381	4541/3/353
goodness-of-fit on F^2	1.207	0.95	1.035
R(F); R_w(F) [I>2σ]	0.08/0.1305	0.0554; 0.1059	0.0341; 0.0665
R; R_w (all data)	0.1213/0.1439	0.1065; 0.1244	0.057; 0.0731
Largest peak/hole (e $Å^{-3}$)	0.56/-1.12	0.767/ -0.510	0.45/−0.44

VITA

KAIGE SHI
Born, HENAN, CHINA

2005-2007	Bachelor of Chemistry Nanyang Normal University Nanyang, China
2007-2010	Master degree in Inorganic Chemistry Zhengzhou University Zhengzhou, China
2014-2018	Master of Science in Chemistry Doctoral Candidate in Inorganic chemistry Florida International University Miami, FL.
	Graduate Teaching Assistant Graduate Research Assistant Florida International University Miami, FL.

PUBLICATIONS AND PRESENTATIONS

1. K. Shi, L. Mathivathanan and R. G. Raptis. Crystal structure of μ_6-chlorido-nonakis(μ-4-chloropyrazolato)bis-μ_3-methoxo-hexacopper(II). Acta Cryst. 2017. E73, 266–269.

2. K. Shi, L. Mathivathanan and R. G. Raptis. Selective CO_2 adsorption on Cu-pyrazolato MOFs. ACS meeting, New orleans, USA, March 17, 2017.